CZECH TECHNICAL UNIVERSITY IN PRAGUE

DEPARTMENT OF MECHANICS, BIOMECHANICS AND MECHATRONICS

MECHANICAL ENGINEERING

Dissertation

Developing Trabecular Structure

Eren Pehlivan, MSc

Supervisor: Prof. RnDr. Matej Daniel, Ph.D

Co-supervisor: Prof. Ing. Ján Džugan, Ph.D

Study programme: Mechanical Engineering

Study branch: Biomechanics

2019   Prague

Type of publication	Ph.D. Dissertation
Title	Developing trabecular structure
Author	Eren Pehlivan, MSc
Supervisor	Prof. RnDr. Matej Daniel, Ph.D.
	Department of Mechanics, Biomechanics and
	Mechatronics, Faculty of Mechanical Engineering,
	Czech Technical University in Prague, Czech Republic
Co-supervisor	Prof. Ing. Ján džugan, Ph.D.
	Research and development
	Director Member of the Board of Directors
	Comtes fht a.s. Dobřany, Czech Republic
University	Czech Technical University in Prague
Faculty	Faculty of Mechanical Engineering
Department	Department of Mechanics, Biomechanics and
	Mechatronics
Address	Technická 4, 166 07 Prague 6, Czech Republic
Number of page	118
Number of figures	89
Number of table	18

Declaration

I declared that thesis is entirely my own work and that where material could be construed as the work of others, it is fully cited and referenced, and/or with appropriate acknowledgement given.

……………………………….

Eren Pehlivan

In Prague 2019

Annotation

Additive manufacturing can produce a regular three-dimensional mesh of tiny interconnected wires that form a porous structure. It is reasonable to assume that the properties of single wires/struts, geometry of the mesh and the post-treatment method affect the performance of each unit-cell and the whole porous structure. Within this study, we have evaluated the effect of these variables on mechanical behavior of a regular porous structure in a series of experiments and numerical models. We have shown that the build orientation of individual elements of porous structure is significant for small diameters. Static and dynamic tests of rhombic dodecahedron structure showed excellent repeatability and they corresponds well to the results of analytical and FEA models. Original post-treatment methods of porous structure were developed and it was shown that these methods can predictively modify mechanical response of the whole structure. In addition to the knowledge of mechanical behavior, the presented research also verifies a set of methods for testing of metal porous structure used in orthopedic applications.

Keywords: Additive Manufacturing (AM); Selective Laser Melting (SLM); Titanium Alloy; Surface treatment; Hot Isostatic Press.

Anotace

Pomocí metod aditivní výroby je možné vytvořit jemnou porézní strukturu podobnou kosti, která se skládá ze vzájemně propojených trámců. Můžeme předpokládat, že vlastnosti jednotlivých trámců, geometrie sítě nebo jejich technologická úprava ovlivní mechanické vlastnosti celé porézní struktury. Cílem předložené studie je systematicky studovat tyto jednotlivé vlivy v sérii experimentálních testů a s nimi propojených matematických modelů. V rámci naší studie jsmě dokázali, že směr stavby malých trámců v komoře výrazně ovlivňuje jejich mechanické vlastnosti. Pro celou rhombickou dodekahedronovou síť jsme ukázali výbornou opakovatelnosti výsledků a dobrou shodu s analytickými a MKP modely. V rámci práce byly studovány původní metody následného zpracování porézní struktury and bylo ověřeno, že pomocí těchto metod je možné dosáhnout predikovatelnou změnu mechanických vlastností. Kromě získání původních znalostí o mechanickém chování porézní struktury, poskytuje předložená práce také soubor metod k testování porézních kovových struktur využívaných k ortopedickým aplikacím.

Klíčové slovo: Aditivní technologie; Selektivní tavení laserem; Slitinami titanu; Povrchové úpravy kovů; Izostatické lisování za tepla (HIP)

Acknowledgments

List of symbols

ρ^*/ρ_s	Relative density	N/a
$E_A = P/(U x SP)$	Applied energy density	J/mm3
P	Laser power	W
U	Scan velocity	mm/s
SP	Scan spacing between parallel scan lines	mm
YS	Yield strength	MPa
UTS	Ultimate tensile strength	MPa
A	Elongation after fracture	n/a
E_x	Young's modulus in the x-direction	GPa
E_y	Young's modulus in the y-direction	GPa
E_s	Young's modulus of the solid	GPa
σ_x	Stress in x-direction	MPa
σ_y	Stress in y-direction	MPa
σ_s	Stress of the solid	MPa
σ_Y	Yield stress of the porous structure	MPa
σ_{Ys}	Yield stress of the bulk material	MPa
ε_x	Strain in x-direction	n/a
ε_x	Strain in y-direction	n/a
ε_s	Strain of the solid	n/a
t	Strut thickness	mm
l	Strut length	mm
F_x	Load in the x-direction	N
F_y	Load in the y-direction	N
γ	Poisson's ratio	N/a
r	Radius of the struts	mm
θ	The main angles of rhombus faces	Degree
b	Side dimension of the strut	mm
U_1	Displacement in x-direction	mm
U_2	Displacement in y-direction	mm
U_3	Displacement in z-direction	mm

Table of contents

Chapter 1: Introduction

Additive manufacturing (AM) of titanium alloys is rapidly becoming a global trend for biomedical industry. Biocompatible titanium and its alloys are mostly used as an AM material for joint and bone replacement. AM from biocompatible metal alloys has the potential to revolutionize the design and production of joint replacements [1]. The AM process could create custom shapes of implants adjusted for individual patient, and/or optimize implant' surface [2]. The remarkable possibility of AM is in manufacturing porous structures resembling the geometry of a trabecular bone. It was proposed that bone-like structure could increase the longevity of joint replacement by reducing the stress-shield effect and by enhancing osteointegration [3][4][5].

The porous structure could be considered as the three-dimensional mesh of interconnecting struts [6]. The mechanical properties of the porous structure are given by the geometry of the mesh and by the properties of individual struts [7][8]. It can further be adjusted by tuning open-cell architecture, strut thickness (relative density) and choice of materials [9][10][8][11]. The variation in the properties of single struts is usually neglected. The unit cell intrinsically consists of struts built at various angles and possibility of different thickness [12][13]. It was shown that building orientation affects the mechanical properties of AM components. In addition, the small elements produced by AM might exhibit a large variation in mechanical properties [14].

Selective laser melting (SLM) is a widely used AM method for creating arbitrarily complex and predictable porous 3D structures [15][16]. SLM forms an implant from titanium powder by melting the powder layer by layer and forming the solid structure in the melted region. The bulk titanium could contain internal pores as a result of SLM process. These internal defects influence strength considerably. It was shown that hot isostatic pressing (HIP) can be used effectively to reduce internal defects of AM metals. The effect of HIP is well documented for solid structure, its potential advantage for porous structures has not been described in the previous literature.

The SLM methods produce not only internal defects but gives also a very rough surface. During the AM process, some powder particles are partly melted and remain loosely connected at the surface. It was suggested that the released particles can have adverse long-

term metabolic, oncogenic and immunologic effects [17][18][19]. Loosely attached powder could be removed from the surface of solid implant by polishing or machining. Cleaning of un-melted titanium particles from porous implant surface is not straightforward but could be considered as a crucial for further in-vivo application. In this study, dynamic compression and quasi-static mechanical tests were carried out in order to (a) identify the effect of HIP treatments and (b) determine the effect of chemical etching on mechanical properties in porous samples.

Analytic and numerical approach help to improve understanding of the mathematical background of cellular structure. The previous works mainly focused on tetrakaidecahedral cellular structures since it is widely used in the automotive industry. In this study, rhombic dodecahedron structure was investigated since the same structure was used for mechanical tests. 2D and 3D analytic models were used to compare with numerical approach in order to develop a representative model for complex porous components. The present study is concerned with modelling and simulation of the mechanical behavior of regular open cell porous structures by the finite element method. Mathematical model of this study also illustrates that material data can play a vital role in calculating mechanical response cellular architecture.

Chapter 2: Review of literature

2.1   *What is cellular structure?*

The word 'cell' is known as the Latin cella which means a small compartment, an enclosed space. A cellular solid is one made up of an interconnected network of solid struts or plates which from the edges and faces of cells [20]. The Mentioned struts can be grouped in 3; line connector, faces connectors or plate connectors, Figure 2.1. Foam structure is also known as a cellular solid and provide a wide range of benefits.

a) Balsa wood   b) Trabecular bone   c) Polyethylene foam
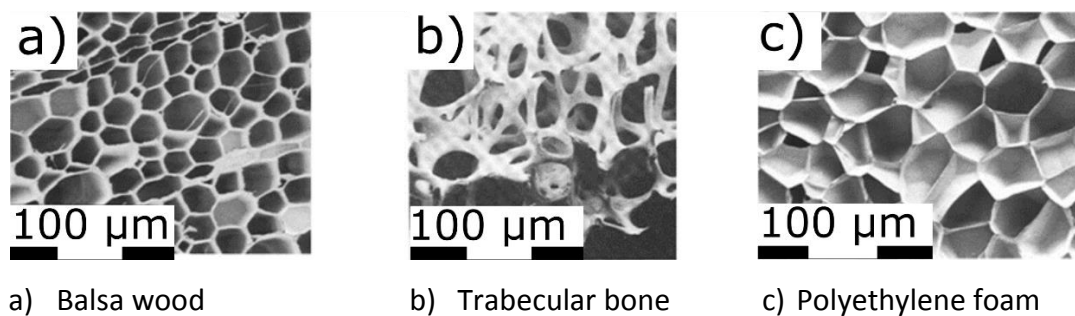
Figure 2.1 Foam and connector types[21]

2.2   *Cellular structure in nature*

In nature, cellular structure materials can be seen everywhere. Foam like materials consists of pores and connector. In the application environment, the shape of the unit cell can be adapted according to needs in time. For example; honeycombs, cork, coral, and wood have natural evolution to provide certain mechanical benefit. And also it is known that bones have different cellular structure with variety of density range according to function area

Figure 2.2. For instance, porous structure in skull has different shape than femoral bone cells because different cell structure can bear with different types of loading. Understanding the mechanical properties of cellular solids can lead to improved materials design and performance.

a) Bread

b) Chocolate
   bar

c) Malteser

d) Meringue

e) Potato
   Chip

f) Cake

Figure 2.2 Foam types in nature [22]

2.3 *Benefit of porous structure in nature*

The porous structure is able to deliver elastic mechanical properties and surprisingly suitable flexible range of application area. The trees contain wood cells and pores which help to distribute substance for the others cells. On the other hand, they can provide st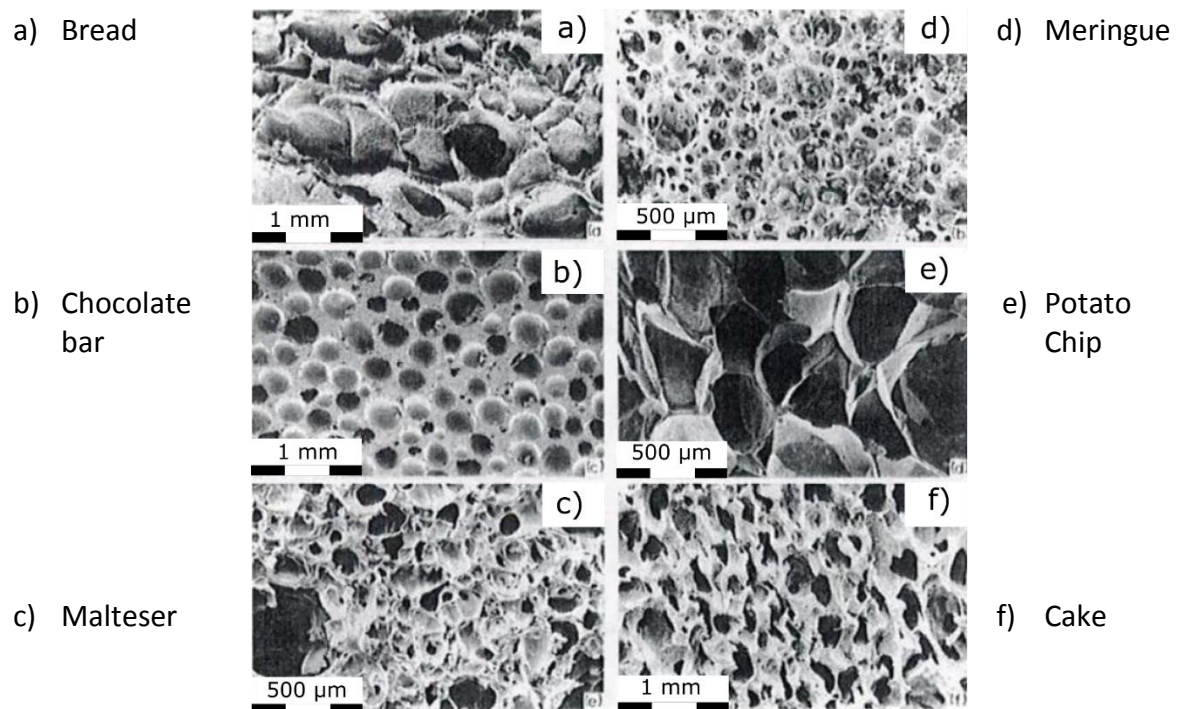rength to stand against strong winds and wild environmental conditions. Moreover, cellular architecture also provides thermal benefit for live tissues in nature.

2.4 *Parameters affect properties of cellular structure*

The porous structure is able to provide special feature than solid materials. It is well-known that any material can be foamed by thermal application for instance; ceramics, glasses, metals composites. There are several description to understand the cellular structure, the honeycomb is the foundation and simplified description of porous architecture and it is widely used term for open and closed cells. The foams can be shaped by applying heat sintering technique. This technique is commonly used for the materials such as polymers and aluminium. Several different methods exist for metallic foam fabrication such as, metallic foam can be formed in the by melting process by adding foaming agents (gas or gas-producing solids) during solidification [23].

a)

b)

a) Foam shape   b) Honeycombs shape

Figure 2.3 Comparison between a cellular solid and a solid with isolated foam [24]

Understanding the properties of honeycombs allows us to define new applications and improve design parameters for existing ones. Relative density is the parameters affects directly the mechanical performance (ρ^*/ρ_s), and it can be adjusted by the cell shape such as closed or open cell. Material type is also parameter to be considered for affecting mechanical response of the design. For instance, the stiffness of the metal structure can be adjusted by making lighter for biomedical application. On the other hand, cell geometry such as convex hull or rhombic dodecahedron are also vital for integration with other material such as epoxy or bone cells for interpenetrating phase composites behaviour. Despite the mechanical performance is depending on several parameters, thermal performance is dedicated by material types and cell geometry.

2.5   *Cellular structure of metal material*

Any material can be foamed by heat sintering. However not all material can be additively manufactured. Materials selection charts are used to aid engineers in choosing the optimal material for a specific task Figure 2.4. Based on a certain set of design criteria, these charts help to narrow down the choices of available materials for a given application. Elastic modulus, strength, density and cost are some of the primary properties that materials selection charts map out, however, many other properties are charted where a given application requires them, such as impact resistance [25]. Titanium, aluminium and stainless steel are widely used for additive manufacturing application.
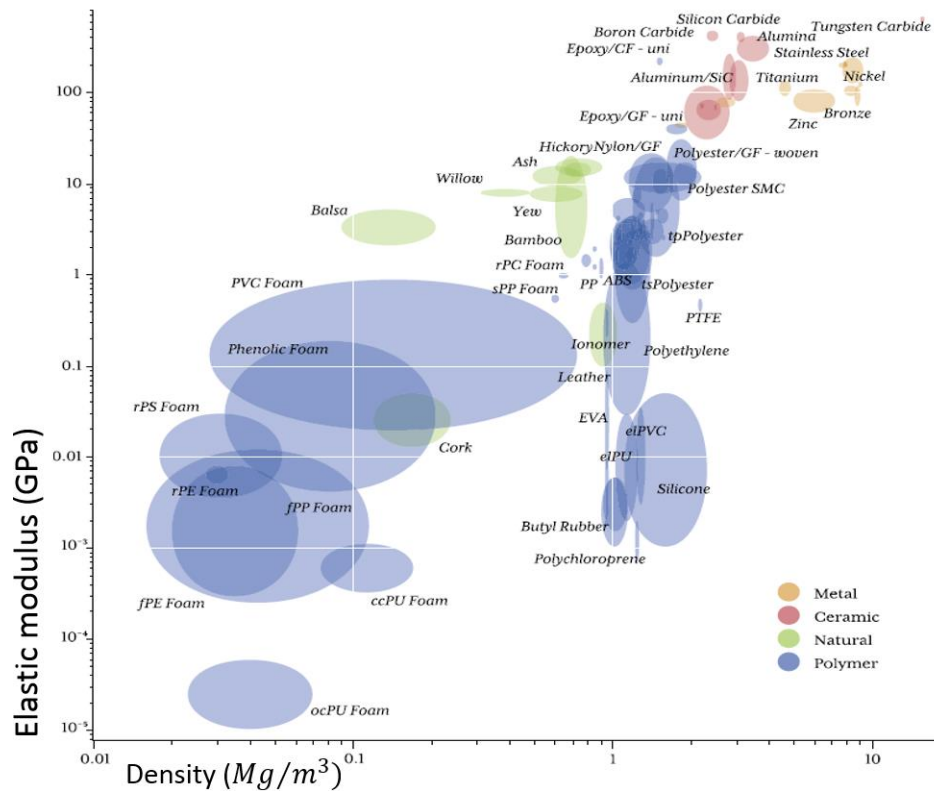
Figure 2.4 Typical material selection chart [26]

2.6   *Additive manufacturing state of the art*

Additive manufacturing is the formalized term for what used to be called rapid prototyping and nowadays it is known as 3D Printing. The term rapid prototyping (RP) is used in a variety of industries to describe a process for rapidly creating a system or part representation before final release or commercialization [27]. Unlike conventional manufacturing subtractive processes, in which a tool is used to remove unwanted material from a work piece to fabricate a part. Additive manufacturing (AM) is ''a process of joining materials to make objects from 3D model data, usually layer upon layer [28] . In recent years, AM has received significant attention in both the popular press and in scientific journals; in fact, from 2011 to 2012 the number of publications on AM jumped by an order of magnitude, from 1600 to 16,000 [29]. The first method to create a three-dimensional object layer by layer using computer-aided design (CAD) was rapid prototyping, developed in the 1980s to produce models and prototype parts. The main advantage of the Additive Manufacturing (AM) is its ability to create almost any possible shape and this capacity is run by the layer-by-layer manufacturing. AM technology is most commonly used for modelling, prototyping, tooling through an exclusive machine or 3D printer. AM is largely used for manufacturing short-term prototypes but it is also used for small-scale series production and tooling applications[30]. The demand of AM

machines is increasingly growing since the 1990s. Due to the evolution of rapid prototyping technologies, it has become possible to obtain parts representative of a mass production within a very short time. AM perfectly fits into the numerical design and manufacturing chain. AM is very complementary with the reverse engineering to reproduce or repair a model [31]. It also helps to create light weight structure with adjustable stiffness according to the application area.

2.7   *Metal printers SLM and EBM*

AM is a layer manufacturing process that allows generating complex 3D parts by consolidating successive layers of powder material on top of each other. Selective laser melting (SLM) and electron beam melting (EBM) are relatively new technique. AM technologies can allow fabrication of complex, multi-functional metal component with powder bed melting [32].

Electron beam melting (EBM) has become a successful approach to powder bed fusion. In contrast to laser-based systems, EBM uses a high-energy electron beam to induce fusion between metal powder particles. In the EBM process, a focused electron beam scans across a thin layer of pre-laid powder, causing localized melting and re-solidification per the slice cross section, Figure 2.5.
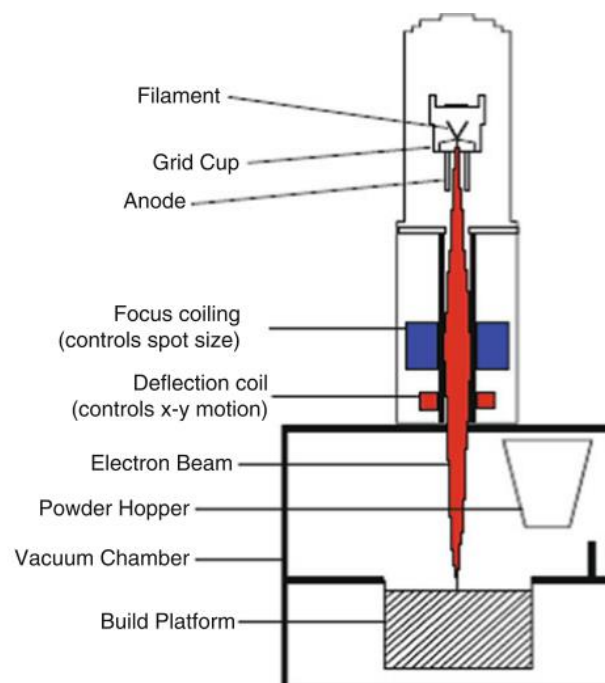

Figure 2.5 Schematic of an EBM apparatus. [33]

The working atmosphere environment is a vacuum for EBM and preheating is one of the key feature. The scan speed is very fast and magnetically driven. It has moderate energy consuming despite almost poor surface finishing. Post surface finishing commonly needs to be done. Resolution of the features medium if we compare to other application such as selective laser melting. Medium powered size commonly is used and it is an advantage or a disadvantage regarding the industry. One of the important consideration is, it can be used only for the metal (conductors) materials. SLM can be defined as powder bed fusion process used to produce objects from powdered materials using one or more lasers to selectively fuse or melt the particles at the surface, layer by layer, in an enclosed chamber [34]. The powder bed is in inert atmosphere or partial vacuum to provide shielding of the molten metal. An energy source (Laser or electron beam) is used to scan each layer of the already spread powder to selectively melt the material according to the part cross section obtained from the digital part model. When one layer has been scanned, the piston of building chamber goes downward and the piston of the powder chamber goes upward by defined layer thickness.
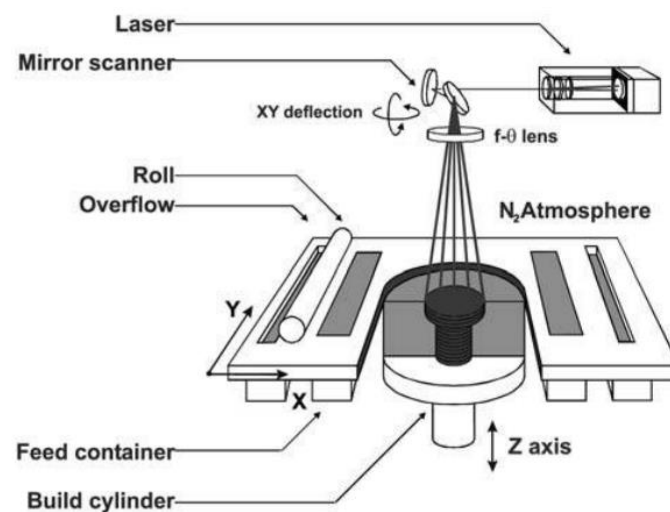
Figure 2.6 Schematic of SLM apparatus[35]

This cycle is repeated layer by layer, until the complete part is formed [36]. The special feature of laser cusing machine is the stochastic exposure strategy based on the island principle. Each layer of the required cross section is divided into number of segments called "islands", which are selected stochastically during scanning, Figure 2.7. This strategy ensures thermal equilibrium on the surface and reduces the component stresses [37].

Figure 2.7 Island hatching principle of printing[38]

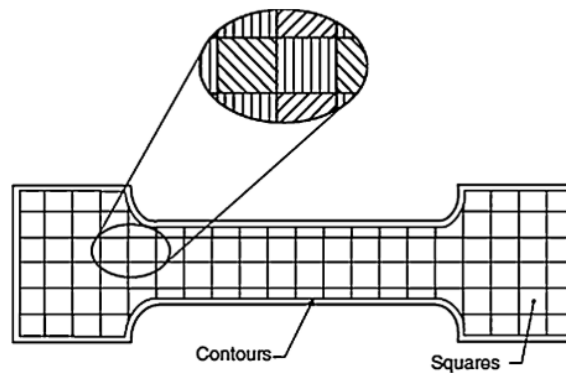Most of these systems use one fibre laser of 200W to 1 KW capacity to selectively fuse the powder bed layer. The build chamber is provided with inert atmosphere of argon gas for reactive materials and nitrogen gas for non-reactive materials. Power of laser source, scan speed, hatch distance between laser tracks and the thickness of powdered layer are the main processing parameters of these application [39]. Layer thickness can be adjusted according to material being used. There is another issue would affect the mechanical performance is melt pool formation. Melt pool size and melt pool depth are a function of absorbed energy density. A simplified energy density equation has been used by numerous investigators as a simple method for correlating input process parameters to the density and strength of produced parts [40].
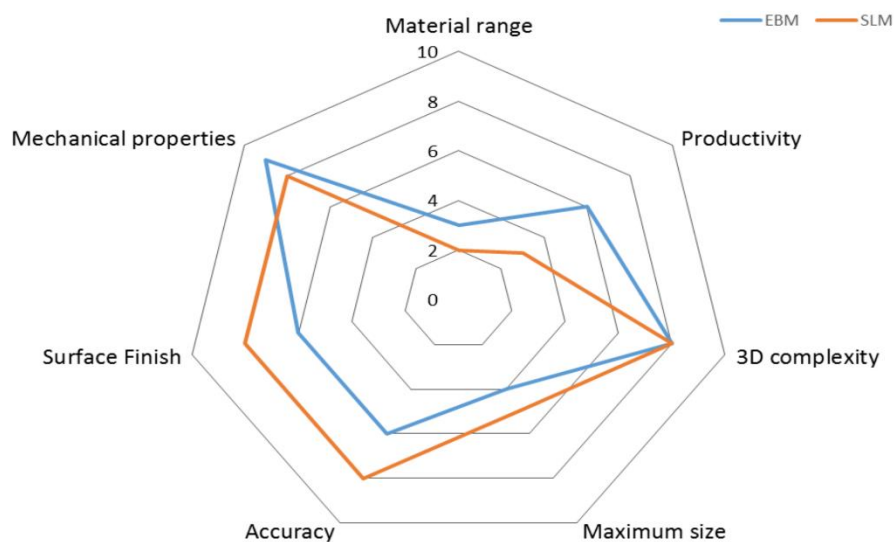

Figure 2.8 Technology comparison – EBM –SLM [41]

Figure 2.8 and Figure 2.9 represent difference between EBM and SLM, as it can be seen that both machines have pros and cons and they could be suitable for the industry they will be used. The major benefit of EBM is, it can create less residual stress due to pre-heating of powder ability which is able to create less thermal gradient. On the other hand, this feature compromises to create small samples or parts since powders are relatively already merged.

$$E_A = P/(UxSP)$$

P	Laser power
U	Scan velocity
SP	Scan spacing between parallel scan lines
E_A	Applied energy density

``	Electron beam melting	Metal laser melting
Thermal source	Electron beam	Laser
Atmosphere	Vacuum	Inert gas
Scanning	Deflection coils	Galvanometers
Energy absorption	Conductivity-limited	Absorptivity-limited
Powder preheating	Use electron beam	Use infrared or resistive heaters
Scan speeds	Very fast, magnetically driven	Limited by galvanometer inertia
Energy costs	Moderate	High
Surface finish	Moderate to poor	Excellent to moderate
Feature resolution	Moderate	Excellent
Materials	Metals (conductors)	Polymers, metals and ceramics
Powder particle size	Medium	Fine

Figure 2.9 Differences between EBM and SLM [27]

2.8 *Application area of AM*

Aerospace industry   Automotive industry   Defense Industry   Medical Industry

Figure 2.10 AM part in different industries [42]

Since there is a several way to create porous structure, application area would be decisive for the method. For instance EBM is able to create the part with less residual stress, however it is struggle to manufacture small component. Lightweight structure could be beneficial for industries such as automotive, aerospace, defence and medical. One of the key benefits of early-stage vehicle design with the assistance of a 3D printer is the ability to start small and scale up rapidly, well before assessment or the part reaches the assembly line [43].Moreover, increases in strength without a corresponding increase in weight could potentially lead to AM even being used to make the body in a while for automobiles in the future. Another advanced material of note is carbon-fibres. Carbon fibres is used to make lightweight auto components such as fenders, car roofs, and windshield frames through conventional techniques. In addition, AM can also provide high strength and lightweight parts. Low density-high strength ratio is not only parameters defence and aerospace industry are seeking, ability of impact performance also is vital. As it is known that porous structure has great energy absorption performance which is suitable for the defence industry. On the other AM has wide range of medical device applications and benefits.

2.9   *Additive manufacturing in medical application*

Medical device industry consist of several classification depending on the time of the medical device being inside the human body and they call; class I, class II and class III medical devices. This consideration may affect the material choose and method because of the living tissue interaction. Since computational tomography technology evolving to get better resolution, AM has taken advantage to create custom made medical device. Commercially available software can provide a solution from CT files to create 3D model nowadays, AM is able to deliver a surface freedom of the design such as suitable body shape or complex bone form. There is also material flexibility for the surgical tool, depending on the application area, parts can be manufactured by metal or plastic. There is a limitation for AM in medical application, it is often necessary to apply post treatment for the parts being developed. Medical device industry is highly regulated environment and limitation comes from the regulation aspects, since AM is still relatively new application. For instance, Custom cranio-maxillofacial implant contains example of generating 3D model from CT documents and AM parts to replace damaged bone section, Figure 2.11. It is quite good example of, how it would be difficult to manufacture lightweight implant such as cranio-maxillofacial with conventional way. It would be time consuming moreover, it would not completely mimic the actual skull shape.

Figure 2.11 Custom Cranio-Maxillofacial implant [44]

As an example, during fracture surgical operation, the medical plate implant or rods get manipulated by the surgeons in order to make their shape more anatomical. AM naturally can deliver the anatomical product which save operational time. 3D printer is also able to provide patient-specific surgical instrument such as femoral cutting block that can save several operation steps and time during the surgical operation of total knee replacement, Figure 2.12.

Figure 2.12 Customised femoral cutting block [45]

2.10   *Porous structure in implant application*

Figure 2.13 shows that mathematical relationship with stress distribution. Regardless of the reputation of the model accuracy, Wollff's methods of analysis express that bone does adapt itself in response to regular loading. Bone response regarding regular load is crucial for bone remodelling and health of the bone. Stress distribution become very vital for trabecular bone and the most commonly excepted criteria for strength of bone. Porous structure tends to provide increased subtract surface that bone cells can grow inside to porous. It increase the

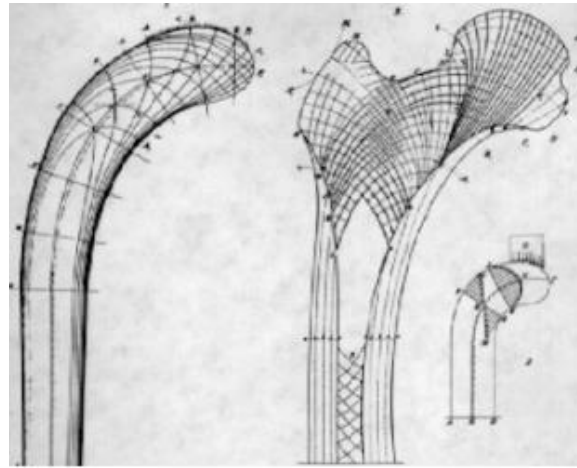bone anchoring. AM also provides low density implant which is suitable for orthopaedic application.

Figure 2.13 Culmann crane diagrams[46]

2.11 *Porous structure stress shielding effects on orthopaedic implant*

Medical implants are able to deliver property of mimicking to damage bone part. Stress shielding or stress protection occurs when the metal implants inserted in-vivo system. Although rigid metal plates stabilize the fracture site, help maintain contact between bone fragments, and allow early weight bearing and patient mobility, the higher stiffness of the implant results in bone loss as a result of decreased physiologic loading of the bone [47]. Stress shielding also reduces the quality of the remaining bone stock leading to a significantly increased risk of fracture and aseptic loosening with revision surgery. This is particularly concerning for the future, as the number of revision implant is projected to rise [48]. Approaches to reduce stress shielding are mainly based on reducing the implant stiffness. Methods to achieve this aim include: modification of the geometric profile of the implant, modification of its material properties, or a combination of both material and geometrical modifications. Geometric modifications include geometric variation of the implant cross section, density [49]. AM can tailor the material stiffness and geometric shape for decreasing stress shielding.

Chapter 3: Aim of the work

Trabecular or porous structures are widely used in the biomedical industry in order to achieve ideal bone integration. The current porous structures are stochastic in principle and used as a surface coating that is based on their manufacturing using plasma spray. Additive manufacturing (AM) is capable to deliver bulk porous structure with controlled geometry. The porous structure consists of elements at the limit of AM accuracy that has not been studied extensively so far. The purpose of this study is to evaluate mechanical properties of trabecular metal structure created by using additive manufacturing technique for orthopedic application. The aim of this study is to test the hypothesis that the AM cellular structure mechanical properties are influenced by open-cell architecture, strut thickness, relative density, and choice of materials.

Specific aims of the study is:

- To determine the size effect of AM small samples on their mechanical properties
- To quantify and explain the effect of post-treatment methods on mechanical properties of AM porous structure
- To assess the role of environmental conditions in the human body on the mechanical behavior of the cellular structure.

To address problems above, hierarchical experimental and theoretical approaches reflecting the porous material structure are introduced within this study.

Chapter 4: Method

4.1   *Mechanical characterization of porous connectors*

The porous structure could be considered as the three-dimensional mesh of interconnecting struts [6]. The mechanical property of the porous construct is given by the geometry of the mesh and by the properties of individual struts and connecting elements [7][8]. There are multiple studies dealing with the effect of mesh geometry on mechanical properties of the porous structure. In these studies, the mechanical properties of the porous material are derived from the unit cell [50][51]. The unit cell intrinsically consists of struts build at various angles and could have also different thickness [12][13]. It was shown that building orientation affects the mechanical properties of AM components [14]. In addition, the small elements produced by AM might exhibit large variation in mechanical properties.

The testing sample size corresponds to the strut size used in porous joint replacement components, Figure 4.1.

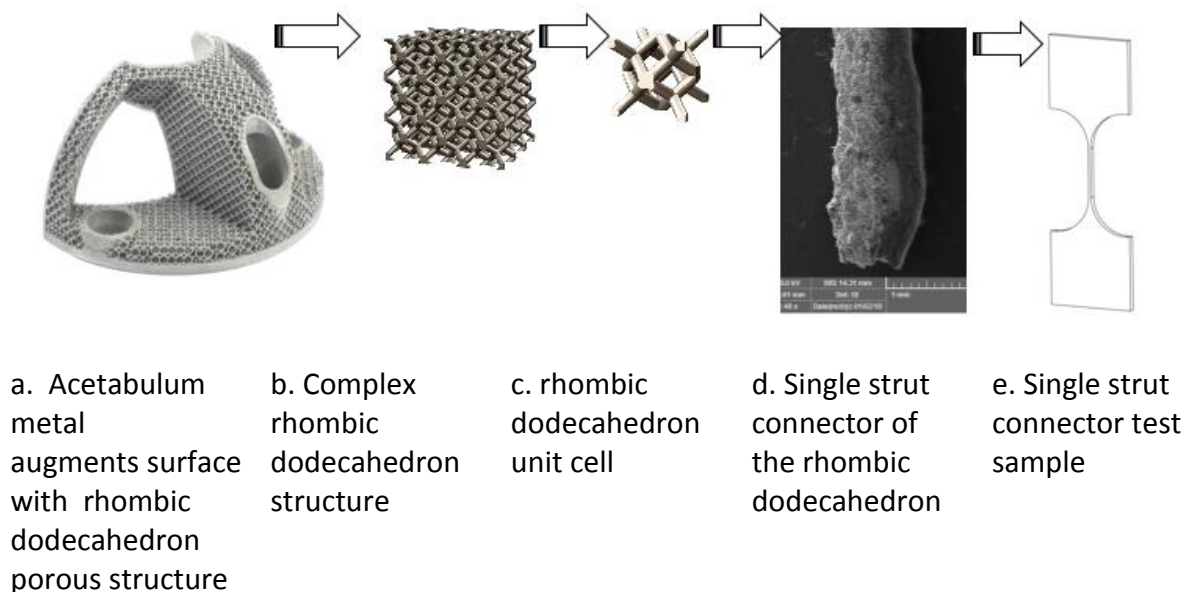| a. Acetabulum metal augments surface with rhombic dodecahedron porous structure | b. Complex rhombic dodecahedron structure | c. rhombic dodecahedron unit cell | d. Single strut connector of the rhombic dodecahedron | e. Single strut connector test sample |

Figure 4.1 Root of single strut application area [52]

The sample were fabricated from Concept laser CP-Ti Grade 2 powder consisting of particles with size ranging from 45 to 100 μm [53]. Chemical composition of raw material is defined in Table 4.1 while the mechanical properties are listed in

Table 4.2. The data are valid for unalloyed CP-Ti according to ASTM F67, while it can been expected that additively manufactured material might have higher yield strength than reference material [54].

Table 4.1 Chemical composition of titanium grade 2 [54]

	C	Fe	O	N	H	Ti
Concept Laser Grade 2 CP-Ti	0,008%	0,03%	0,25%	0,003%	0,00015%	Balance
CP-Ti Grade2, Required	<0,08%	<0,3%	<0,25%	<0,03%	<0,015%	Balance

Table 4.2 Mechanical properties of titanium grade 2 [54]

	Yield Strength (YS)	Ultimate Tensile Strength (UTS)	Elongation	Reduction of Area
Concept Laser Grade 2 CP-Ti	530-570 MPa	600-620 MPa	15-20%	>20%
CP-Ti Grade2, Required	275 MPa	345 MPa	55%	>30%
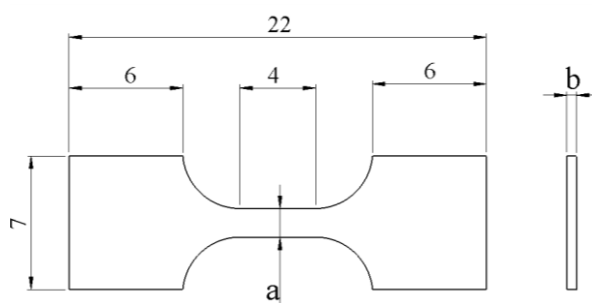
Figure 4.2 Technical drawing of small tensile specimens (mm) [52]

Figure 4.3 Concept Laser M2 SLM machine [55]

The computer-aided design package SolidWorks (Dassault Systemes SolidWorks Corp., Waltham MA) was used to design computer models of the plate tensile specimens (Figure 4.2). The thickness of the samples (b) was designed to be 0.5 mm while the width of the

sample (a) ranged from 0.15 mm to 4.2 mm (Figure 4.4). The designed cross-sectional area has a shape of a rectangle with area ranging from 0.07 mm^2 to 2.10 mm^2.

Additive manufacturing was performed by the Concept Laser the M2 cusing machine (Concept Laser GmbH, Lichtenfels, Germany) that adopts selective laser sintering method. Following parameters were in accordance with manufacturer's recommendation: building chamber is not pre-heated, the laser beam power was 200W, the scan speed was 7 m/s, the layer thickness was 20µm, and the offset distance was 75µm. Concept Laser's patented 'island' scan strategy was applied [56].

Table 4.3 Specimen numbers and orientations

Building orientation	Number of Sample
ZXY	46
YZX	27
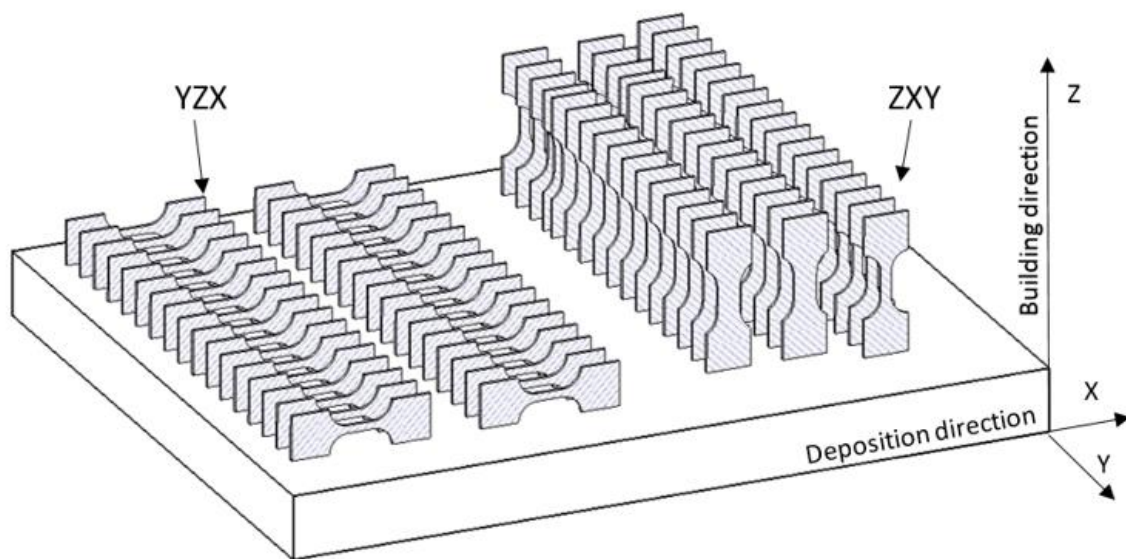
Figure 4.4 Sample printing and deposition direction on the platform [52]

Two orientations of samples with respect to the building direction were chosen. Figure 4.4 describes the orientation of samples. ASTM WK49229 [57] was used denoting the building direction as Z (Figure 4.5a) while the ground plane is denoted as XY (Figure 4.4). The first group contains samples built in a vertical orientation, where the tensile direction (Figure 4.5b) coincides with the building direction (orientation ZXY, Figure 4.4). On the other hand, the tensile direction is perpendicular to building direction in the second group of samples

(orientation YZX, Figure 4.4). The number of samples is shown in Table 4.3. There was not applied post-treatment after the deposition process.

A) Printing direction and building layers   B) Tensile direction and
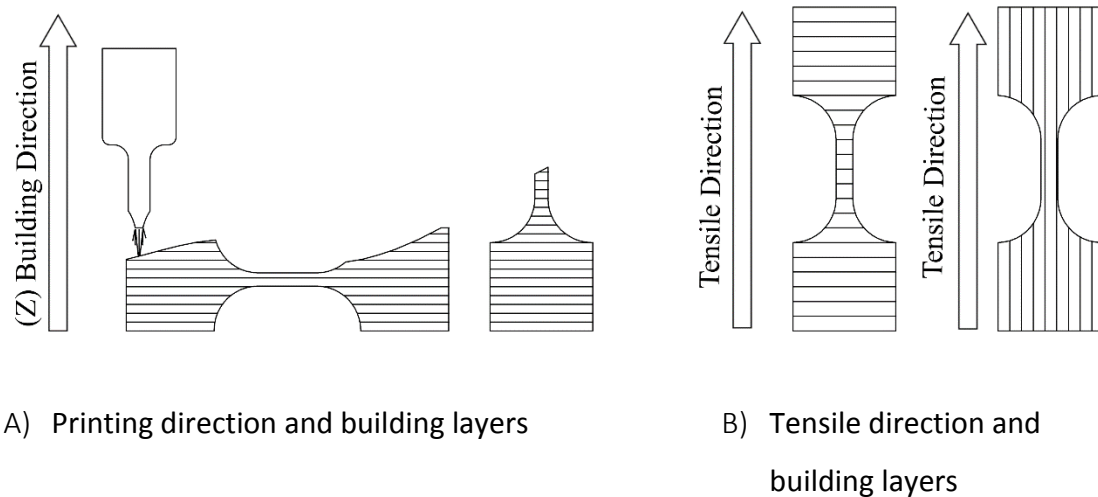   building layers

Figure 4.5 printing and tensile directions [52]

Tensile tests at room temperature were carried out under quasi-static loading conditions. Miniaturized specimens according to Figure 4.2 were tested using a test method based on ASTM E8 [58]. Fixed cross- head velocity was set at 0.2 mm/min. The test specimens' cross-sectional area (So) was measured prior and after the test using stereomicroscope in order to allow subsequent evaluation of tensile test parameters such as yield stress (YS), ultimate tensile strength (UTS), elastic modulus (E) and elongation after fracture (A). Tests were carried out by the small size testing system with the load-cell capacity of 5kN. Longitudinal strain was measured by the digital image correlation (DIC) system Sorbriety (Sobriety, Czech Republic) that was used in 2D set up as the virtual extensometer. The system was calibrated prior each batch. Stochastic speckle pattern was applied to all tensile specimens by airbrush.

ZXY and YZX building orientation surfaces have been investigated with scanning electron microscope (SEM) Tescan VEGA-3 LMU (Tescan, Czech Republic). Geometrical accuracy of additive manufacturing was evaluated using optical 3D coordinate measuring machine RedLux (RedLux Ltd. Southampton, UK). The machine uses confocal probe to map the surface roughness up to ~0.5µm.

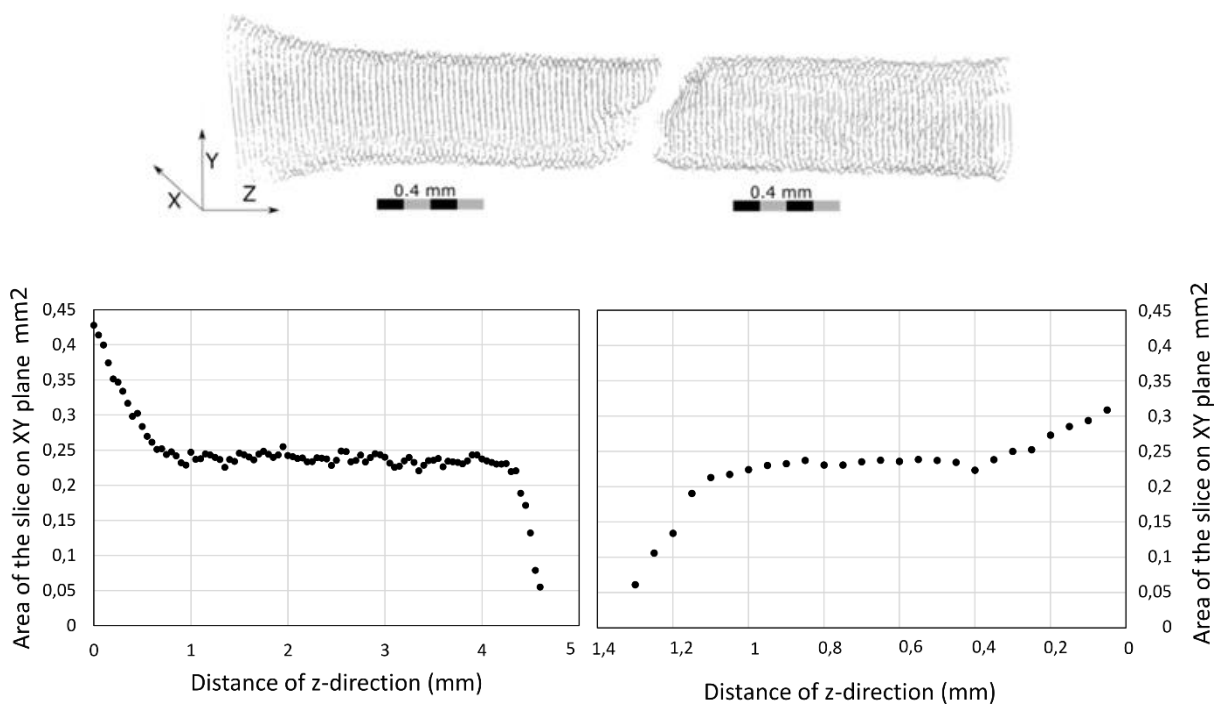Figure 4.6 Micro-tensile Tests Machine [59]

Figure 4.7 the surface scan of the sample fragments obtained after tensile testing, the sample was manufactured in ZXY orientation [52]

Scans were performed in the sample tensile direction with helix track of the confocal probe. The helix pitch was 0.05 mm. The data were projected onto the XY plane, and the cross-section area was estimated by the convex hull using Matlab (Mathworks, Matick, MA, USA),

Figure 4.7 represent the cross-sectional areas of the sample after the tensile testing along the testing direction. The discontinuity in the cross-sectional area corresponds to the fracture.

a) RedLux   Ltd.   b) Point   cloud   of   c) Cross-section area of
   Southampton, UK)   RedLux scan   single strut
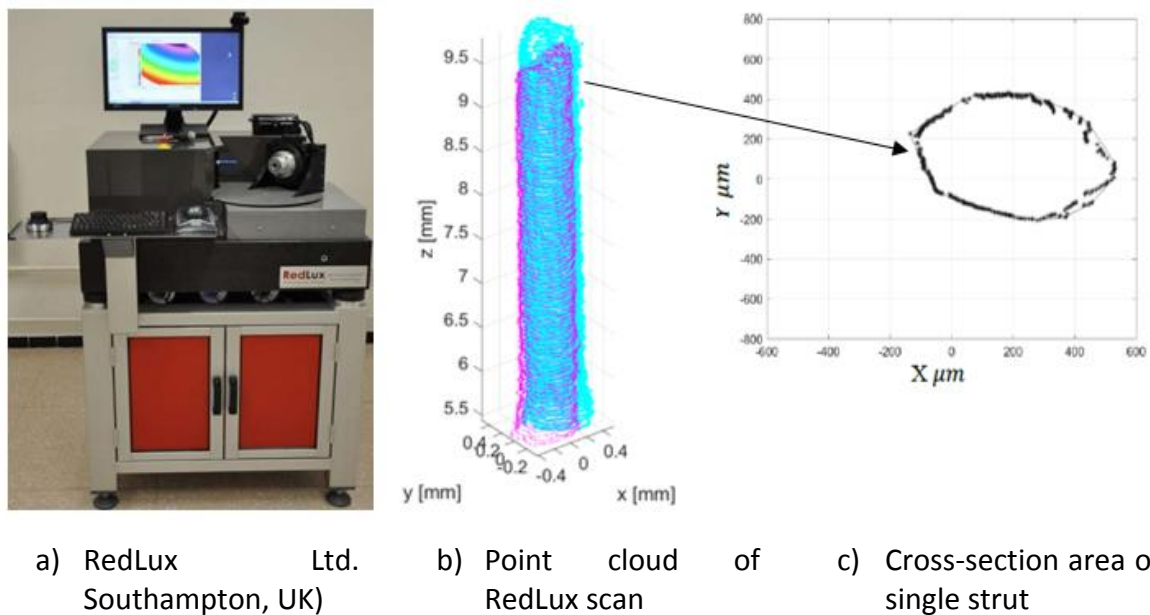
Figure 4.8 RedLux method of geometrical investigation

After the tensile test, the samples were sent to the RedLux measurement. RedLux is non-contact coordinate measuring machine (CMM) which provides 3D capture. It is mounted on an anti-vibration platform, the machine is unaffected by environment and gives on-screen results for analysis as soon as the measurement is completed. The machine has a white light confocal sensor, which allows for analysis relevant surfaces without touching them and therefore potentially affecting the extent of the damage of the small fragile sample [60].

4.2   2D Porous analytic-numeric approach

One of the well-known examples of honeycombs is hexagonal cell. The honeycombs foundation is the idea of porosity structure in two dimension geometry. Therefore, it helps to understand the simplified porosity structure [61].
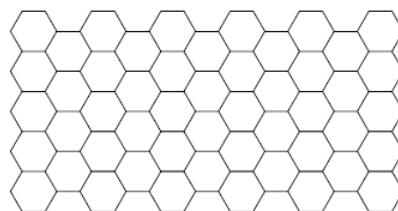

Figure 4.9 Regular Honeycombs [62]

It is considered, three dimensions cellular structure would be defined as a foam shape which consists of interconnected networks like honeycombs [63]. Two typical types of cellular structures can be seen as widely closed and open cell structure. Lightweight structures and compliant mechanisms have been investigated up to now. Cellular mechanisms are designed to transform motions and forces.
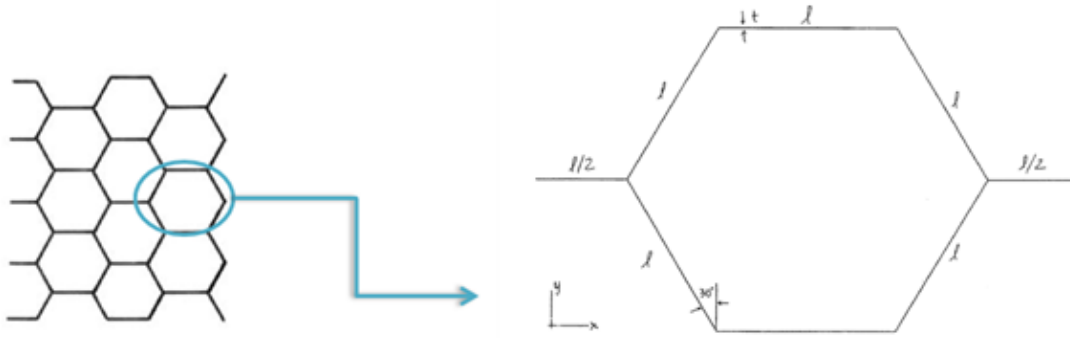

Figure 4.10 Unit honeycomb cell [64]

Unit cell approach one of the technique gives a chance to compare analytic calculation and finite element method. This technique evaluates the computer base calculation because since computational calculation will be used for complex architecture. As it was mentioned that mathematical models of foam have simplified as honeycombs. Therefore, unit-cell is chosen as a hexagonal geometry, Figure 4.10. The elastic modulus for a unit hexagonal cell was calculated with displacement and momentum in order to gain delivered an analytical phrase. For a regular hexagonal honeycomb (Figure 4.10) with linear elastic walls of uniform thickness is t, side length is 1, and elastic modulus is E.

Theoretical calculation of elastic modulus in the plane;

$$\frac{E_x}{E_s} = \frac{E_y}{E_s} = \frac{4}{\sqrt{3}}\left(\frac{t}{l}\right)^3$$

Ex* and EY* are elastic modulus in the x- and y-directions, respectively. The thickness to length ratio, t/l is given as a function of the relative density $\frac{\rho^*}{\rho_s}$ by;

$$\left(\frac{t}{l}\right) = \frac{\sqrt{3}}{2}\left(\frac{\rho^*}{\rho_s}\right)$$

This equation is used by condition under $t/l < 0.2$. Calculation can be only use small t/l values. It was also calculated an analytical expression for the yield strength of a hexagonal unit cell with elastic-perfectly plastic cell walls [65];

$$\left(\frac{t}{l}\right) < 3\left(\frac{\sigma_{ys}}{E_s}\right)$$

Plastic collapse occurs when the bending moment in the cell walls reaches the fully plastic moment. Two moments are balanced, the plastic yield stress of the regular hexagon reduces to;

$$\frac{\sigma_x}{\sigma_s} = \frac{\sigma_y}{\sigma_s} = \frac{2}{3}\left(\frac{t}{l}\right)^2$$

In order to reach analytic calculation results, wall thickness, relative density, wall length elastic modulus are defined as;

$E\_x/E\_s = E\_y/E\_s = 4/\sqrt{3}\ (t/l)^{\wedge}3$

$\sigma\_x/\sigma\_s = \sigma\_y/\sigma\_s = 2/3\ (t/l)^{\wedge}2$

In order to find elastic modulus components, x and y directions.

Wall thickness (t)
Wall length (l) $\Big\}$ $t/l = 0.13$

Relative density,
Elastic modulus (E) $\Big\}$ $\rho^{\wedge}*/\rho\_s = 0.15$
                              $E=1$
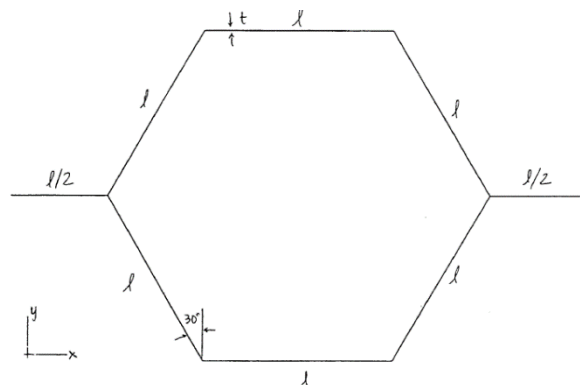
Unit hexagonal honeycomb finite element calculation is carried out with Abaqus (Hibbitt, Karlsson, & Sorensen, Inc., Pawtucket, RI) software. Each network wall defines as a beam (According to Timoshenko Beam Theory). Therefore, Beam was decided as B22 mesh element. Abaqus input file (Inp.) was prepared by AutoCAD software (Autodesk, San Rafael, CA) and design as a regular hexagon and exported to dxf. file format for "gCAD3D" software that would help to transform dxf. file to Inp. file.
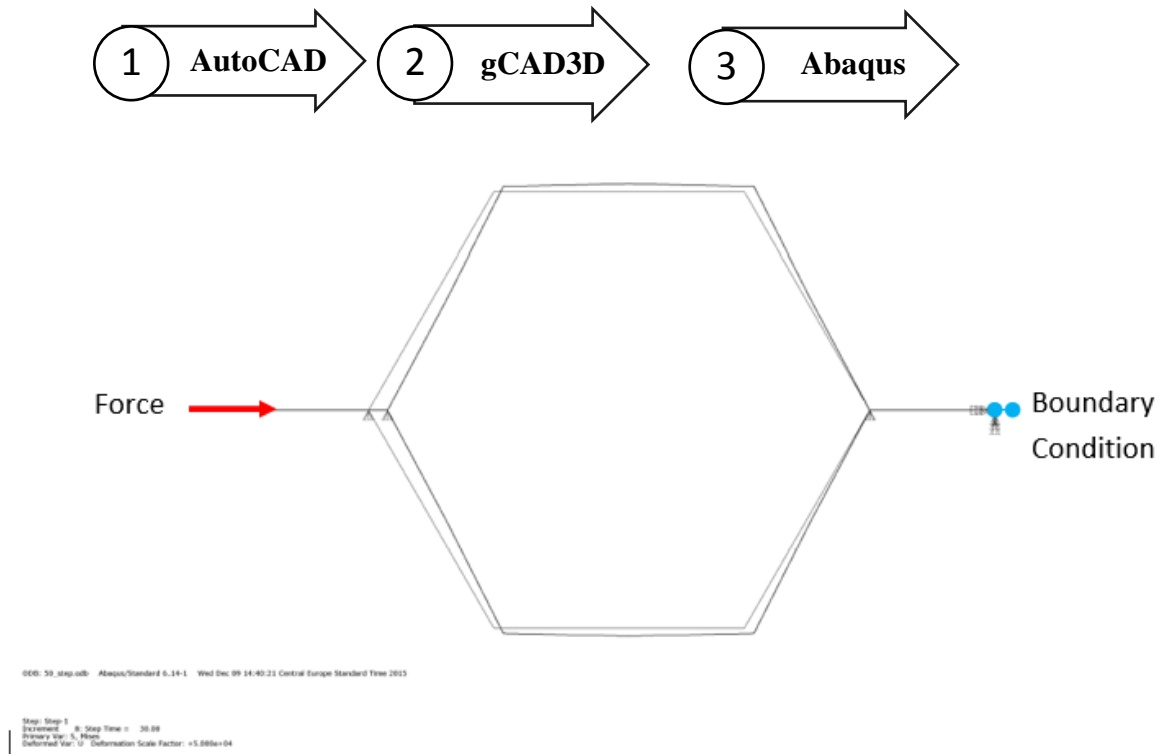
Figure 4.11 Unit honeycomb cell deflection results in Abaqus [64]

In order to reach x-direction of elastic modulus, the force was applied in x-direction, Figure 4.11, and boundary condition was applied at the end of the regular hexagonal honeycomb.
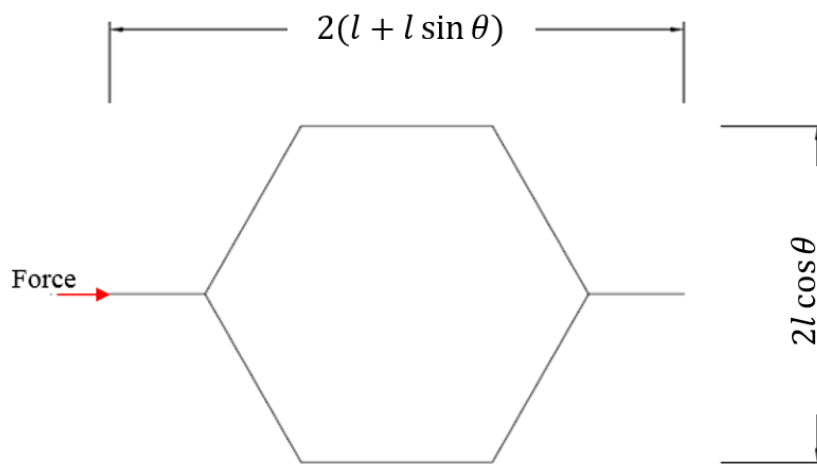

Figure 4.12 Regular hexagonal honeycombs general dimensions [64]

Stress [x-direction]------------------------------------- $\sigma_x = \dfrac{F_x}{2blcos\theta}$

Strain [x-direction]------------------------------------- $\varepsilon_x = \dfrac{U_x}{2(l + lsin\theta)}$

Stress, strain, and x-direction of elastic modulus components were calculated by using reaction force and displacement. The first equation gives us a stress contribution of x-direction and the second equation explain strain in the x-direction. Therefore, x-direction of Young modulus can be calculated by using the conventional following equation;

$$E_x = \frac{\sigma_x}{\varepsilon_x}$$

4.3   *2D Complex honeycombs approach*

Printed material is considered as a perfect condition however, some of the network components might not be welded or laser beam may miss the powder target. Moreover, the path of the software sometimes can fail to complete the hatching target. Following calculation shows that the concept of regularity and network reduction results. Developing new approach under different circumstances in order to understand simple 2D porosity structure may help to carry out complex 3D models by reducing the computational cost.

It was defined previously, regular honeycombs determined according; t/l=0.13, E=1 and γ=0.3 condition. Moreover, all structures have 5 hexagonal cells of rows and 11 hexagonal cells of columns. Figure 4.13 illustrates general features.
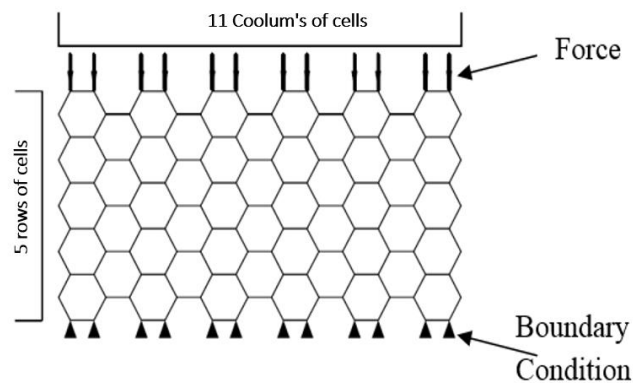

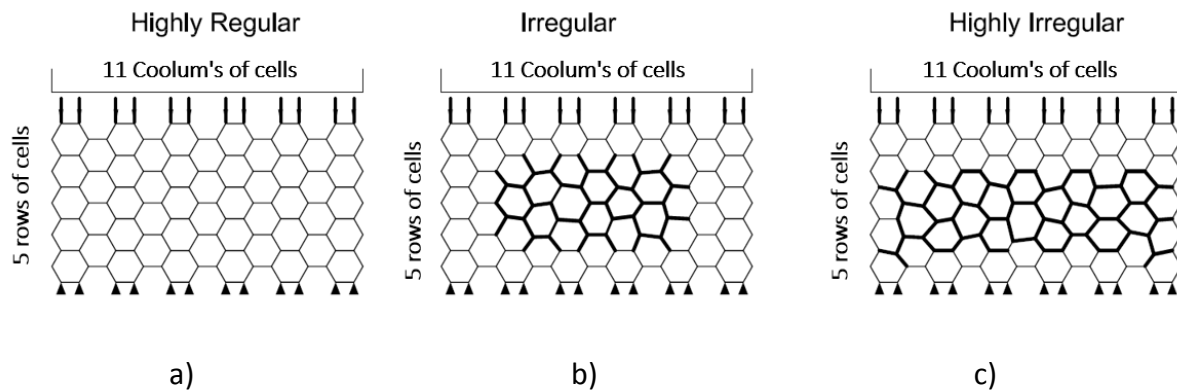Figure 4.13 Regular hexagonal honeycombs [64]

Figure 4.14 a) Regular b) Irregular c) Highly Irregular hexagonal honeycombs [62]

Figure 4.14 shows that three types of structure were investigated in order to understand different mesh architecture results. Bold network lines represent modifications, struts thickness-length ratio was changed. Therefore, the highest Von Misses stress distribution location were changed and adjusted due to the stress flow diagram.
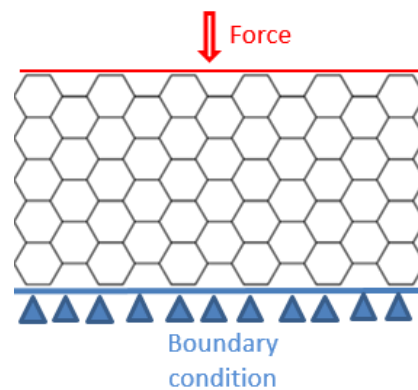

Figure 4.15 Force and boundary condition definition [64]

Figure 4.15 illustrates the boundary condition which was defined as no displacement and torsion, the applied force was decided in the static test condition. During the investigation, B22 beam structure was used for FEM calculation.
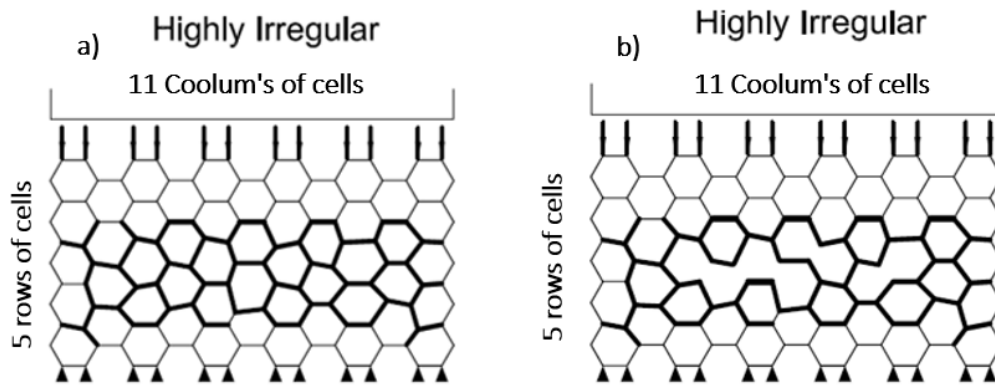
Figure 4.16 a) ''Highly Irregular'' and b) ''Highly Irregular network reduction'' hexagonal honeycombs with network reduction [64]

Figure 4.16 illustrates irregular 2D and connector reduced 2D structure. 3D printer is not always able to create perfect geometry and there will be some of the missing network components or the connectors may be failed in time under the repetitive load. Therefore, those missing network components may lead to high-stress concentration on different location. Moreover, this simplified concept gives us a chance to understand the behaviour of cellular structure.

4.4   *Mechanical response of CP-Ti porous structure under compressive loading*

Commercial implants with porous architecture are supposed to deal with compression load commonly in vivo environment.
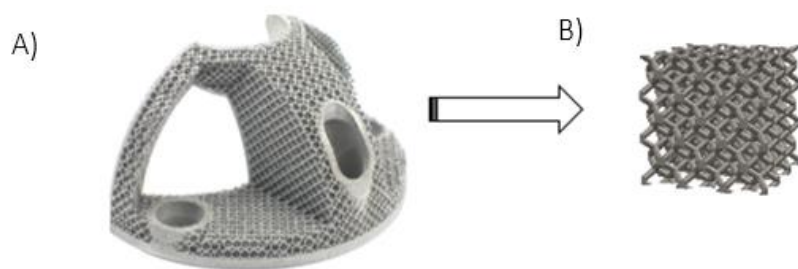
(A) Acetabulum metal augments implant surface with rhombic dodecahedron porous structure

(B)   Complex   rhombic   dodecahedron structure

Figure 4.17 Origin of the application area of cubical porous structure [66]

The samples were fabricated from Concept Laser CP-Ti Grade 2 powder consisting of particles with size ranging from 45 to 100 µm [53]. The data are valid for unalloyed CP-Ti according to ASTM F67, while it can be expected that additively manufactured material might have slightly higher yield strength than the reference material [54]

The computer-aided design package SolidWorks (Dassault Systemes SolidWorks Corp., Waltham MA) was used to design computer models of the cubical specimens. Connector struts thickness were set with 0.3 mm. Unit-cell was set as 2 mm. Relative density is 20%.

Figure 4.18 SLM chamber of cubical sample manufacturing

Additive manufacturing was performed by the M2 cusing machine (Concept Laser GmbH, Lichtenfels, Germany) that adopts selective laser melting method. The process parameters were in accordance with manufacturer's recommendation: building chamber was not pre-heated, the laser beam power was 200 W, the scan speed was 7 m/s, the layer thickness was 20 µm, and the offset distance was 75 µm. Concept Laser's 'island' scan strategy was applied [56]. No post-treatment was applied after the deposition process.

The experiment has been carried out in Czech Technical University laboratory. Materials-testing machine MTS 858 Mini Bionix (MTS, Eden Prairie, USA) was used. 2500N load cell has been used, 15 samples were used for test. Although samples were designed as 6x6x6 mm in CAD environment, manufactured samples dimensions were slightly different than CAD. We set the experiment in loading direction parallel to building direction. Cross-section area was predefined parallel to building platform.
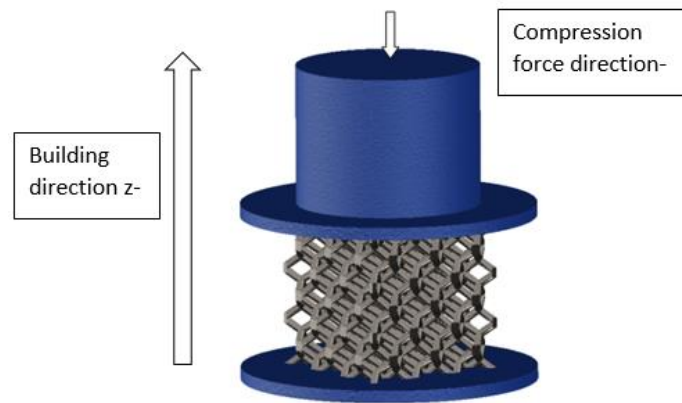
Figure 4.19 Building and compression force direction

Cross section area was design as 36 mm² however, manufactured part contains 40.4165 mm² mean value and the standard deviation is 0.3502 mm². All the pre-test measurements were done with digital micrometer. The mean height of the cubical samples is 6.0697 mm and the standard deviation is 0.01 mm.
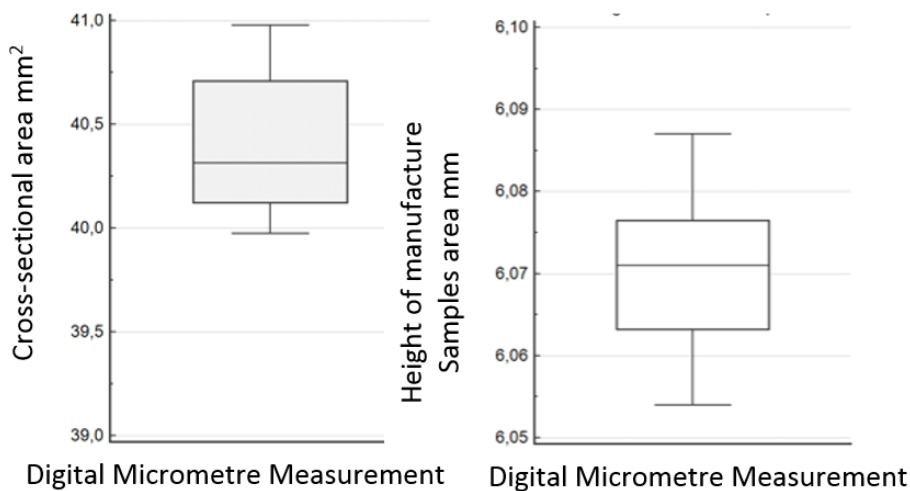

Figure 4.20 additively manufactured cross-sectional area and height result for 15 samples

There is 12.2% mean error on the cross-section manufacturing. Nevertheless, there is only 1.16% mean error occurred in terms of the height of manufactured parts. The cross-sectional error is vital for stress calculation since mechanical compression test was carried out according to ISO 13314 (Mechanical testing of metals-ductility testing-compression test for porous and cellular metals)[67]. Static test was run in 80 seconds for each sample and it was

aimed at 50% compression deformation. 20%-70% loading-unloading slope was applied in order to identify elastic gradient.
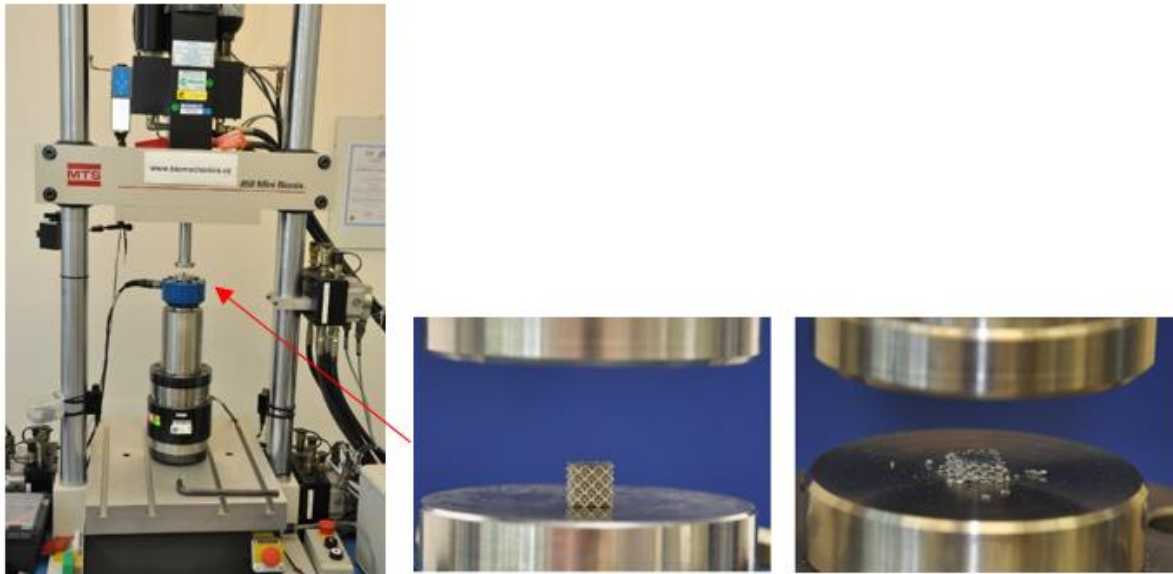

Figure 4.21 Compression testing set-up

Figure 4.21 shows the illustration of sample placing into the testing machine. After running test, the sample platform was cleaned and maintained smooth surface for next sample. Each samples has an identical bag and initial for traceability for further investigation.

Figure 4.22 Traceability and storing samples after and before compression test

Compression test of the porous structure is vital for the validation of the application area such as acetabulum cup, Figure 4.17. It is known that orthopaedic implant such acetabulum cup is supposed to deal with compression stress often. Although it has to bear with the static and dynamic load. It was tested in the experiment only static approach. But it should be considered that the same structure also face with dynamic load during its application.

4.5   *Surface treatment effect on mechanical response of TILOP porous structure*

manufactured by SLM

Our previous study shows that surface may affect the performance of individual mechanical response. Moreover, the surface of the individual connectors contains un-melted powder particles which will contact with living tissue [68]. The increasing use of orthopaedic implants and, in particular, of hip and knee joint replacements for young and active patients, has stimulated interest and concern regarding the chronic, long-term effects of the materials used.

In this study, samples were fabricated with TILOP pure titanium (OSAKA Titanium Technologies Co., Ltd., Japan) which is titanium with low oxygen powder. Oxygen level effects on the metallurgical properties of the powder and eventually its mechanical performance [69]. Since TILOP powder has homogenous spherical particles, it was expected a good mechanical response. The computer-aided design package SolidWorks (Dassault Systemes SolidWorks Corp., Waltham MA) was used to design computer models of the cubical specimens. Connector struts thickness were set with 0.3 mm. Unit-cell diameter was set as 2 mm. Relative density is 20%. Porous samples were designed with 6x6x6 mm cubical structure. Additive manufacturing was performed by the M2 cusing machine (Concept Laser GmbH, Lichtenfels, Germany) that adopts selective laser melting method. The process parameters were in accordance with manufacturer's recommendation: building chamber was not pre-heated, the laser beam power was 200 W, the scan speed was 7 m/s, the layer thickness was 20 μm, and the offset distance was 75 μm. Concept Laser's 'island' scan strategy was applied [41].
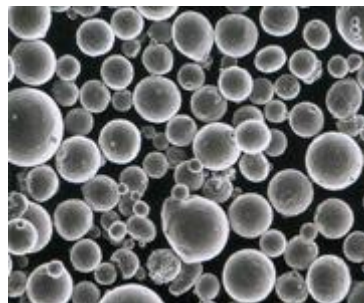

Figure 4.23 TILOP (Gas-atomized titanium powder) [70]

Surface treatment was carried out at the Department of Metal and Corrosion Engineering UTC Prague. The samples diameters were decreased in ethanol in ultrasonic bath for 5 minutes

prior etching. After surface eroding, samples were etched for a selected time (3 min or 6 min) in mixture of 20 ml HF, 200 ml HNO3 and 780 ml demineralised water. Specimens were after that washed by demineralised water and dried in air steam. The thickness of the beam was evaluated from SEM images in image software. 45 struts were measured for each group for statistical distributions.

Cross section area of porous samples was design as 36 mm^2 however, SLM accuracy may manufacture components slightly different than design parts. Strut thickness can also effect on the diameter of cross-sectional area of the sample.

Table 4.4 Strut thickness regarding post treatment

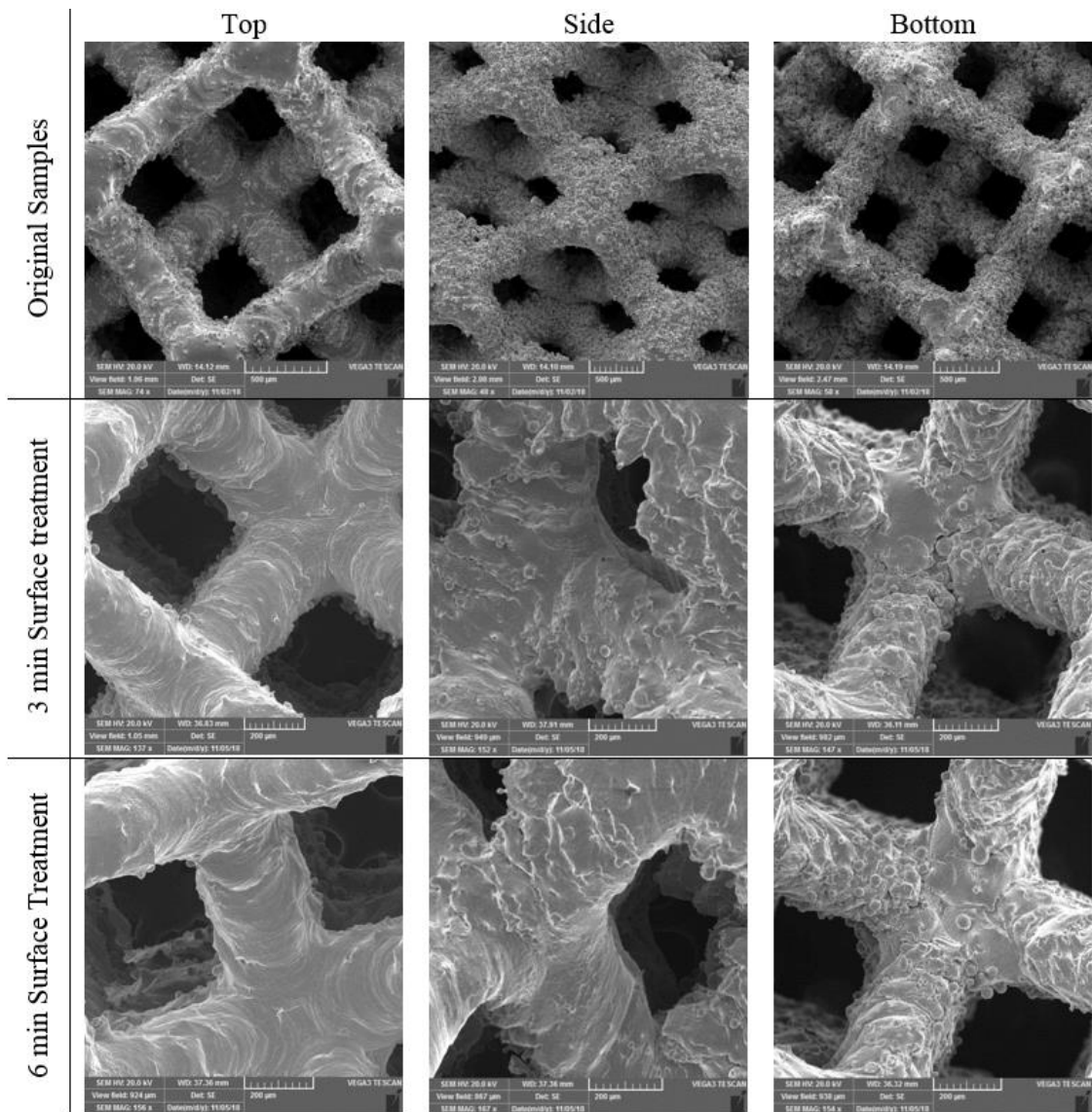|	As-built	With 3-minute surface treatment	With 6-minute surface treatment
Single strut thickness	380 ± 20 mm(*0.001)	323 ± 18 mm(*0.001)	297 ± 16 mm(*0.001)

Figure 4.24 Rhombic dodecahedron connectors surface quality after acid treatment

Figure 4.24 shows the surfaces after etching treatment. Surface treatment can clear the spikes on the surface which may reduce a notch effect. Connector struts mechanical performance will be decreased since the diameter change. The diameter of struts can affect density and diameter of cross-sectional area.

Samples area divided within to the groups according to the post-treatment process. Table 4.5 represents the sample description and codes.

Table 4.5 Sample groups and description

Group No	Sample description	Sample Code	Sample No
Group 1	3 min surface treatment	PT3S_1	1
		PT3S_2	2
		PT3S_3	3
Group 2	6 min surface treatment	PT6S_1	4
		PT6S_2	5
		PT6S_3	6
Group 3	As-built	PTWT_1	7
		PTWT_2	8
		PTWT_3	9
		PTWT_4	10
		PTWT_5	11

Table 4.6 Cross-sectional area results of rhombic dodecahedron samples

	3 min surface treatment PT3S	6 min surface treatment PT6S	AS built PTWT
Cross-sectional area of rhombic dodecahedron	36.32 ± 0.12 mm^2	35.83 ± 0.09 mm^2	36.76 ± 0.15 mm^2
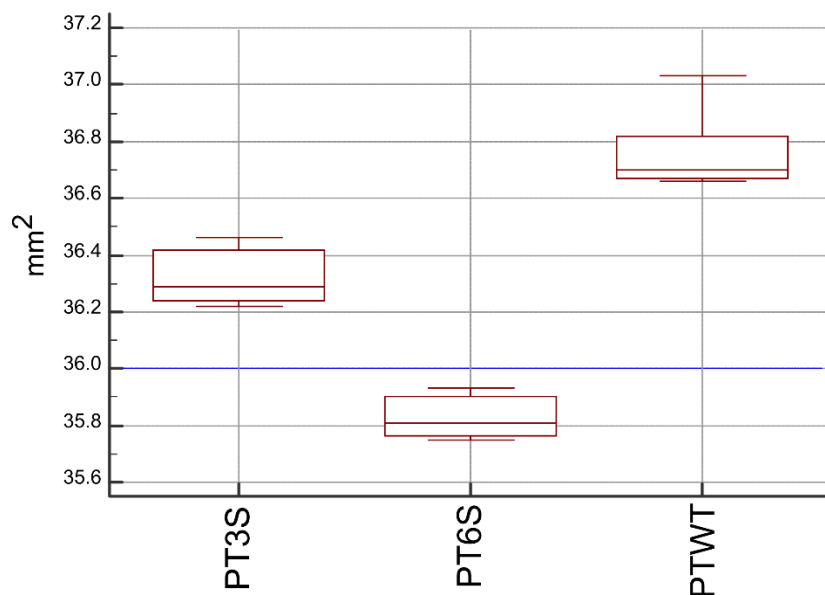
Figure 4.25 Porous sample Cross-sectional area measurement

Table 4.6 shows that cross-sectional area can be depended on the treatment method. Measurement of cross-sectional area was done with digital micrometre. Surface treatment can decrease the cross-sectional area up to 2.5% which may affect mechanical response.

The experiment has been carried out in Czech Technical University laboratory. Materials-testing machine MTS 858 Mini Bionix (MTS, Eden Prairie, US) was used. 500N load cell has been used and each static test took approximately 80 seconds. Mechanical response parameters were calculated according to ISO 13314 (Mechanical testing of metals-ductility testing-compression test for porous and cellular metals)[67]. Elastic modulus was calculated from 30% and 70% loading and unloading slope from the stress-strain diagram.

4.6   *Mechanical response of Titanium alloy porous samples with HIP and surface treatment*

The longevity of joint replacements can be increased with improving bone anchoring [3]. Solid titanium alloys genially are stiffer than bones and this mechanical mismatch could lead to bone ingrowth, lack of bone resorption and eventually loosening of the orthopedic implant [71][72][73]. Regardless of titanium' good mechanical response, it also has outstanding resistance to corrosion [11]. Cleaning of un-melted titanium particles from porous implant surface is considered as a crucial. Titanium porous structure failure in the human tends to realize particles which can create concern regarding long term metabolic, oncogenic and immunologic effects[17][18][19].

In this study, titanium alloy powder (CL 41TI ELI) has been used during selective laser melting (SLM) operation which is widely used AM methods for creating arbitrarily complex and predictable porous 3D structures [15][16]. Cubical testing samples design was selected from commercially available acetabulum augments implant, and unit cell architecture was chosen rhombic dodecahedron, Figure 4.26. During the investigation, samples have grouped according to their post-treatment method. In order to achieve a better mechanical response, hot isostatic pressing (HIP) operation was applied to a group of samples. Identify to cleaning effect on mechanical properties and geometry, surface etching method was carried out for as-built and HIP treated samples.

Figure 4.26 (A) Acetabulum metal augments implant with rhombic dodecahedron porous structure surface and (B) Rhombic dodecahedron cubical element [66]

The Samples were manufactured from Consept Laser titanium alloy grade 23 (CL 41TI ELI) powder [74]. The computer-aided design package SolidWorks (Dassault Systemes SolidWorks Corp., Waltham MA) and Materialise/Magics (Magics - Leuven, Belgium) software were used to design computer models of cubical samples. Dimensions of cubical sample were set 6 mm, and 2 mm rhombic dodecahedron open unit-cell was used, Figure 4.27. Relative density was defined 20% due to strut thickness which was 0.3 mm. The rhombic dodecahedron unit cell consists of 12 identical rhombic faces with 24 edges and 14 vertices [11].
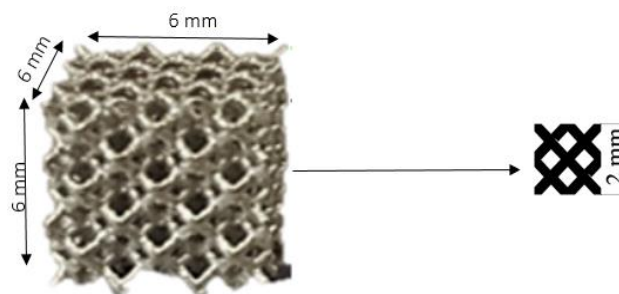
Figure 4.27 Compression samples dimension [66]

M2 cusing machine (Concept Laser GmbH, Lichtenfels, Germany) that adopts selective laser melting (SLM) method was used for additive manufacturing performing. SLM process was carried out with manufacturer's recommendation; building chamber was not pre-heated, the laser beam power was 200 W, the scan speed was 7 m/s, the layer thickness was 20 µm, and the offset distance was 75 µm. Concept Laser's 'island' scan strategy was applied [56]. Furthermore, surface etching and hot isostatic pressing (HIP) were applied to some groups of

samples. The surface etching was aiming the decreasing surface roughness and reducing partly melted powders. Surface treatment start with 5 minutes prior etching in ethanol in ultrasonic bath. After removing certain level of particles on the surface, samples were etched for a selected time (3 minutes or 6 minutes) in mixture of 20 ml HF, 200 ml HNO3 and 780 ml demineralised water. Specimens were washed with demineralised water (in US bath) and dried in air steam. The thickness of the connector struts was evaluated from scanning electron microscope (SEM) Tescan VEGA-3 LMU (Tescan, Czech Republic) with ImageJ software. Hot isostatic pressing (HIP) was carried out at Bodycote Bourgogne (Bodycote HIP Ltd.). HIP was followed through with high-pressure argon gas (1020 bars) and steady high temperature (900 °C). The applied pressure was isostatic due to argon gas which helps to develop a decreasing internal defect. First of all, samples were heated up to 900 °C in 5 hours then they spent 4 more hours at the set temperature with steady isostatic pressure. Afterward, specimens were cooled down slowly to room temperature, the cooling process also took 5 hours. Samples were divided into 6 groups according to post-treatment method and each group contains 4 samples, Table 4.7.

Table 4.7 Sample description and group definition

Group code	Name of the group
SNHHTNS	Sample No Heat, HIP and surface treatment
SWHIT	Sample with HIP treatment
SWS3T	Sample with Surface treatment 3 min
SWS6T	Sample with Surface treatment 6 min
SHITS3T	Sample with HIP treatment with surface treatment 3 min
SHITS6T	Sample with HIP treatment with surface treatment 6 min

Two types of geometrical measurement was done in order to identify geometrical accuracy and effect of post-treatment. Connector strut thickness measurement was done in order to identify the surface treatment effect on the connector diameters. The strut thickness measurement was realized on two samples with at least 45 measurements on each. This approximately corresponds to two measurements on every strut. The results are presented as mean ± standard deviation.

Mechanical compression test was carried out with MTS 858 Mini Bionix testing machine (MTS, Eden Prairie, USA) with 5 KN load cell. The loading speed was set at a constant of 0.1 mm/min, it aims to maintain a constant strain rate according to ASTM E9. The deformation was measured with the linear variable differential transformer (LVDT) and elastic gradient was calculated as the slope of the stress-strain curves between 30% and 70% of the plateau strength according to ISO 13314). 0.2% offset method was used for determining the compressive proof stress and maximum first strength was obtained from the diagram.
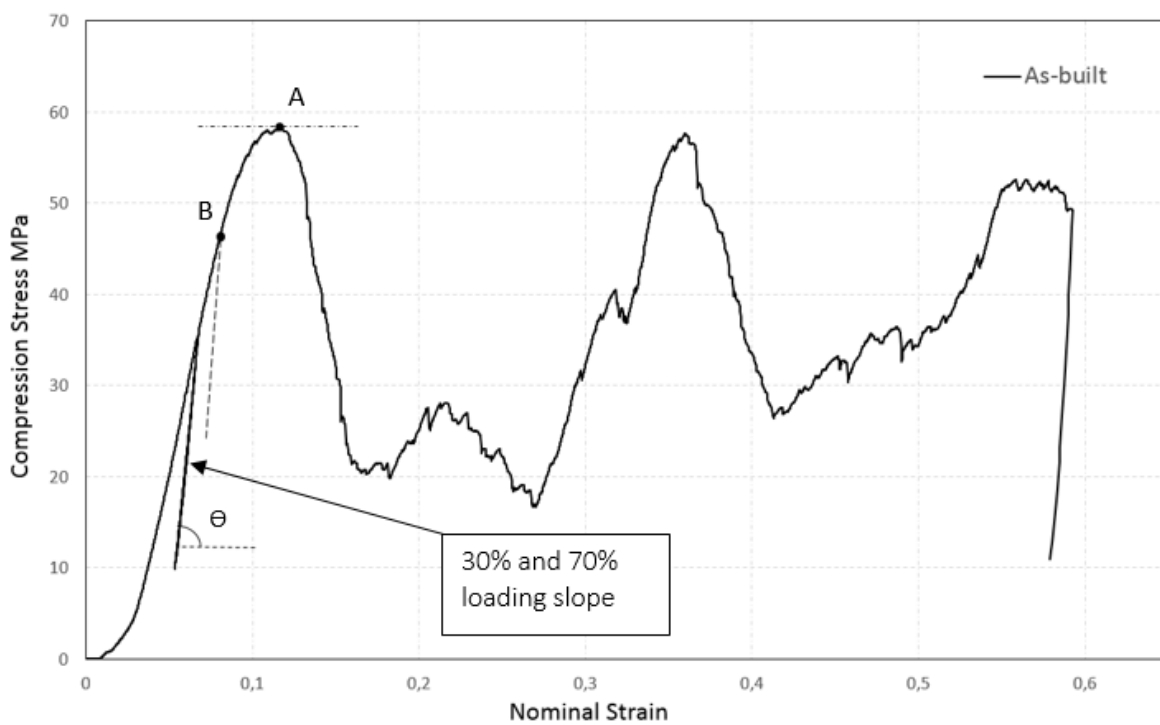
Figure 4.28 Compression test stress-strain diagram according to ISO 13314. Elastic gradient tangent of ''Θ'', ''B'' is 0.2% offset compressive proof stress and '''A'' is maximum first strength [66]

Implants with porous structure such as acetabulum cups are supposed to handle compression strength often. Deformation of the open-cell structure may affect bone attachment in the long term [75]. Porous structure mechanical performance can be improved by post-treatment and it may also help in-vivo response.

4.7   *3D porous structure analytic approach*

Open cell rhombic dodecahedron has orthotropic behaviour and material properties are affected by the bending of the edges. The material definition could play a vital role for determining mechanical response assumption.

Mechanical tests were carried out with rhombic dodecahedron 2 mm unit-cell and 20% density. Strut connectors were adjusted 0.3 mm thickness by defining according to density. The analytic calculation is also calculated with the same condition with mechanical test in order to compare mechanical test results.
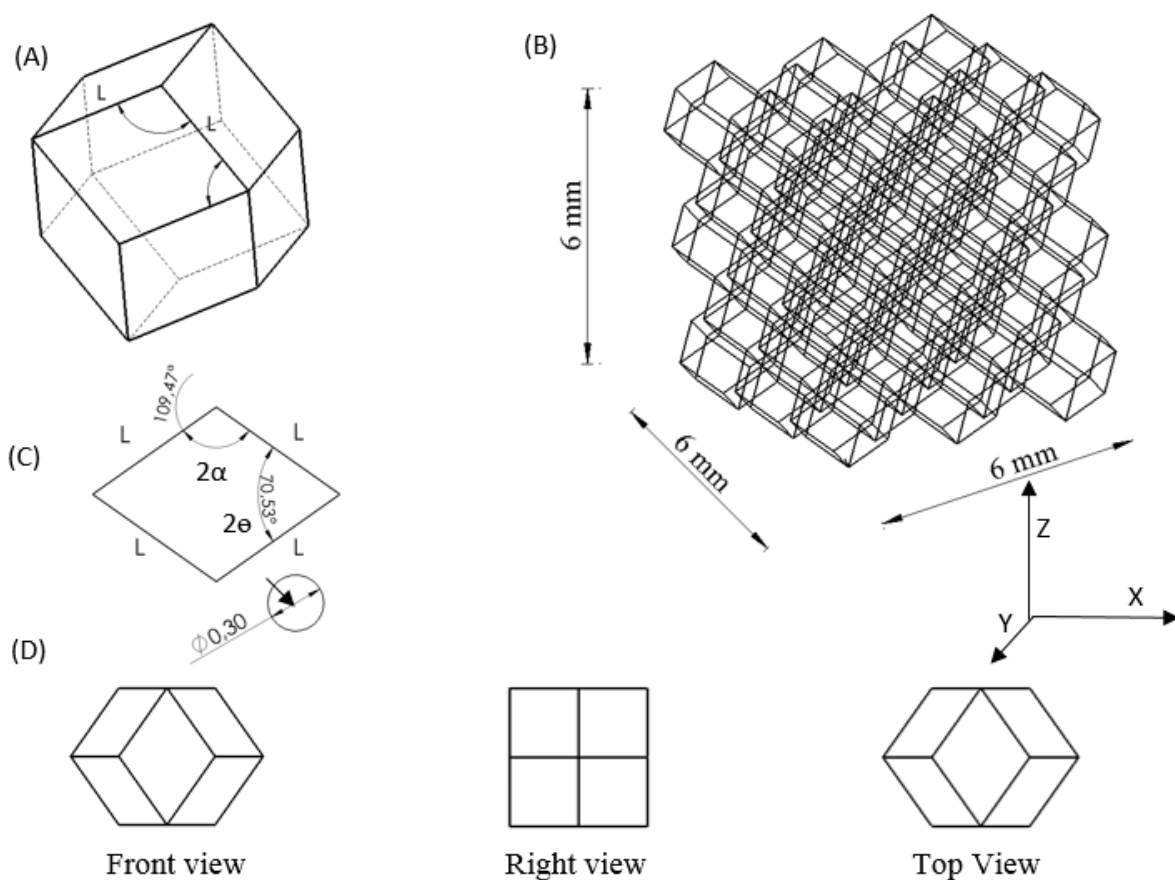
Figure 4.29 Schematic of a regular rhombic dodecahedron structure. (A) Rhombic dodecahedron unit cell comprises 12 identical rhombuses, (B) tessellated rhombic dodecahedron cellular structure with 27unit cells, (C) unit cell 12 identical rhombuses, with edge length [76]

The unit cell of the rhombic dodecahedron consists of 12 identical rhombic faces with 24 edges and 14 vertices. Each face of a rhombic dodecahedron is a rhombus, with 2α= 70.53°

and $2\theta= 109.47^\circ$. Strut shape is circular and thickness is 0.3 mm. For a 3-D rhombic dodecahedron cellular structure of infinite size, each cell edge is shared by three adjacent unit cells, so the effective relative density of a 3-D tessellated cellular structure denoted $\rho = (3\sqrt{3}/2)\pi(r/l)^2$. The cell edge material behaviour was taken as plastic, and comprised the elastic modulus, E_s.

Table 4.8 Rhombic dodecahedron formulas

Relative density formulas [77]	$\rho = \frac{3\sqrt{3}}{2}\pi\left(\frac{r}{l}\right)^2 - \frac{27\sqrt{2}}{4}\pi\left(\frac{r}{l}\right)^3$
Analytical elastic modulus [78]	$\dfrac{E_1}{E_s} = \dfrac{E_2}{E_s} = \dfrac{27\dfrac{sin\theta}{sin2\theta}}{\dfrac{3l^4}{\pi r^4} + \dfrac{18l^2}{\pi r^2}}$ $\dfrac{E_3}{E_s} = 9\pi\, r^4\, \dfrac{cos\,\theta}{2l^4\,sin^2\theta} \qquad \theta = 54.73^\circ$
Analytical yield stress modulus [77]	$\dfrac{\sigma y_1}{\sigma y_s} = \dfrac{\sigma y_2}{\sigma y_s} = \dfrac{3\sqrt{6}}{8}\left(\dfrac{b}{l}\right)^3$

Relative density could be depending on the unit-cell type open or close. Moreover, in this research open cell structure have been investigated. Connectors thickness or size of the unit cell affect directly to relative density. The volume of structure is occupied by the connectors and corners. Therefore, the relative density function of total struts per volume.

NOMENCLATURE

r	Radius of the struts	m
l	Length of the struts	m
A	Cross-sectional area of the struts	m^2
θ	the main angles of rhombus faces in a rhombic dodecahedron unit cell	degree
ρ	Relative density, dimensionless	
b	Side dimension of the strut	m
E_s	Elastic modulus of the bulk material	Pa
E	Elastic modulus of the unit cell	Pa
σ_Y	Yield stress of the porous structure	Pa
σ_{Ys}	Yield stress of the bulk material	Pa

It can be assumed that 3D rhombic dodecahedron mechanical response could be calculated by 2D honeycombs approach. Connector can be calculated as a beam. This approach will be used for FEA verification.
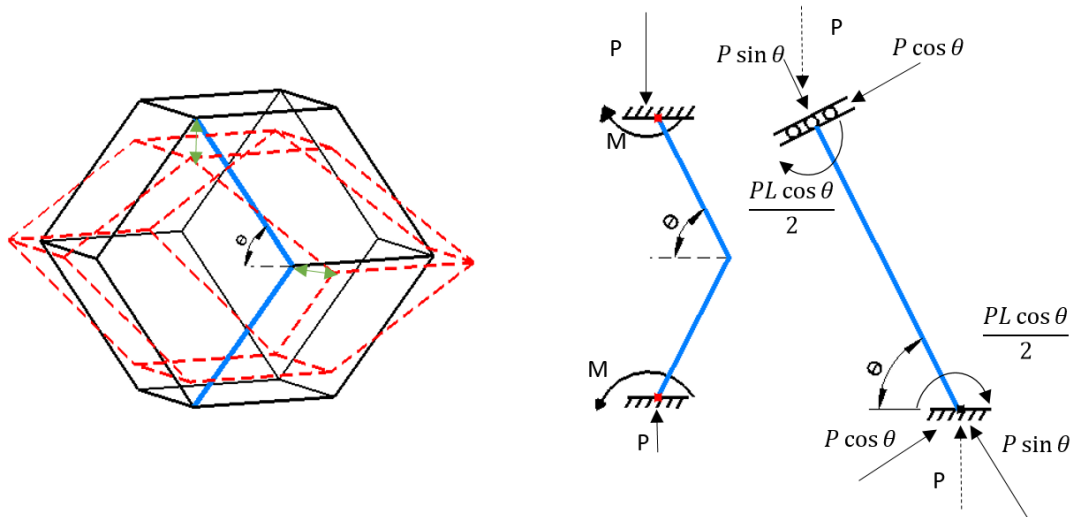

Figure 4.30 Schematic of a rhombic dodecahedron unit cell under uniaxial compression. The deformed and un-deformed shapes are shown by dashed and solid lines. Uniaxial compression in direction [76]

The strut length (l) is 0.87mm. The thickness of strut is $2r$=0.3 mm. The values are enough to define relative density by using equation in Table 4.8. The displacement of the unit cell under an applied force is used to derive the analytical relationships that describe the elastic modulus [79].

4.8   *Numerical approach of 2D porous structure*

Porous structure mechanical response can be changed with number of cells, cell topology, strut diameter, and cell size. Boundary condition and loading condition may affect the mechanical response of the mathematical model [78][80].

In this study, the static test of finite element model is developed in order to create representative model for further calculation. Commercial product such as acetabulum cup augmentation consist of porous surface and calculation and predicting mechanical behaviour. It may help to improve implant corresponding response.

Cubical rhombic dodecahedron porous structure is developed with 6x6x6 mm dimensions by using SolidWorks (Dassault Systemes SolidWorks Corp., Waltham MA). Porous structure unit

cell was chosen as 2 mm rhombic dodecahedron. Connector diameters is designed for 0.3 mm and circular.
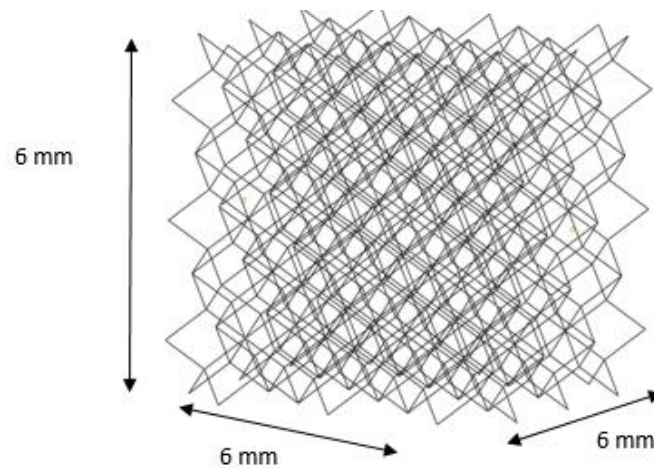
Figure 4.31 Cubical porous FEA model

It is assumed that struts behave like a beam and smooth surface. In a real application, struts contain partly melted powder. In this study, cubical porous samples were designed with 27 rhombic dodecahedron unit-cell, Figure 4.31. The parametric model was created with Body-Centred Cubic (BCC) seed points. BCC help to improve cell generation and it can help to make regular or irregular structure. In this study regular open cell architecture was used.
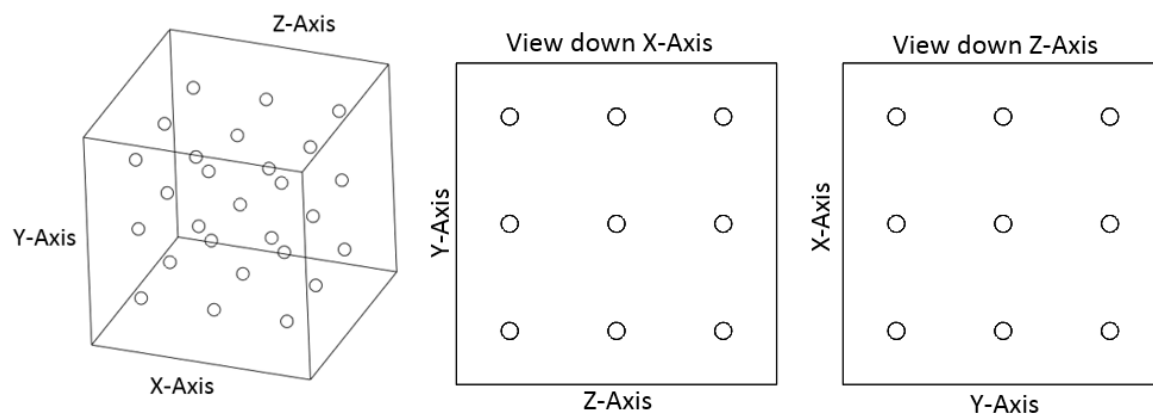
Figure 4.32 Body-Centred Cubic (BCC) seed point cloud [80]
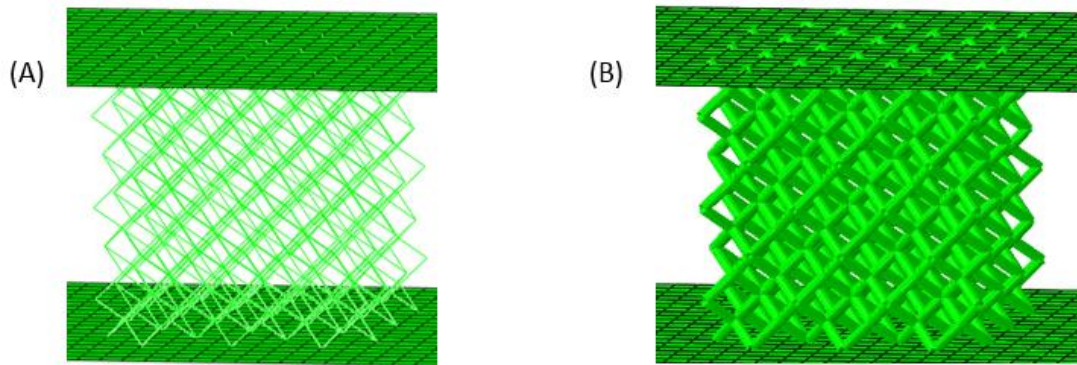
Figure 4.33 Thickening process for generation of 3D wet foams: (A) dry foam (B) "thickening" wet connectors
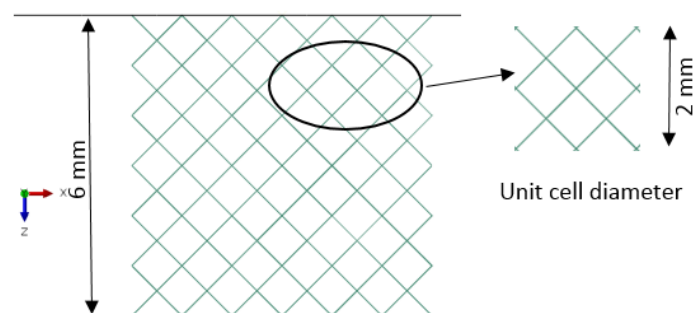
Figure 4.34 Dry cell and unit cell diameter

Abaqus (SIMULIA, Providence, RI) software was used for the finite element modelling. As it was discussed previously, the beam approach of numerical model can be reliable for complex 3D cellular calculation. Dry cell was used for decreasing computational cost.
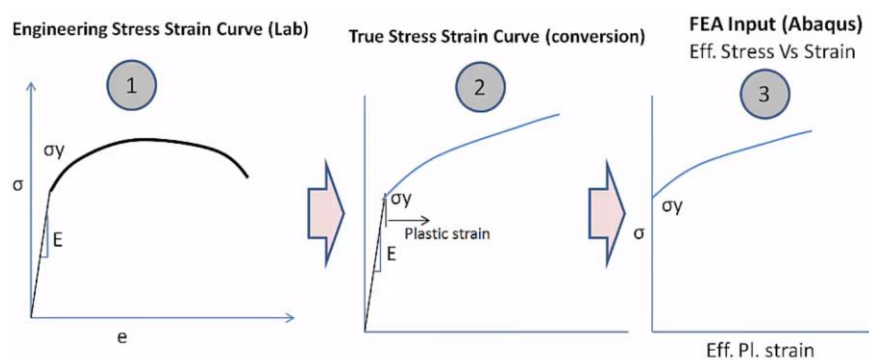
Figure 4.35 Material data modification for Abaqus input [81]

Concept Laser pure titanium tensile test data were used for material definition. Figure 4.35 shows that modification were done for importing pure titanium raw material parameters.

2 parallel rigid blocks were designed to mimic compression test. Calculated and used material properties for pure titanium; elastic modulus is 50 GPa, Poisson's Ratio is 0.3 and material plastic region adjusted according to Figure 4.35. Material data were chosen from previous single strut study.
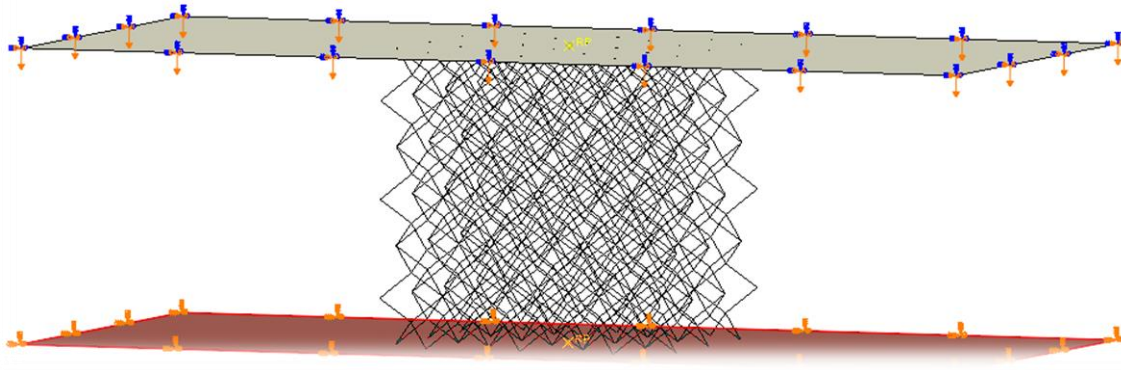
Figure 4.36 Load and boundary condition of the FEA model

Figure 4.36 illustrates that boundary conditions and applied displacement. Since it is a static analysis total displacement was set 2 mm in the z-direction. Boundary conditions was applied as encastre (U1=U2=U3).

4.9   *Dynamic response of porous structure with post treatments*

Concept laser titanium grade 23 (CL 41TI ELI) has been used during selective laser melting (SLM) [74]. The computer-aided design package SolidWorks (Dassault Systemes SolidWorks Corp., Waltham MA) and Materialise/Magics (Magics - Leuven, Belgium) software were used to design computer models of cubical samples. Cubical porous samples dimension was adjusted 6 mm and 2 mm rhombic dodecahedron open regular unit cell was used.

Selective laser melting (SLM)M2 cusing machine (Concept Laser GmbH, Lichtenfels, Germany) was used for AM process.   SLM manufacturer's recommendation was set during the manufacturing process; building chamber was not pre-heated, the laser beam power was 200 W, the scan speed was 7 m/s, the layer thickness was 20 μm, and the offset distance was 75 μm. Concept Laser's 'island' scan strategy was applied [56]. Surface treatment was carried out with 2 steps, 5 minutes initially etching in ethanol in ultrasonic bath was done then, samples were etched for selected time 6 minutes or 3 minutes in the mixture of 20 ml HF, 200 ml HNO3 and 780 ml demineralised water. Porous samples were washed with demineralised water and dried in air steam. The thickness of the connector struts was evaluated from

scanning electron microscope (SEM) Tescan VEGA-3 LMU (Tescan, Czech Republic) with ImageJ software. The strut thickness measurement was realised on two samples with at least 45 measurements on each. This approximately corresponds to two measurements on every strut. The results are presented as mean ± standard deviation. Hot isostatic pressing (HIP) was carried out at Bodycote Bourgogne (Bodycote HIP Ltd.). HIP process contains high-pressure argon gas (1020 bars) under high temperature (900°C). HIP process tends to decrease internal defect by using argon gas pressure at high temperature.

Table 4.9 Sample description and group definition

Group code	Name of the group
B	As-built
H	HIP treatment
B3	Surface treatment 3 min
H3	HIP treatment with surface treatment 3 min
B6	Surface treatment 6 min
H6	HIP treatment with surface treatment 6 min

Figure 4.37 IMATEK-IM10 resting machine [82]

Samples were grouped in 6 groups according to post-treatment method. 54 samples were manufactured for the impact test. 3 different environmental conditions were formed in order to simulate in-vivo conditions.
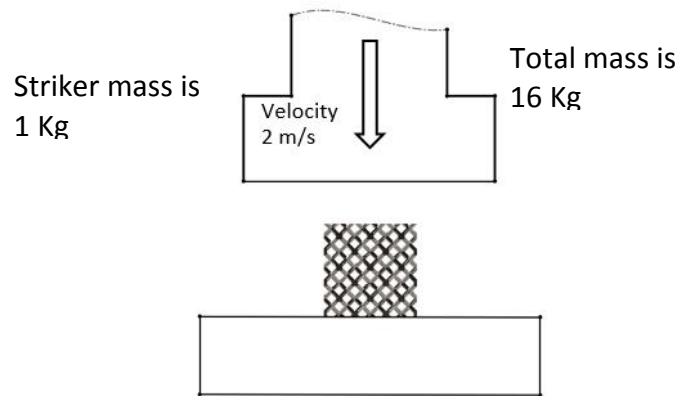
Figure 4.38 Dynamic test set-up

Impact test was carried out in the air, water, and blood like material [83]. The impact tests were performed in a drop test impact machine IMATEK-IM10 (Imatek Ltd., Old Knebworth, UK) with piezoelectric load cell positioned at the impactor root, Figure 4.37. The impact energy is completely supplied by gravity and controlled by the adjustment of the drop height. The IMATEK-IM10 is equipped with three hemispherical impactor devices and with ImpAqt software. The total mass of the impactor goes up to 16 kg, which allows energy peak at a velocity of 2 m/s. In the impact tests the total mass of the impactor was 1 kg [82].

`

``

Chapter 5: Result

5.1   *Single strut manufactured with SLM mechanical response*

Figure 5.1 presents microphotographs of sample surfaces showing the various orientation of the powder grains for samples build in ZXY (Vertical) and YZX (Horizontal) orientation. It is shown that the columnar powder grains growth always in the building direction regardless of specimen orientation, i.e. the samples build in ZXY directions has columnar grains oriented perpendicular to the testing direction while the YZX oriented samples have surface powder grains clustered parallel to the testing direction.
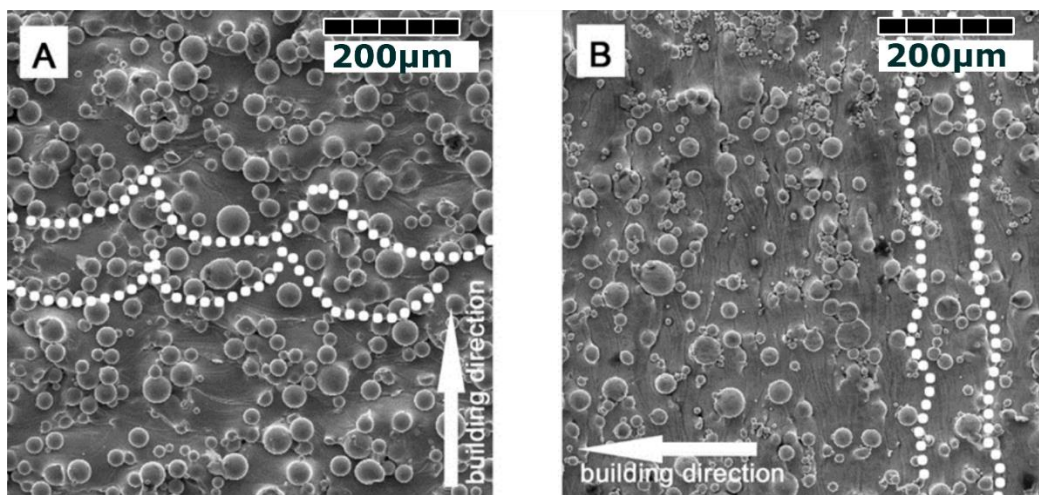
A) Surface of Sample a, printed with ZXY (Vertical) orientation

B) Surface of Sample b with, printed with YZX (Horizontal) orientation

Figure 5.1 Surfaces comparison of sample with ZXY (Vertical) and YZX (Horizontal) building orientation [52]
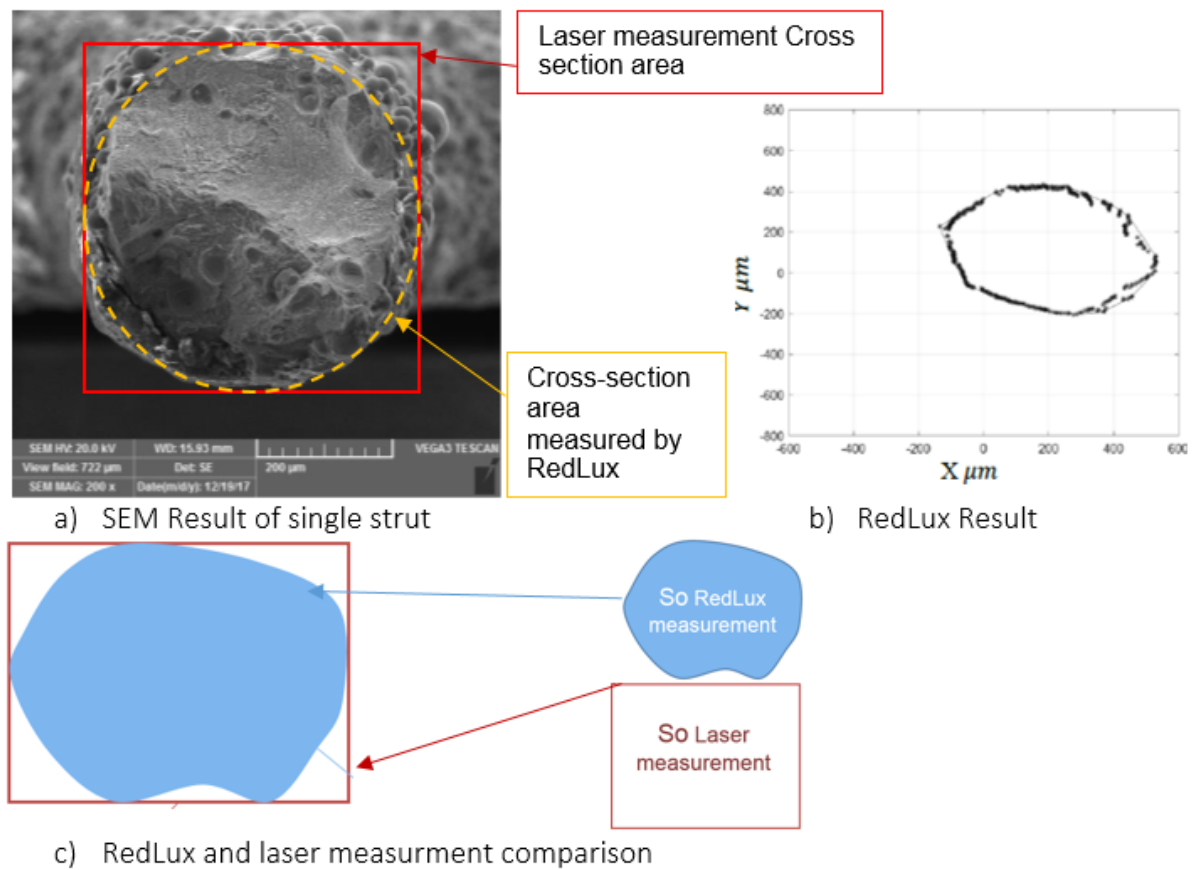
Figure 5.2 Cross-section area measurement comparison

The cross-sectional area of the samples estimated by optical surface scanning is approximately 9% lower than the cross-section area measured by laser scan micrometer or defined in CAD model (mean 9.3%, stdev 14.5% and mean 8.6%, stdev 14.6%, respectively, Wilcoxon paired test p<0.01 for both datasets, Figure 5.3). The CAD design and laser scan micrometers give comparable values of cross-sectional area (mean difference 0.6%, stdev 0.7%, Wilcoxon paired test p=0.16). The absolute relative differences between designed cross-section and optical surface scanning were measured based on the cross-section range from 0% to 40% and the higher values were found in smaller samples. The absolute values of difference in the cross-sectional area between the designed and measured values range from -0.19 to 0.22 mm² across all sizes of studied samples cross-sections. The observed discrepancies are caused by the shape of the samples where the design and DIC measurements assume rectangular cross-section. The real manufactured cross-section of small sample resembles ellipse.
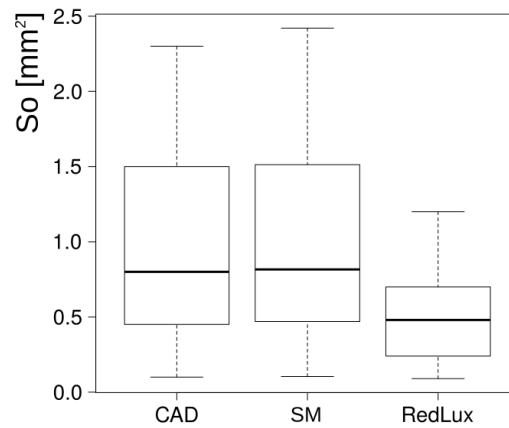
Figure 5.3 Statistical of comparison the geometrical accuracy [52]

Table 5.1 Mechanical result of tensile test [52]

	Elastic Gradient E (MPa)	Yield Strength YS (MPa)	Ultimate Tensile Strength UTS (MPa)	Elongation After Fracture A (%)
ZXY built orientation	0.70±0.27	613.94±139.29	676.46±145.89	10.59±10.17
YZX built orientation	0.68±0.24	405.29±142.84	469.88±144.63	9.84±5.42

The internal structure affects also material properties determined by the tensile test (Table 5.1). The ZXY build sample exhibits significantly higher yield strength and ultimate strength than YZX samples. There is no significant difference in the elastic modulus and the elongation among tested samples. However, the measured data indicate that mechanical properties could depend also on the sample size. Therefore, a two-way analysis of covariance ANCOVA was conducted to compare the main effects of the sample orientations and cross-sectional areas and the interaction between the sample orientations and size of the cross-sectional area on the yields strength. The main effect for sample orientation in the building chamber yielded an F-ratio of $F_{(1,62)}=48.64$, $p<0.001$ indicating the significant difference between ZXY (mean 613 MPa and stdev 139 MPa) and YZX (mean 405 MPa and 143 MPa) oriented samples. The main effect for the cross-sectional area yielded an F-ratio of $F_{(1, 62)} = 2.45$, $p=0.12$, indicating that the effect for the cross-sectional area was not significant. However, the interaction effect was significant, $F_{(1, 62)}=22.96$, $p<0.001$.

To further study this interaction, samples were divided into two groups according to their cross-sectional area (So): (I) with a cross-section smaller than 1.5 mm^2 and (II) represents samples with a cross-sectional area larger than 1.5 mm^2.

Table 5.2 Number of samples and their orientation in two groups divided according to the cross-sectional area [52]
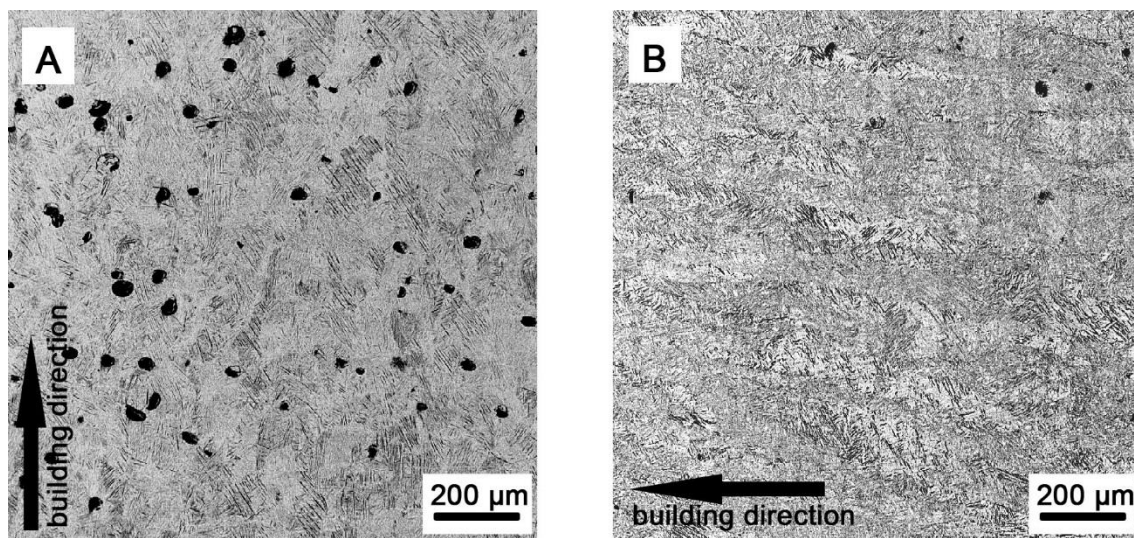
Group	So	ZXY	YXZ
I	<1.5mm^2	30	18
II	>1.5mm^2	9	8

Figure 5.4 Metallographic result of samples with a different orientation (YZX (horizontal) and ZXY (vertical) building orientation) [52]

The building direction influence not only the surface structure, but it has a considerable effect on the internal structure. As an example, we show the internal microstructure of two samples with ZXY and YZX built orientation (Figure 5.4). Both samples have a cross-section area lower than 1.5mm^2. The sample with ZXY building orientation has a finer microstructure but contains a considerably higher number of pores.
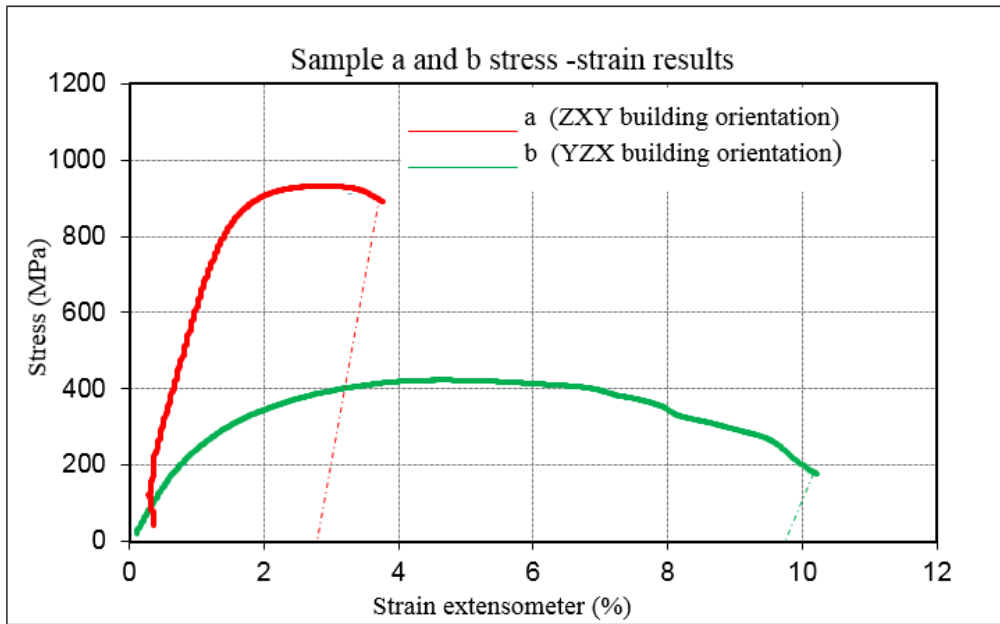
Figure 5.5 Stress-strain result of sample a and b with building orientation ZXY and YZX respectively. The red lines represent specimens built with ZXY orientation and green line represent YZX orientation respectively
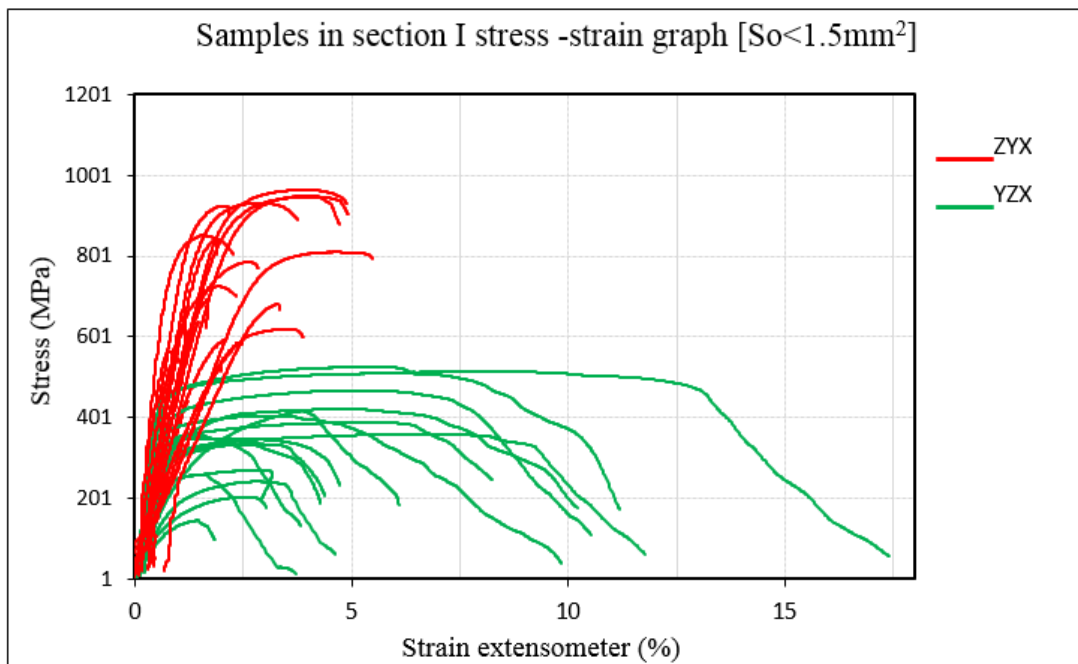
Figure 5.6 Samples in section I and II (So<1.5mm2) stress-strain results. The red lines represent specimens built with ZXY orientation and green line represent YZX orientation respectively [52]

The sample microstructure determines its mechanical behaviour. The sample build in ZXY orientation has considerable higher yields strength than sample build in YZX orientation. However, the internal defects conditions low elongation in sample build in ZXY orientation. This behaviour was observed in samples with small cross-sectional area, Figure 5.5. Samples with higher cross-sectional area, the yield strength is almost the same, while the elongation is higher in ZXY built samples, Figure 5.6.
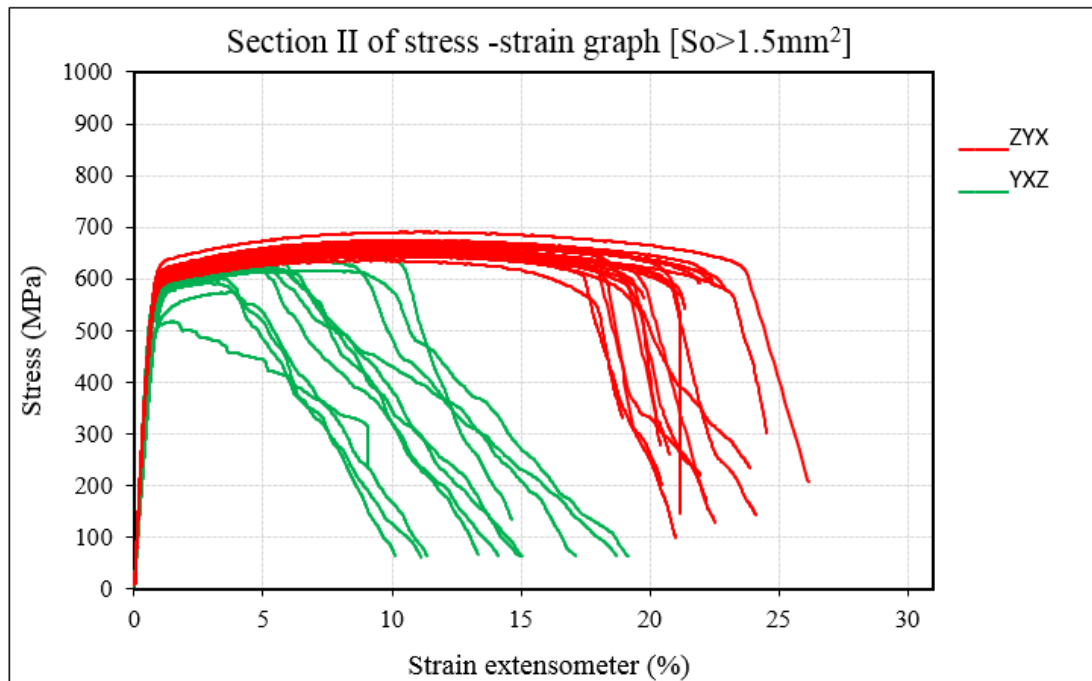
Figure 5.7 Section II (So>1.5mm2) samples stress-strain results. The red lines represent specimens built in ZXY orientation and green lines represent YZX built orientation respectively [52]

The ZXY samples have higher strength than YZX samples in small samples (group I), (Wilcox test p<0.01, Figure 5.6) that is in agreement with results presented in Table 5.1. However, these two groups also differ in elongation. The ZYX samples have almost brittle behaviour with limited elongation. The behaviour changed for larger samples (group II, Figure 5.7), where the yield strength is almost the same in the both ZXY and YZX group while the elongation in ZYX samples is larger than in XYZ oriented samples.

The results for the yield strength are summarized in Figure 5.8. Our results indicate that the orientation effect is crucial for small samplers (So<1.5 mm^2) while it is less important if the cross-sectional area is larger than 1.5 mm^2.
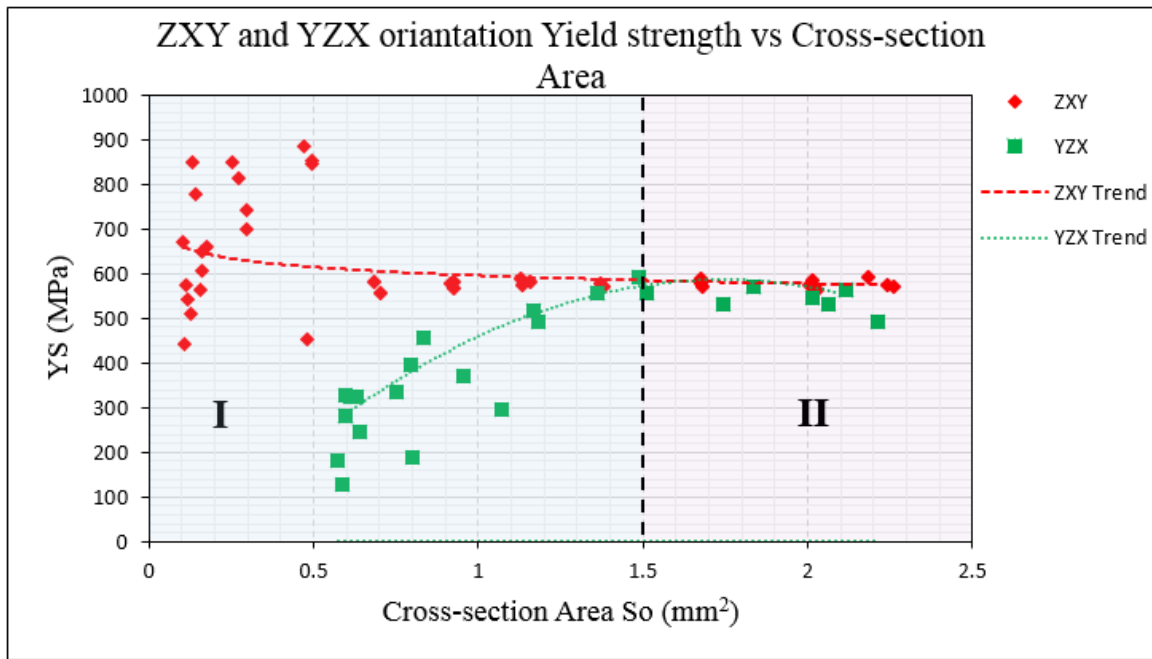
Figure 5.8 Yield strength (YS) for small struts-like specimens with different cross-section and building orientation. The group I and II are defined on the base of the cross-sectional area (group I: So<1.5 mm2 and group II: 1.5 mm2<So). Red symbol and dash line show the result of the sample with ZXY building orientation. Green square symbol and dotted line illustrate the result of specimen build in YZX orientation [52]
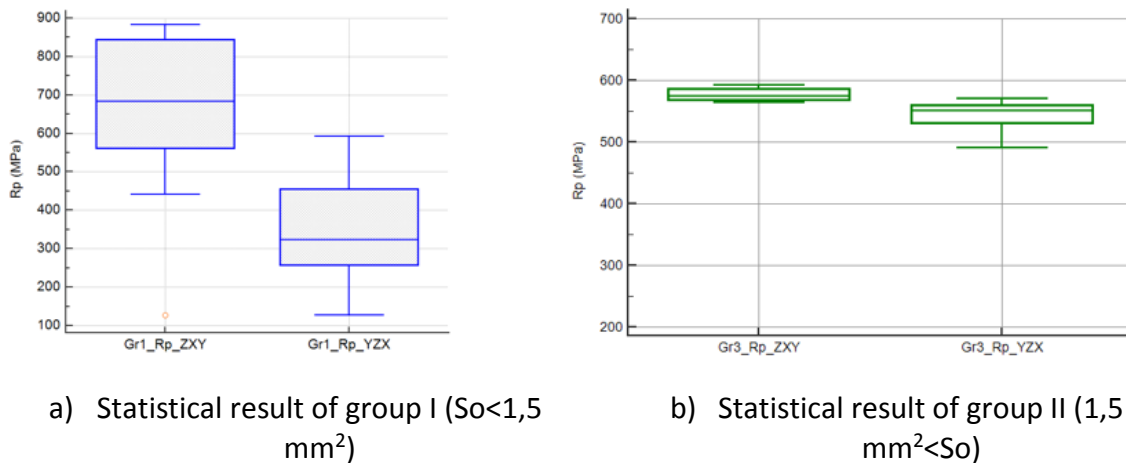
a) Statistical result of group I (So<1,5 mm^2)

b) Statistical result of group II (1,5 mm^2<So)

Figure 5.9 Yield strength statistical result of group I and II (So<1.5 mm2 and 1.5mm2<So, respectively) [84]

5.2   *Unit-Cell approach and 2D Analytic-numeric comparison*

Analytic results and finite element results were compared and the %6.5 difference was found on elastic modulus in x-direction. Analytic calculation based on the unit cell beam approach. Our previous study of geometrical and mechanical aspect was applied numerical approach as well. The result was satisfied to move further for complex calculation. Developed FEM approach of unit hexagonal cell can be used for complex and irregular 2D and 3D structure.

Analytic calculation and mechanical properties of unit-cell	FEA approach mechanical properties of unit- cell
$$\frac{E_x}{E_s} = \frac{E_y}{E_s} = \frac{E^*}{E_S} = 4.61x10^{-3}$$ $$\frac{\sigma_x^*}{\sigma_{ys}} = \frac{\sigma_y^*}{\sigma_{ys}} = \frac{\sigma_{pl}^*}{\sigma_{ys}} = 1.13x10^{-2}$$	$$\frac{E_x^*}{E_s} = 4.64x10^{-3}$$ $$\frac{E_y^*}{E_s} = 4.59x10^{-3}$$ $$\frac{\sigma_x^*}{\sigma_{ys}} = 1.21x10^{-2}$$ $$\frac{\sigma_y^*}{\sigma_{ys}} = 1.10x10^{-2}$$

5.3   *Developing complex 2D honeycombs with beam approach*

a)   b)   c)
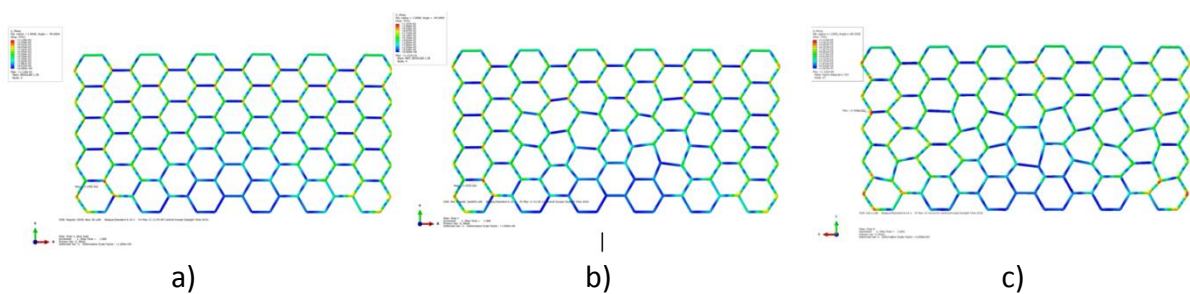
Figure 5.10 Regular b) Irregular c) Highly Irregular hexagonal honeycombs Abaqus Von Misses stress distribution [62]

Figure 5.10 shows that maximum Von misses stress location affected by irregular honeycombs architecture. Maximum stress location gives an idea to redesign the structure and avoiding high stress on the critical section. On the other hand, the changing orientation of struts

(angels or thickness-length ratio) effects on stress flow or distribution. As a result of that, it may provide a positive approach during the designing cellular structure on the contrary it may fail to the whole system if they are not considered.

Those missing network components may lead to high-stress concentration on different location which can be seen in Figure 5.11. Moreover, this simplified concept gives us a chance to understand behaviour of cellular structure.
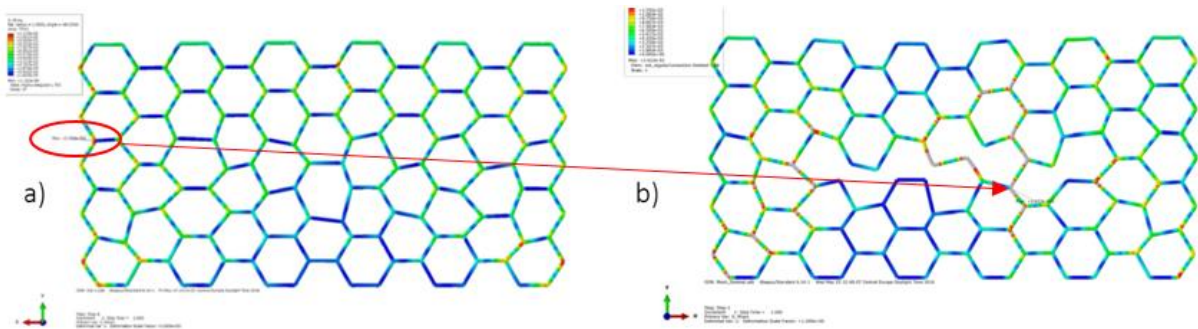

Figure 5.11 a) ''Highly Irregular'' and b) ''Highly Irregular network reduction'' hexagonal honeycombs with network reduction

It can be clearly seen that failing or removed struts affect the system mechanical response. Therefore, it was expected that since porous structure density was decreased and struts have to deal with the same applied load in the irregular geometry [62].

5.4   *Pure titanium as-built porous structure compressive mechanical response*

Compression test was carried out according to ISO 13314 (Mechanical testing of metals-ductility testing-compression test for porous and cellular metals). Loading-unloading slope was used to analysed elastic gradient.
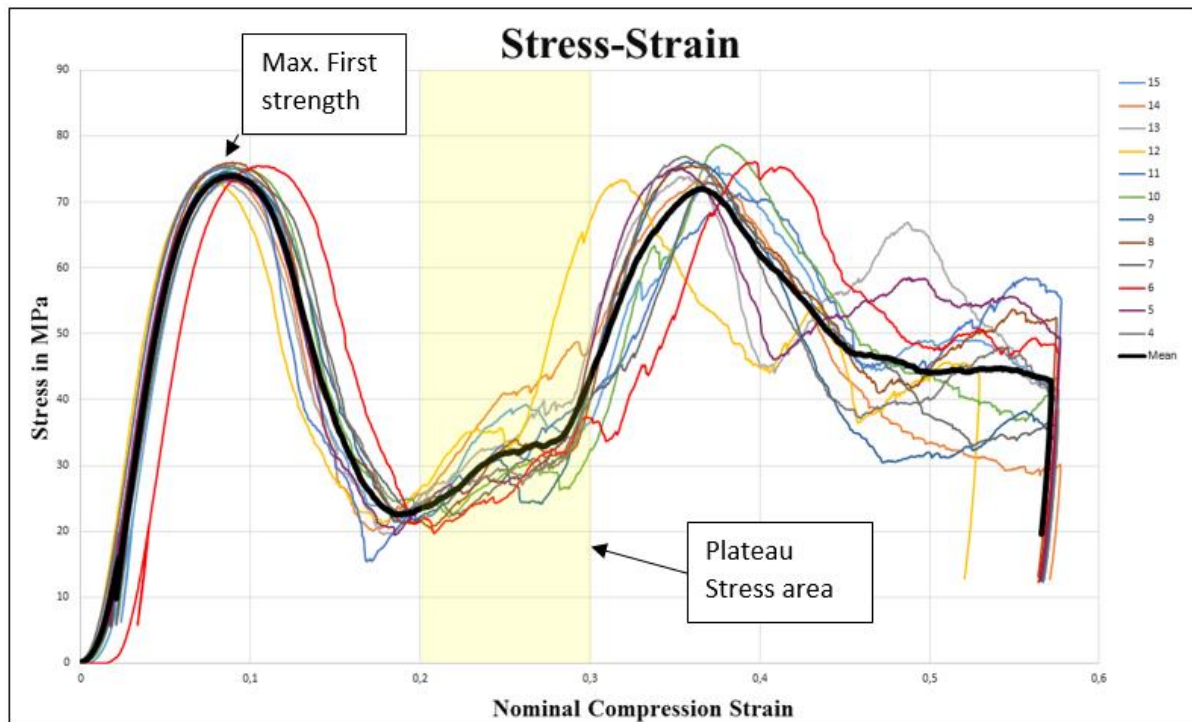
Figure 5.12 Compression test stress-strain diagram for all samples

Figure 5.12 represents the general stress-strain trend of samples. Elastic modulus, plateau stress and maximum the first strength calculated from the stress-strain diagram, Figure 5.12.
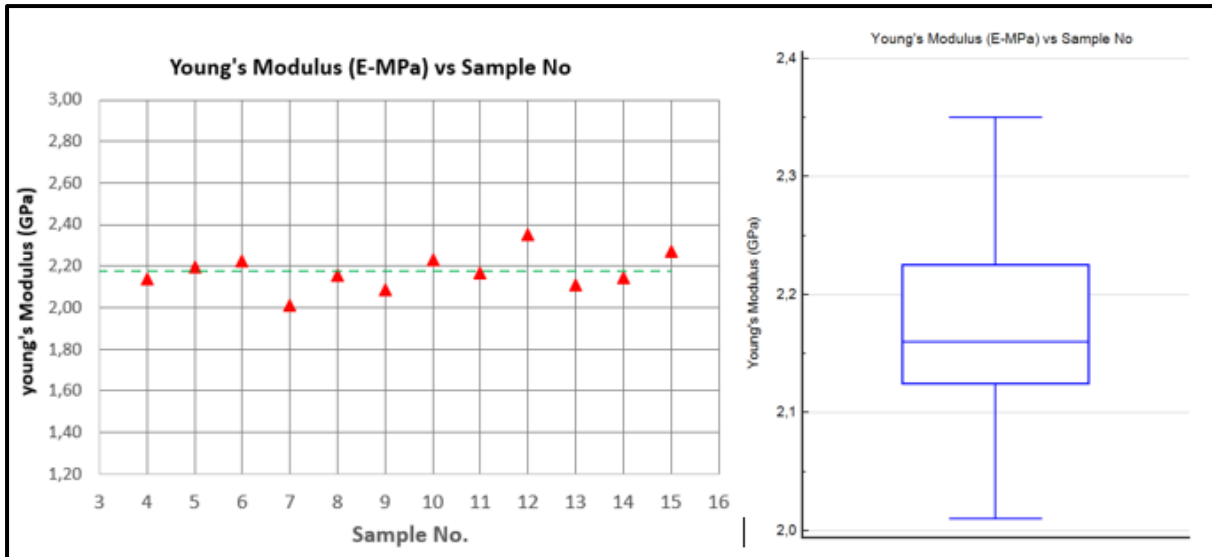
Figure 5.13 Young's modulus results of compression test of CP-Ti

Figure 5.13 illustrates the elastic modulus distribution versus sample number and statistical result. Mean value of elastic modulus is 2.17 GPa for all samples. The lowest and highest values area 2.01 and 2.35 GPa respectively. Standard deviation is 0.09 GPa.
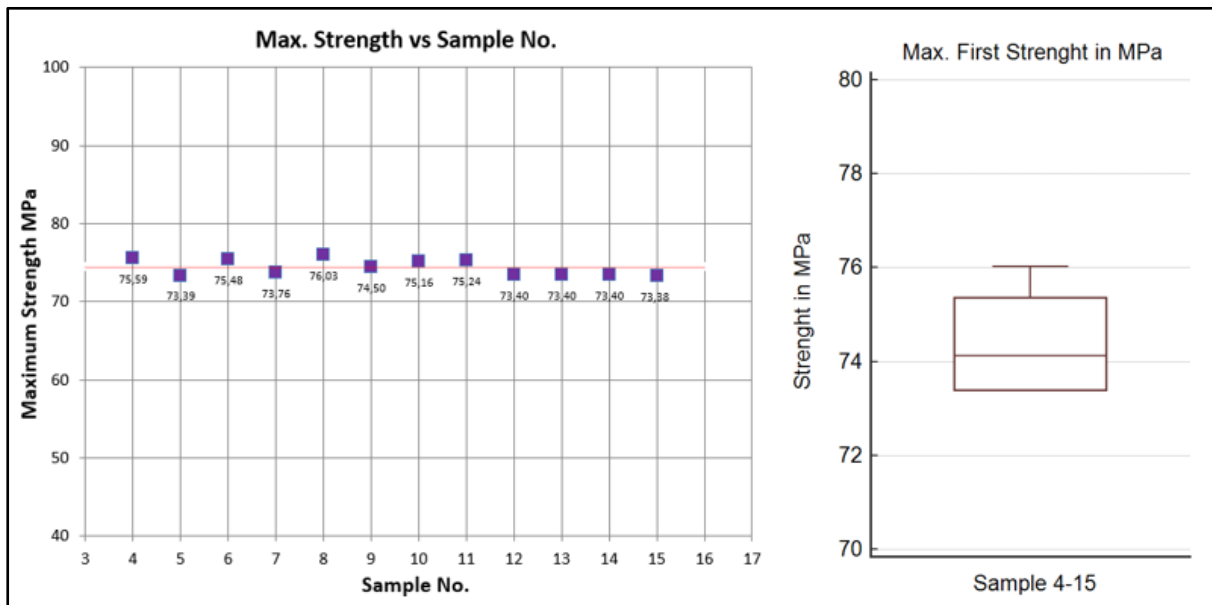
Figure 5.14 Maximum first strength of sample distribution and statistical result

The mean value of maximum strength is 74.39 MPa and the standard deviation is 1.04 MPa. Minimum and maximum value of maximum strengths is 73.38 and 76.03 respectively. This is slightly higher than yield strength value. Solid samples generally tend to have small gap between plateau stress and maximum strength. Therefore, it is important to determine

maximum strength. On the other hand, elongation during the maximum strength is supposed to be considered regarding porous structure design.
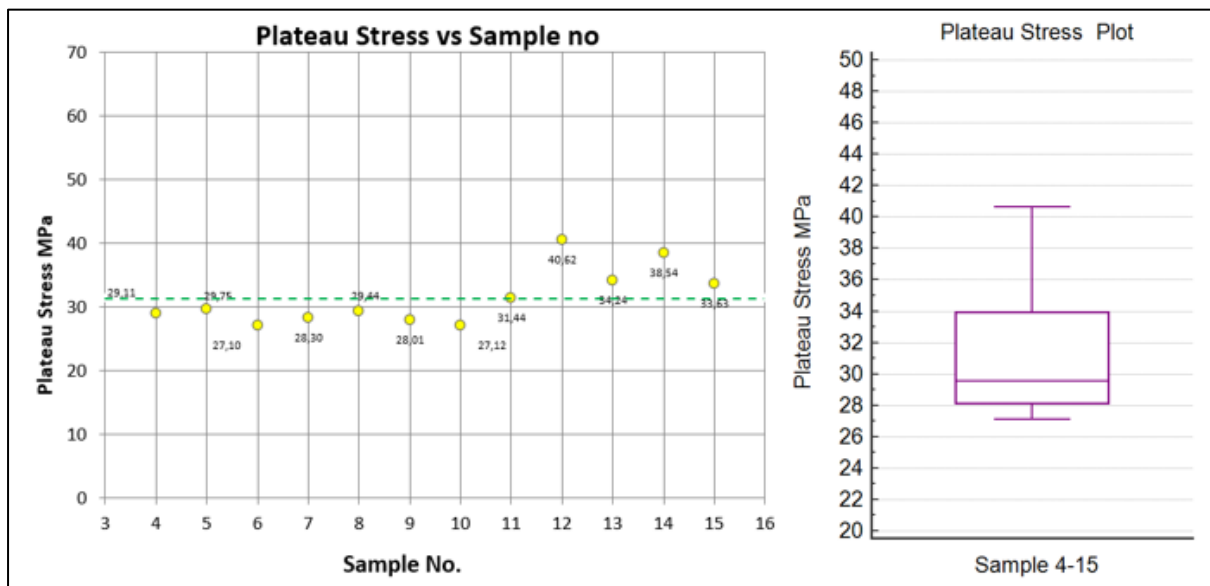
Figure 5.15 Plateau stress of samples distribution and statistical result

The mean of plateau stress of the samples is 31.44 MPa and the standard deviation is 4.46 MPa. The lower and higher values are 27.10 MPa and 40.62 MPa respectively.

5.5   *Pure titanium with surface treatment porous structure compressive mechanical response*

Stress-strain result of the cubical sample with surface treatment and samples without any post-treatment, Figure 5.16. Surface treatment can decrease the highest strength values.
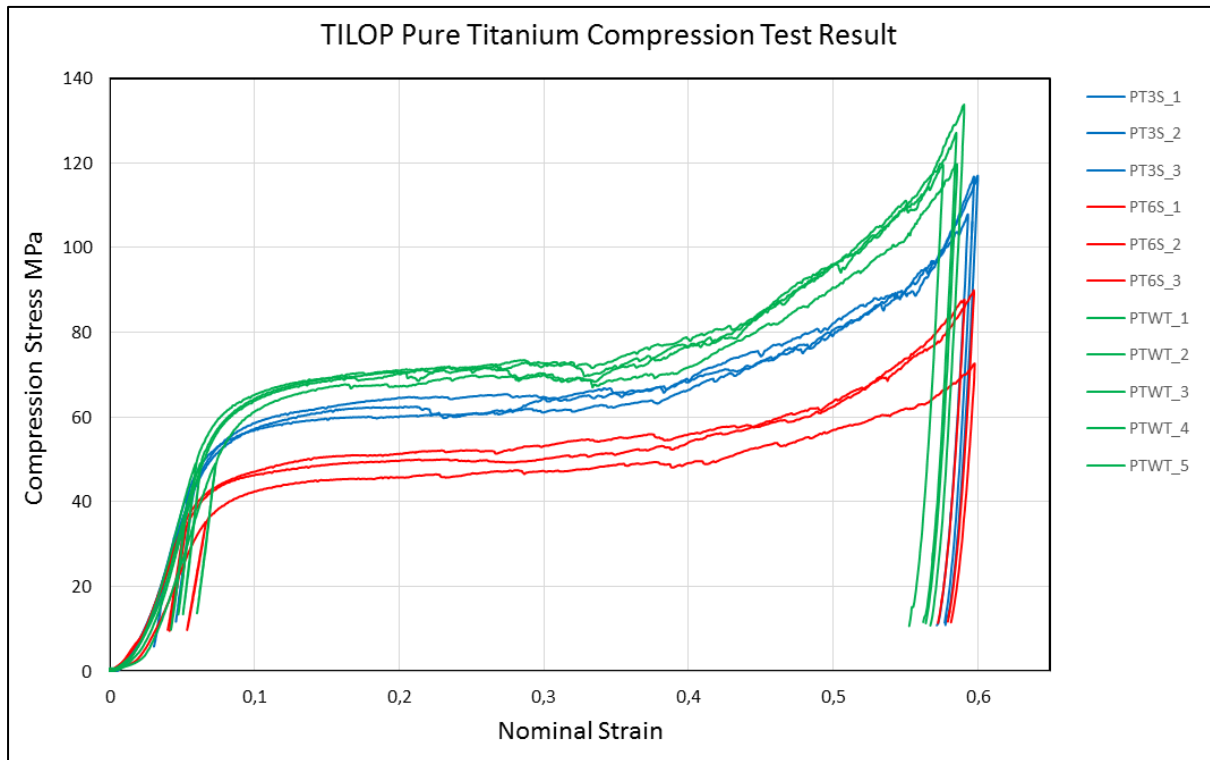
Figure 5.16 Compression stress-strain result of the TILOP pure titanium cubical samples.

Compression strain applied until 3mm deformation. Elastic modulus was calculated by load-unloading slope and it is the recommended the method for calculating porous structure parameters by ISO 13314.

Table 5.3 Mechanical result of compression test of surface treatment samples

	Elastic Gradient (E-GPa)	Yield Strength (YS-MPa)	First Maximum Strength MPa
PT3S	2.45 ± 0.27	38.88 ± 10.12	62.44 ± 2.33
PT6S	2.09 ± 0.11	36.62 ± 0.43	48.85 ± 2.95
PTWT	2.82 ± 0.11	49.63 ± 5.25	70.39 ± 1.94
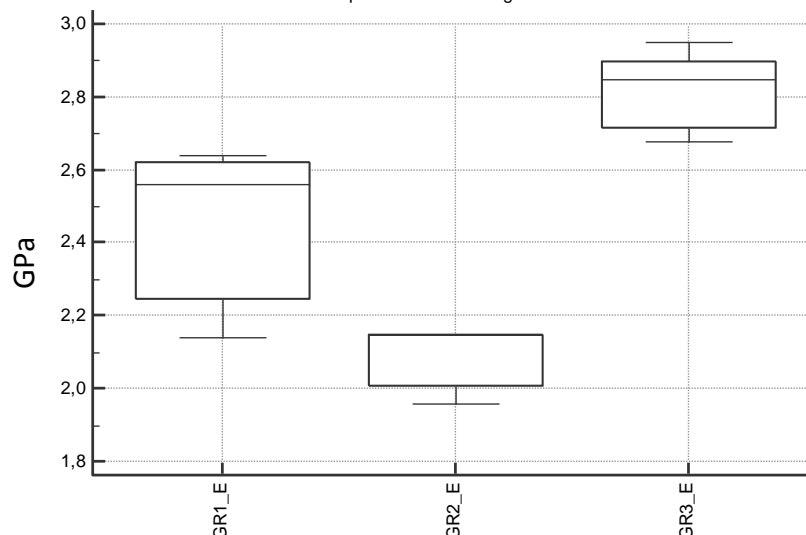
Figure 5.17 Compression test of TILOP pure titanium elastic modulus results

Figure 5.17 illustrates elastic modulus of compression test of TILOP cubical samples. Surface treatment can change mechanical properties and elastic gradient can be depended on the effectiveness of surface treatment which means 6-minute surface treatment can influence porous structure more than 3-minute surface etching. Moreover, surface treatment can decrease elastic modulus by 26%. The difference between the elastic modulus of 3 minute and 6-minute surface treatment is 14.7%. In addition, samples without any surface treatment can reach 2.9 GPa.
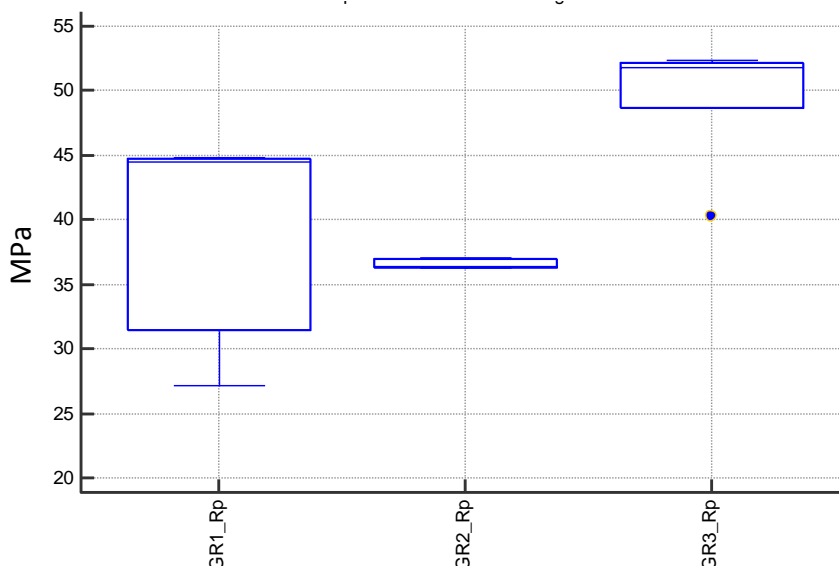
Figure 5.18 compressive proof stress results of the compression test of TILOP pure titanium

Compressive proof stress was calculated with 0.2% offset method. Figure 5.18 shows compressive proof stress result of cubical samples. Sample without any surface treatment has

the highest values with 49.63 ± 5.25 MPa. However, the samples with 6-minute surface treatment can achieve 21.67% lower values than as-built samples. There is also compressive proof stress difference between 3 and 6 minutes of surface treatment by 5.8%.
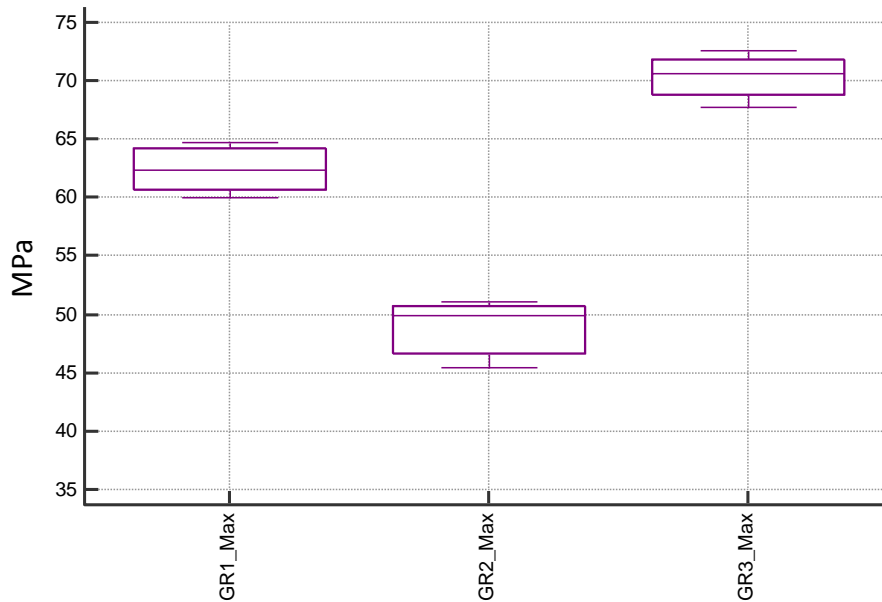

Figure 5.19 The first maximum strength results of compression test of TILOP pure titanium

Figure 5.19 shows the maximum first strength which is quite vital for handling the first phase of the plastic stage. Samples without surface treatment have the highest value with 70 MPa, and it is 11.3% higher than samples with 3 minutes of surface treatment.

PT3S

Sample with surface treatment 3 min

PT6S

Sample with surface treatment 6 min

PTWT

Sample without surface treatment
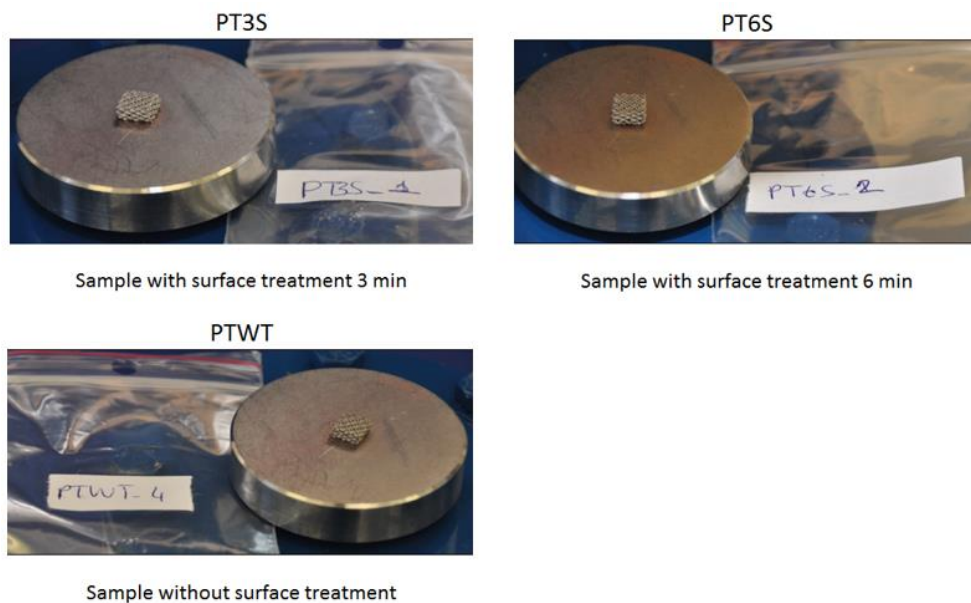
Figure 5.20 Cubical samples deformation after compression test

All metallic surfaces have electrochemical corrosion that reduces the structural integrity of the implant and releases particles that are potentially toxic. The mechanism of corrosion is essentially the galvanic effect [85], based on the thermodynamic driving forces which cause an oxidation/reduction reaction. Every metal has its own reactivity to oxidation and the exposure of metal to synovial or organic fluids produces a gradient-based exchange of electrons and ions from the metal to the solution [86]. Figure 5.20 shows that surface treatment provide releasing un-melted titanium particles under compressive deformation.

5.6   *HIP and surface treatment effect on porous structure*

Table 5.4 Connector strut thinness measurement result

Group no	Group code	Single strut thickness (*0.001)mm
1	SNHHTNS	322 ± 21
2	SWHIT	310 ± 23
3	SWS3T	277 ± 21
4	SWS6T	243 ± 21
5	SHITS3T	287 ± 21
6	SHITS6T	234 ± 18

Single strut measurement was done and compare after the surface and HIP treatments. Cad design of the connector strut thickness was 300 mm (*0.001) however, AM samples without any treatment had slightly bigger strut diameters due to the accuracy of the SLM. The thickness can be decreased with surface post-treatment. Table 5.4 shows that surface etching time would change the diameter of the connectors in the porous structure up to 14%. In addition, surface etching is more effective if samples have HIP treatment.
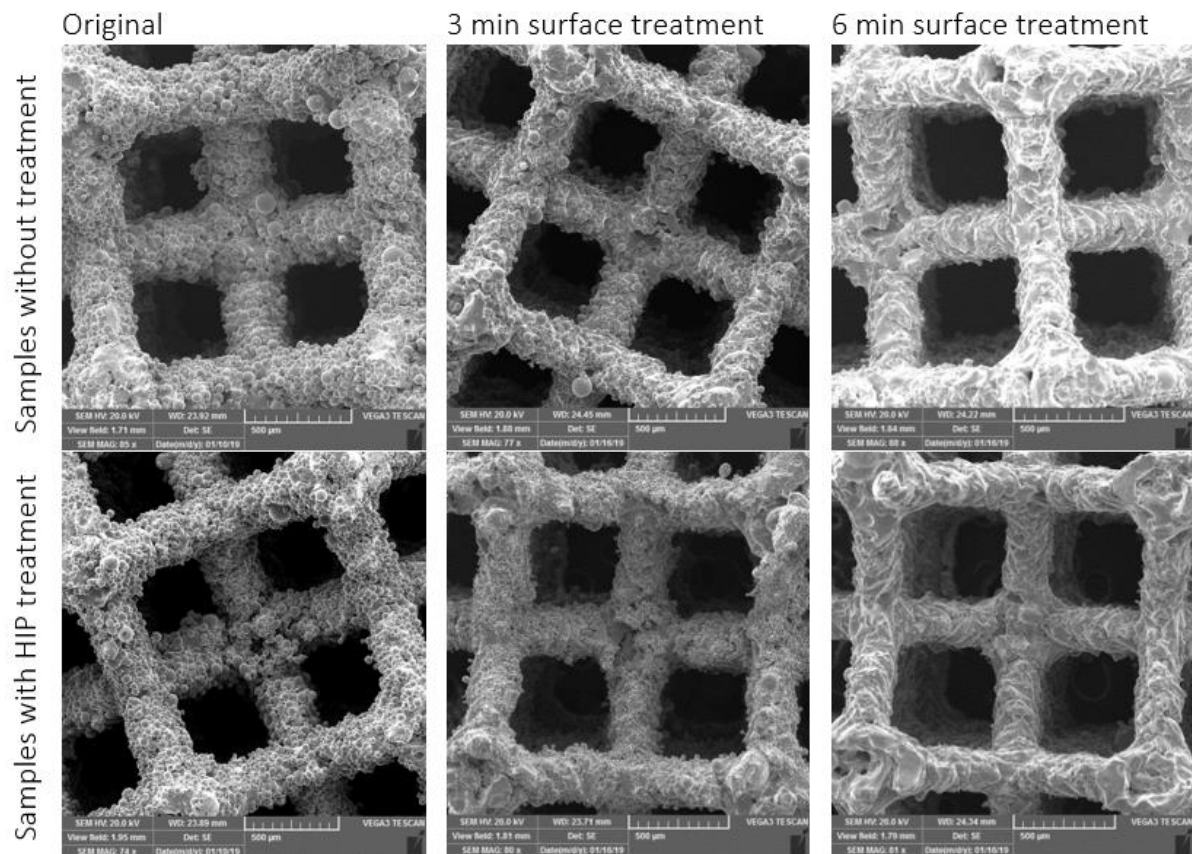
Figure 5.21 SEM result of post-treatment effect on surface [52]

Figure 5.21 shows the surface etching effect on samples without any treatment and samples with HIP treatment. It can be observed that surface etching can remove partly melted powder on the struts and create a smoother surface. However, the process can make struts quite thinner. Furthermore, struts can achieve clear beam form and homogenous shape after etching. This achievement can provide consistent behaviour under compressive loading. Removed particles area not only important for biomedical   approach it may also affect compression stress-strain diagram.
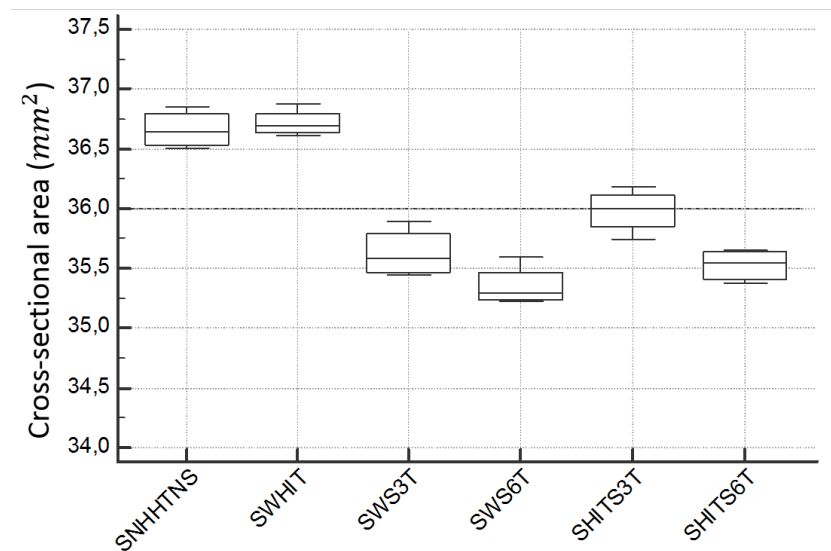
Figure 5.22 Cross-sectional area measurement compression [52]

The cross-sectional area of samples measurements was done with a digital micrometer (Mitutoyo, Mitutoyo Corporation, Tokyo, Japan) for each sample. Figure 5.22 illustrates surface treatment can affect cross-sectional area dramatically. Surface etching can decrease the cross-sectional area up to 3%.

Table 5.5 Compression test mechanical result [52]

No	Group name	Elastic gradient (GPa)	Compressive proof Stress (MPa)	First maximum compressive strength (MPa)
1	SNHHTNS	1.76 ± 0.05	38.70± 0.63	56.87± 0.98
2	SWHIT	1.87 ± 0.05	38.13 ± 0.55	52.67 ± 2.92
3	SWS3T	1.31 ± 0.13	31.66 ± 1.66	44.84 ± 3.63
4	SWS6T	1.23 ± 0.08	30.11 ± 0.43	39.84 ± 2.16
5	SHITS3T	1.48 ± 0.11	31.50 ± 0.94	43.02 ± 4.19
6	SHITS6T	1.34 ± 0.06	28.49 ± 1.24	38.41 ± 1.86

Table 5.5 shows the mechanical result of compression test according to groups. It can be seen that HIP process can deliver an enhanced elastic gradient due to decreasing internal defect [87]. On the other hand, surface treatment can influence almost all mechanical parameters since it tends to decrease strut thickness.
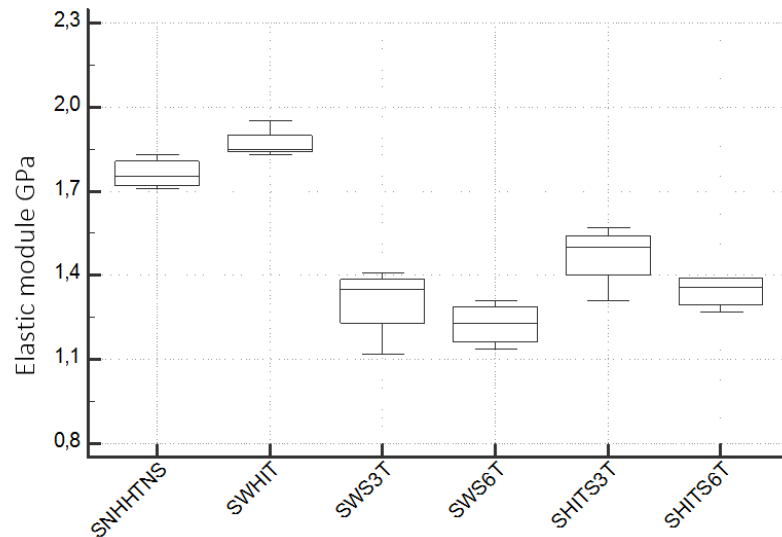
Figure 5.23 Compression test elastic modulus of porous samples comparison according to post-treatment [52]

Elastic gradients were calculated by elastic loading and unloading according to ISO 13314 guidelines [67]. Samples with HIP treatment (SWHIT) achieved the better elastic modulus value and it has 5.88% higher performance than as-built samples (SNHHTNS). It can be seen in Figure 5.23, the lowest elastic gradient was reached with samples with 6 minutes of surface treatment (1.23 ± 0.08 GPa).
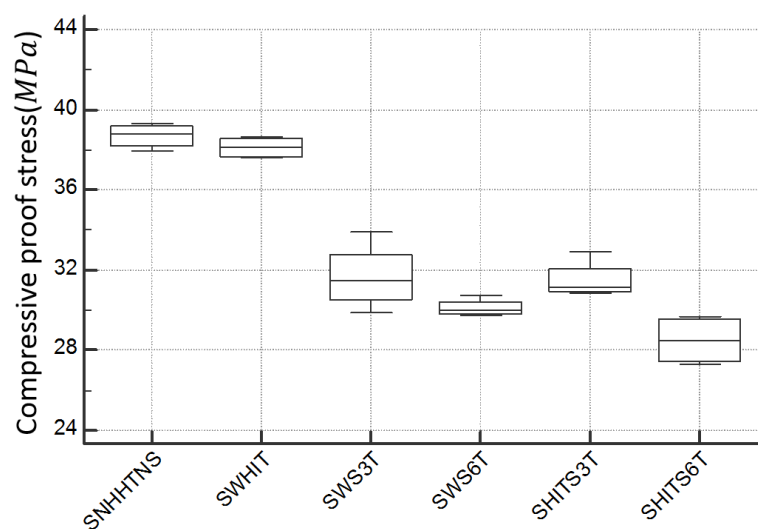

Figure 5.24 Compression test compressive proof stress comparison [52]

Figure 5.24 shows a significant difference between compressive proof stress of samples with surface and without surface treatment. As it can be seen that sample with HIP and 6 minutes surface treatment (SHITS6T) reached the lowest level with 28.49 ± 1.24 MPa. Surface

treatment time did not effect on compressive proof stress significantly. SHITS6T and SHITS3T samples had only 9.5% difference on the average.
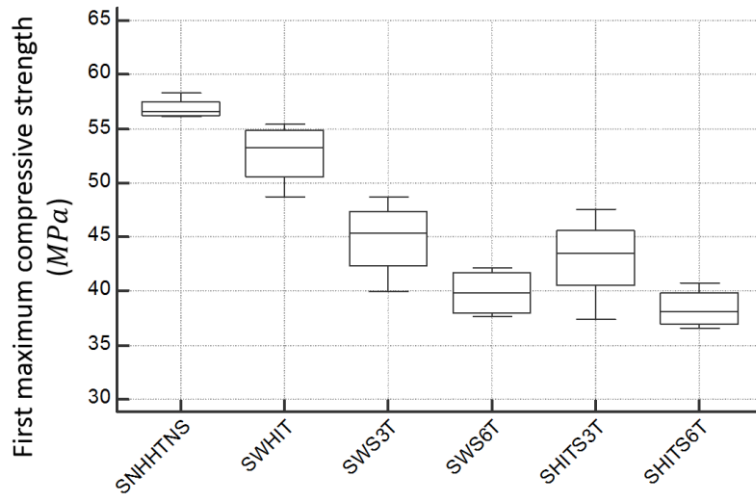
Figure 5.25 Compression test first maximum compressive strength comparison
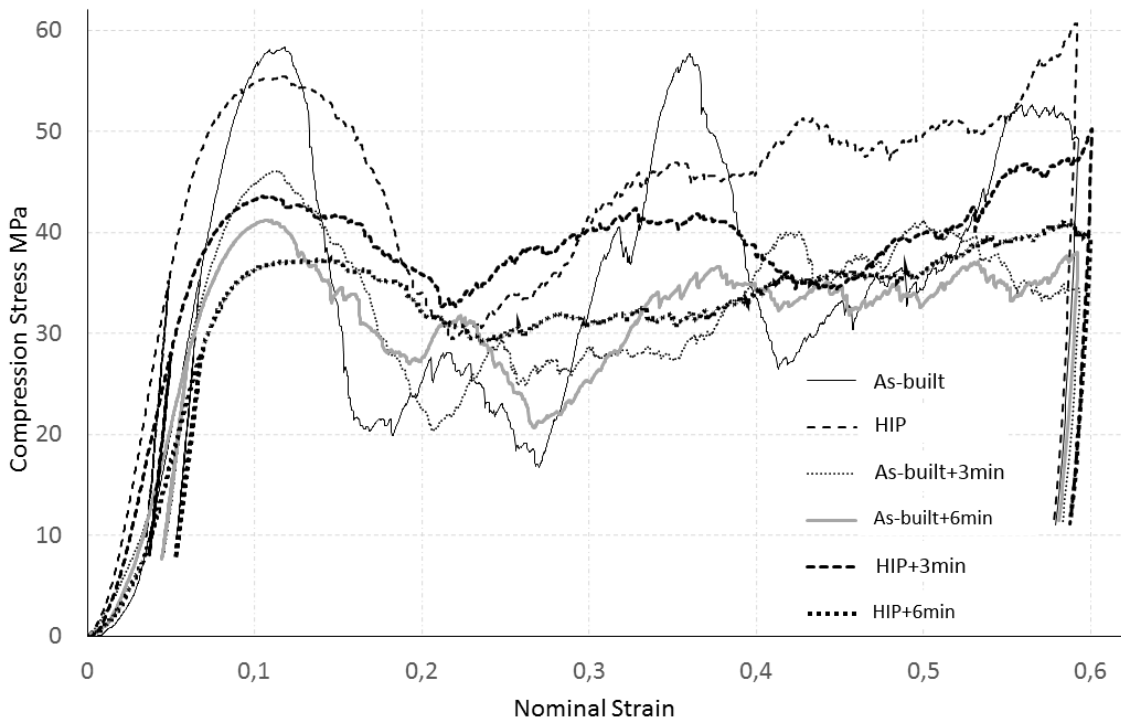
Figure 5.26 Stress-Strain diagram of compression test Ti alloy 23

As-built (SNHHTNS) achieved the highest first maximum compressive strength (56.87± 0.98 MPa), Figure 5.25. HIP treatment can decrease the strength by 7.4%. First maximum compressive strength comparison of samples with surface treatment (SWS3T) and samples with HIP plus surface treatment (SHITS3T) are quite close with the result of 3.5%.
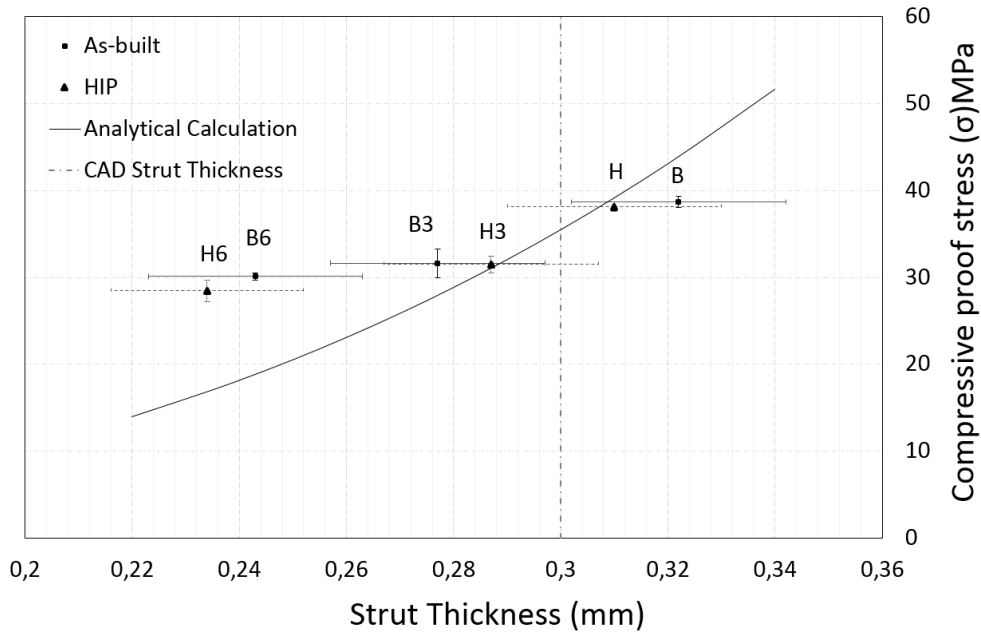
Figure 5.27 Comparison of yield strength of porous samples with post-treatment and theoretical calculation [52]
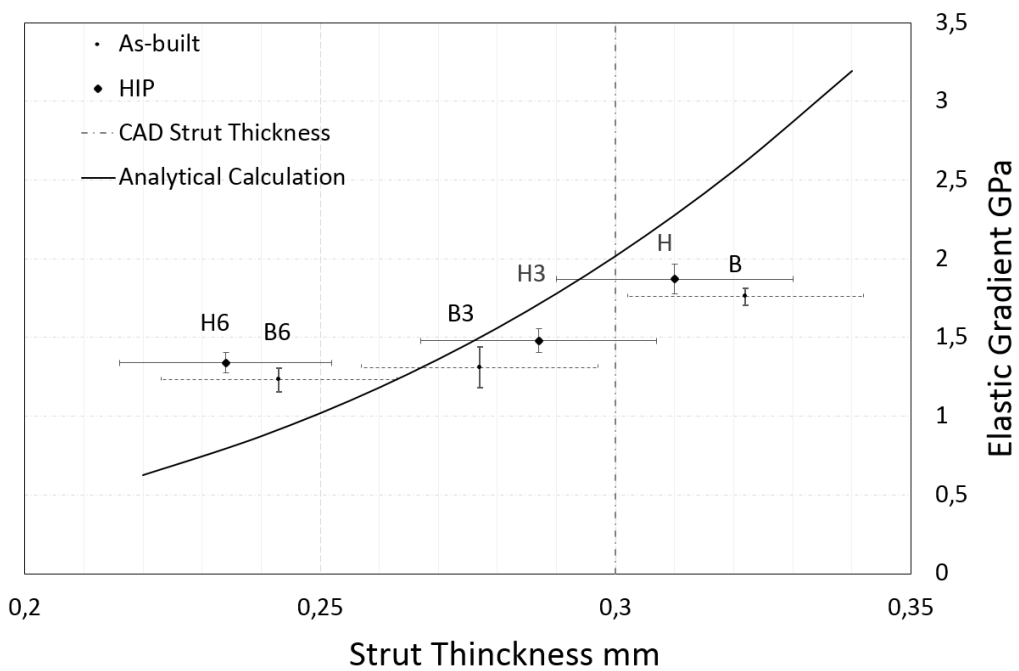
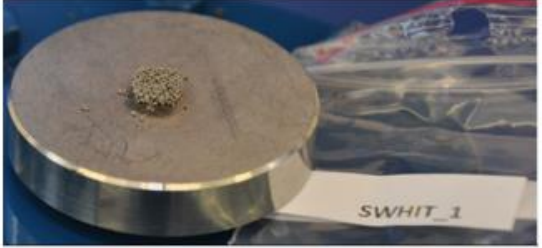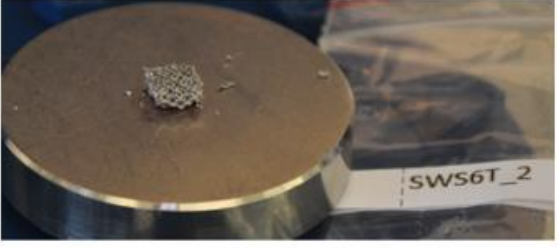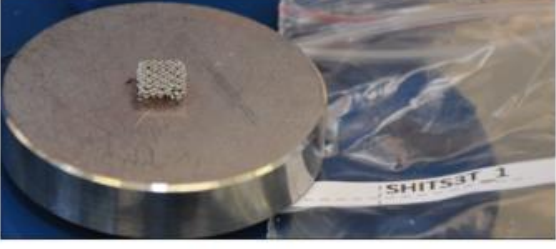Figure 5.28Comparison of elastic modulus of porous samples with post-treatment and theoretical calculation [52]

Figure 5.27 and Figure 5.28 show that surface etching decrease the strut thickness which effect on cross-sectional area and mechanical response. Yield strength trend follows the theoretical calculation which means surface treatment does not affect the porous behaviour. It can be also observed in Figure 5.26.

Table 5.6 Deformation of Ti alloy 23 compression test

SNHHTNS	SWHIT
Sample No Heat, HIP and surface treatment	Sample with HIP treatment
Group 1	Group 2
SWS3T	SWS6T
Sample with Surface treatment 3 min	Sample with Surface treatment 6 min
Group 3	Group 4
SHITS3T	SHITS6T
Sample with HIP treatment with surface treatment 3 min	Sample with HIP treatment with surface treatment 6 min
Group 5	Group 6

Surface treatment effect on deformation can be seen in Table 5.6 Group 6 achieved less titanium particles release after compressive deformation.

5.7   *Analytic calculation of 3D cellular structure*

Bulk material mechanical properties were used for elastic modulus calculation. However, applied bulk material parameters are not reflecting the real problem since connectors have different mechanical properties than bulk titanium. Our previous study also shows that thin struts mechanical properties can be influenced by the size and building orientation.

Table 5.7 Analytic calculation of rhombic dodecahedron result

	Relative density (ρ)	Elastic Modulus (E)	Yield Strength (YS)
Bulk CP-Ti material data	0.24	$E_{1=} E_2,=2.02$ GPa, $E_3=1.19$ GPa	$\sigma y_1=\sigma y_1 =45.19$ Mpa
Single strut CP-Ti material data	0.24	E1= E2,=1.28 GPa,, E3=0.76 GPa	$\sigma y_1=\sigma y_1 =45.19$ Mpa

Bulk material and single strut material properties response of numerical calculation results can be seen in Table 5.7. Analytic density calculation is only 4% difference from the cad design. Mechanical compression mean elastic modulus was 2.17 GPa. If experimental value and analytic result compare, there is a 7% error occurs due to bulk material definition. In the literature, there are few studies have investigated the analytic calculation based on bulk material properties. In reality, struts mechanical properties is quite different than bulk materials. Analytical approach was designed for bulk titanium material. As it can be seen that single strut material data can deliver result with 41% error if the same analytic approach is used.
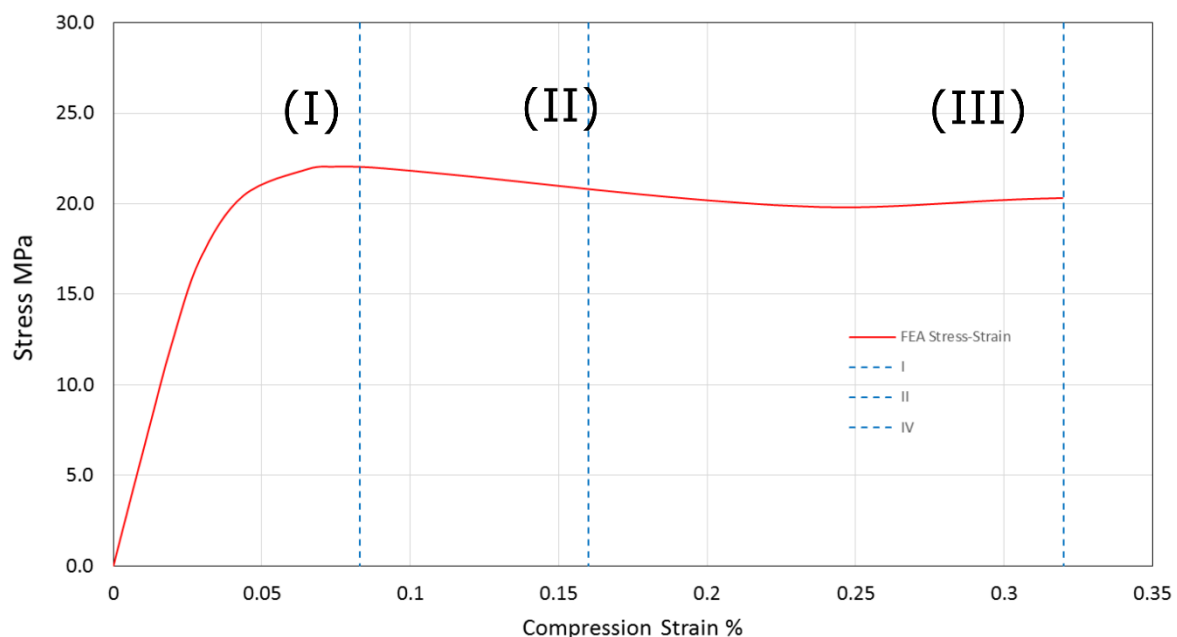
5.8   *Numerical approach of 3D structure*

Figure 5.29 Stress-Strain diagram of FEA calculation

Numerical calculation was developed on beam based calculation which was decribed in the previous sections. Deformation was applied as displacement in order to mimic the compressive mechanical test.

Reaction force was calculated from the reference point which was pre-defined. Stress calculated from reaction force and cross-sectional area. The strain was calculated from displacement, this method is similar to ISO 13314 (Mechanical testing of metals-ductility testing-compression test for porous and cellular metals) [67]. Elastic modulus was calculated as 0.55 GPa with the offset method from the stress-strain diagram, Figure 5.29. Stress-Strain diagram divided into 3 sections.
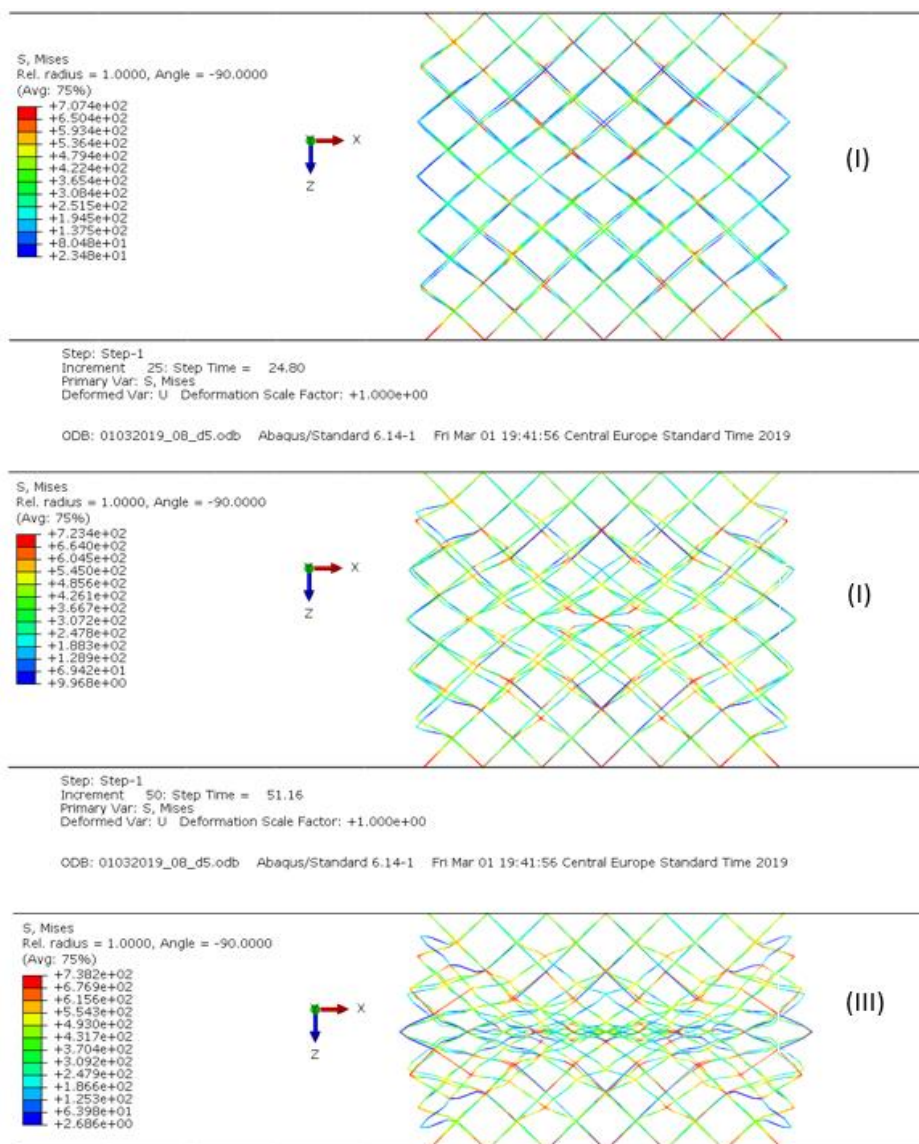
Figure 5.30 Von Mises stress and deformation result of cellular model

The first group contains data until elastic behavior ends. The second group (II) contains the result of plateau stress beginning, where struts get started to collapse. Group 3 illustrates the data where compression test ends and it reached to 2 mm deformation.

Figure 5.30 shows Von Mises stress result and deformation according to compression level. It can be seen that plastic collapse occurs in the second stage. The last stage (III), plastic deformation can be seen clearly.

5.9   *Dynamic behavior of titanium alloy porous structure*

Rhombic dodecahedron lattice structure was manufactured by SLM samples were used for dynamic compression test. The rhombic dodecahedron has a bending dominant structure. Figure 5.31 illustrates deformation of the dynamic test of cubical porous titanium samples. Previously, a cubical porous numerical model was defined as linear elastic and dynamic test deformation showed that they have a common shape of collapse.
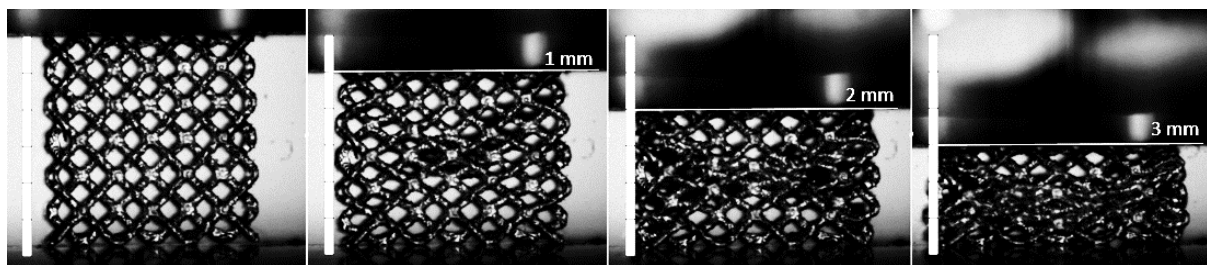

Figure 5.31 Dynamic compression deformation of cubical rhombic dodecahedron samples

Table 5.8 Impact force result of dynamic compression test in a variety of environments

Testing environment	B (kN)	H (kN)	B3 (kN)	H3 (kN)	B6 (kN)	H6 (kN)
AIR	3.03±1.04	3.93±1.72	2.43±0.18	4.3±0.8	2.45±0.46	1.68±0.35
WATER	2.69±0.10	2.38±0.15	1.7±0.13	2.07±0.02	1.66±0.09	2.05±0.23
BLM	2.69±0.34	2.36±0.15	2.19±0.16	1.47±0.53	1.71±0.20	1.42

HIP treatment increased the impact force for the dynamic test in the air by 22% since HIP tends to decrease internal defect. It was also observed that HIP decreased the impact strength by 8%. This effect on the dynamic test can be changed according to the testing environment. Impact force result was decreased in the liquid testing environment, on the other hand, the absorb energy was increased, Table 5.9.

Table 5.9 Impact strength result of dynamic compression test in variety of environments

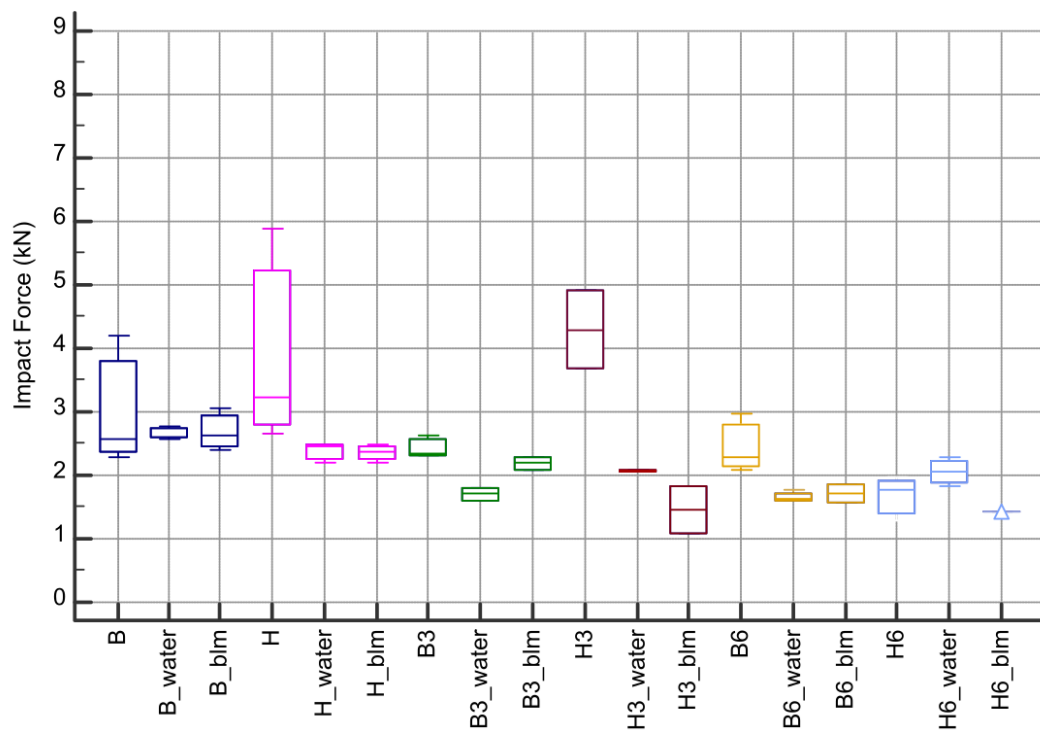| Testing environment	B (J)	H (J)	B3 (J)	H3 (J)	B6 (J)	H6 (J)
AIR	0.6±0.17	0.55±0.21	0.49±0.08	0.71±0.20	0.44±0.09	0.42±0.31
WATER	0.99±0.06	0.76±0.08	0.36±0.07	0.44±0.13	0.44±0.10	0.30±0.05
BLM	0.84±0.26	0.67±0.27	0.79±0.06	0.32±0.21	0.45±0.11	0.39

Figure 5.32 Impact force of dynamic compression test result

Impact force was not significantly changed with the testing environment, Figure 5.32. HIP treatment can decrease impact force slightly due to the fact that strut thickness tends to shrink after HIP treatment so the cross-section area gets reduced after the operation.
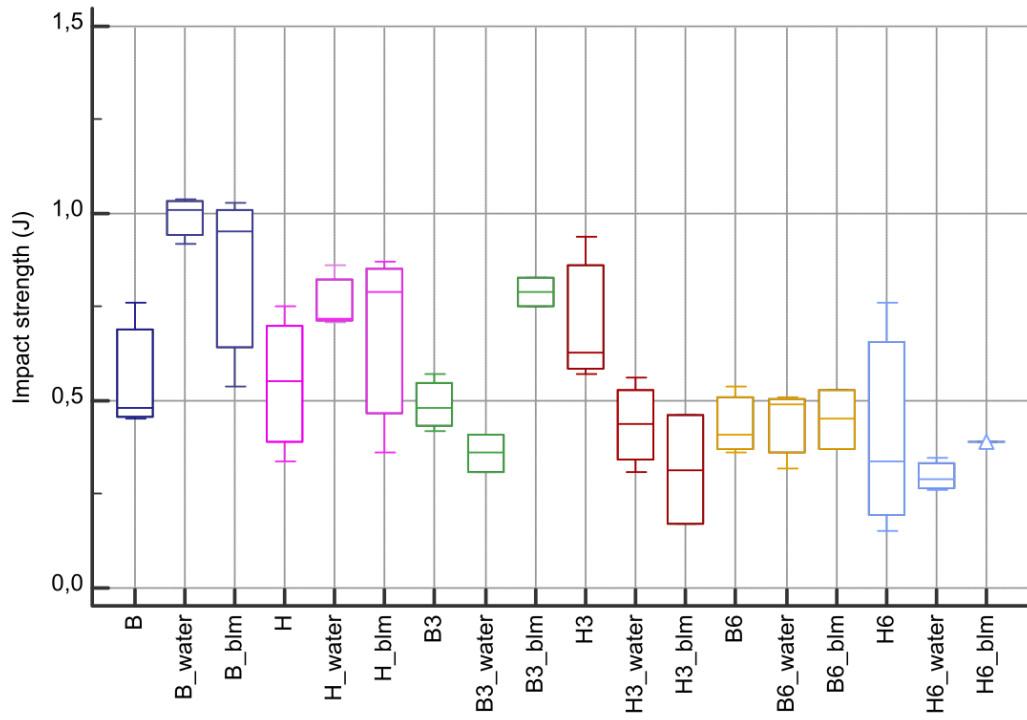
Figure 5.33 Impact strength of dynamic compression test result

Chapter 6: Discussion

The porous structure is becoming trendy application in orthopedic implants [88]. Adjustable geometrical freedom and low-density component can be provided with AM technology for replacing damaged or unhealthy body parts [89]. Un-cemented joint implant surface modification can help to increase bone anchoring therefore, AM can create arbitrarily complex and predictable porous 3D structures[90][91].

Porous structure mechanical properties are important for medical application. It can decrease stress shielding and increase osteointegration [92][93][94]. Therefore, porous structure mechanical properties can be depended on unit-cell architecture, the material used, connector strut thickness and relative density [95]. Optimizing mechanical response of porous structure could be adjusted by strut thickness which changes relative density [96]. In this research pores size adjusted to 0.6 mm which is an optimum value for bone ingrowth [97]. Study of *Mullen et al.,* 2008 shows that the size of the pores can affect bone anchoring significantly [3].

Selective laser melting (SLM) accuracy can be tuned with parameters such as applied energy or beam diameters [98]. In this study, the manufacturer recommended setup was used.

6.1 Single strut size and building orientation effect on mechanical properties

The properties of individual segments of the truss-like porous structure affect its global performance. In this study, it was shown that the building orientation of the struts and its size influence its mechanical properties.

Building direction influences the surface geometry and the microstructure that has in turn effect on mechanical properties. The AM process is primarily tuned to building in the Z-direction, that was observed by finer microstructure (Figure 5.4) and higher yield strength in ZXY (Vertical) than in YZX (Horizontal) built specimens (Figure 5.6, Figure 5.7 and Figure 5.8). However, the larger the cross-sectional area is, the smaller difference in yield strength is between the YZX (Horizontal) and ZXY (Vertical) specimens, respectively (Figure 5.8). It has been also observed a considerable amount of pores for ZXY (Vertical) specimens (Figure 5.4A) that conditioned low elongation, regardless of the specimen cross-section size (Figure 5.6, Figure 5.7). The higher porosity in ZXY (Vertical) samples was reported also in the previous

studies, for review see *Frasier et al., 2014*. The relatively higher porosity could be specific to used SLM setup, including powder, scanning strategy and laser beam power. *Slotwinski et al., 2014* showed that by changing the manufacturing parameters, the porosity could be considerably influenced. However, the study of *Slotwinski et al., 2014* is based on large samples (a cross-sectional area more than 5000 mm^2) and application of small samples used in this study (the cross-sectional area around 1 mm^2) may not be straightforward [99].

Above mentioned results showing the effect of the orientation are in agreement with the previous studies. *Aref Yadollahi et al., 2016* reports the 10% higher yield strength for samples manufactured in the building (Vertical) direction than manufactured in the plane of deposition (Horizontal) based on large samples (the cross-sectional area around 12.56 mm^2)[100].

The previous studies investigated samples with large cross-section areas. The results presented in this study show that the building direction has a much larger effect when the size of the structure is small (cross-sectional area less than 1.5 mm^2). The difference in the yield strength between samples build at different orientation is 79% average (Figure 5.8). If the cross-sectional area is larger than 1.5 mm^2, the difference in yield strength between samples build in different orientation is 6% on average that is comparable to the previous studies. We may conclude, that the orientation effect could be more crucial for fine porous structure than for massive solid AM produced parts.

In addition to the yield strength, the size of the sample and its orientation have an impact on material brittleness. For larger samples, the elongation for ZXY (Vertical) oriented samples is higher than for YZX samples (Figure 5.7). Similar results were observed by Caulfield et al. 2006, Wegner et al. 2012 and Witt, Negi et al. 2015 [101] [102][103]. The new finding in the present study is, that elongation trend is reversed in small samples (Figure 5.6). We may hypothesize, that this effect is process specific. If the sample is built in ZYX direction and the cross-sectional area is small, the building area that laser spot melts is small. The amount of energy applied during the SLM process is a function of laser spot size, scan radius, laser power, scan spacing, and the laser scanner parameters [104]. The smaller the building area, the less optimal hatching distance is achieved and the higher energy is accumulated in the overlapping laser spots. The high melting energy could cause the brittleness of materials [105].

This study was designed to test the structures at the limit of the accuracy of the AM process used. The reaching of the limits for the AM process could be observed in decreased shape and size accuracy for specimens with the small cross-sectional area. It is common engineering practice to measure two perpendicular dimensions and calculate the cross-sectional area as an area of a rectangle. We have observed that the edges designed rectangular cross-section were rounded during the AM process that results in a discrepancy between the designed and actual cross-sectional area. 3D surface measurements using optical methods (confocal probe and digital image correlation) is more appropriate for tiny strut structures.

Current results are based on the static test. Any porous structure in the human body will be loaded dynamically and the fatigue strength should be considered, especially as the properties of AM parts measured in static tests do not guarantee their fatigue performance [106]. When using an implant surface, the porous structure is in contact with body fluids and tissues. The fluids and cells penetrate the structure [107]. Their presence could increase the porous structure density and strength. On the other hand, the interaction of the highly corrosive environment of the human body in combination with the large surface area could result in the failure of the structure[108].

Within this study printed specimen that matched the size and shape of connectors of the porous structure were investigated. However, the struts in the porous structure are always printed in a pack with the whole structure. The presence of surrounding elements may influence thermal gradients and mechanical properties. The most accurate testing will be to isolate the individual element from the whole structure and measure its mechanical properties. Considering the small size of individual elements, this would be technically demanding. Based on the considerable difference between small sample build in a different direction, we believe that the demonstrated method provides results that are applicable also for complex mesh structures.

The advantage of truss structure based on simple shape interconnecting elements is, that the properties of the whole construct could be derived from the unit cell. We have shown, that in designing the optimal unit cell, the directions of individual elements should be taken into account.

6.2 Compressive behavior of pure titanium porous structures

In this study, cubical samples compressive static behavior is quite similar to *L.J. Gibson et al., 1997* research [23]. It was observed that plastic deformation collapse on the plateau level and then at the end of the plateau level stress increases rapidly. The mechanical performance of cellular structures is dependent on factors such as cell topology; the number of cells; geometric parameters, including strut diameter and cell size; material and manufacturing process characteristics; as well as structural boundary and loading conditions [109]. Figure 5.12 illustrates that there is a distribution on the plateau stress level due to stuck powder effect. It affects the deformation of unit cell since there is not any cleaning operation was carried out, Figure 6.1. On the other hand, previously it was explained that the building direction of the struts effects its mechanical performance.
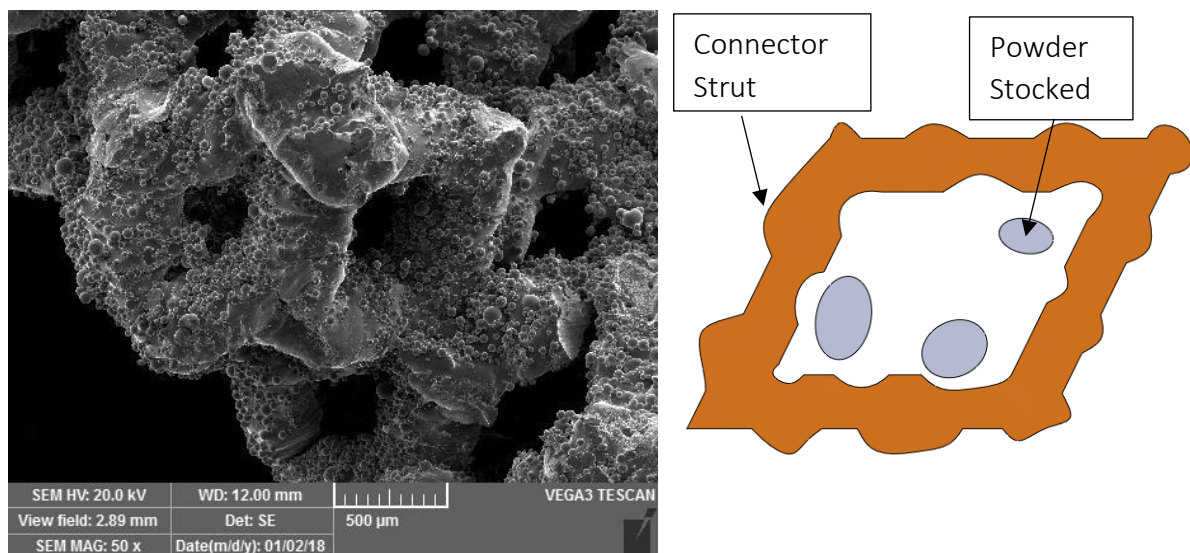

Figure 6.1 Connector strut review and schema of stocked powders

The pure titanium is widely used in biomedical engineering, especially implant industry due to outstanding biocompatible performance. *X.Y. Cheng et al., 2012* [110] studied the elastic modulus of pure titanium can be closer to bone properties. In our research, we also confirmed that porous pure titanium means the elastic module is 1.54 GPa which could be well matched for bone replacement for damaged part since bone elastic modulus is in the range of 0.5-15 GPa. It is quite vital that porous replacement parts density and elastic modulus could decrease stress shielding and extend the life of implants.

Surface treatment affects mechanical properties dramatically and, It is quite necessary for toxicology aspects. It can clean un-melted powders and decrease titanium powder release.

Figure 4.24 shows the effect of surface treatment on the connector struts. Surface roughness can be decreased dramatically by the time of the etching process. It decreases the deformed particles releasing into the body under the compression load. Elastic gradient decrease affectedly with surface treatment. The roughness of the struts gets the beam shape after etching process. Time of the etching process can lower thickness value 1.36% on the average. This thinning operation would affect slightly better for cross-sectional area, Figure 4.25. The highest elastic modulus and yield strength can be achieved with as-built samples. However, as-built samples contain un-melted titanium particles which might be released into the body during the compressive deformation. Titanium accumulation is quite dangerous for the liver and kidney [111]. Even if a small amount of titanium ion accumulation could harm to vital organs such as the liver. Releasing titanium particles can lead to critical conditions. Although, surface etching lower porous structure mechanical performance, it can still be a great match for bone mechanical properties and decrease the stress shielding if it is compared to the solid titanium implant.

6.3 Post-treatment effect on titanium alloy porous structure

Open-cell porous structure mechanical properties would affect bone interaction for orthopedic applications [112]. SLM manufactured components universal performance can be modified with post-treatment technique. HIP treatment was used for reducing internal defects and stress realising which help to improve mechanical response. Surface treatment was used for cleaning partly melted powder and preventing any toxicology outcomes in orthopaedic use [113]. In this study, it is shown that regular porous structure mechanical response was affected by surface and HIP treatment. The surface treatment by chemical etching was used for cleaning partly melted powder, while the HIP treatment reduced internal porosity [114][115][116].

Strut thickness and cross-sectional area can influence the mechanical performance of open-cell porous structure[110]. During the compression loading, the consistent structure provides uniform deformation which means that equivalent connector struts deal with a similar loading. The perfect porous structure should provide stable mechanical properties with small scattering between samples. Despite rough structure in as-build samples (Figure 4.28), they provide low variation between the samples. The surface etching smooths surfaces but adds imperfections in struts diameters that increase variations between the samples.

The effectiveness of surface etching degree can be influenced by post-processing. Surface treatment can erode for 3.7% more in the samples with HIP treatment (SHITS6T) than in the samples without HIP treatment (SWS6T), Table 5.4. A similar trend can be observed in overall porous samples dimensions, Figure 5.22.

It was shown by Song et al., 1999 [117] and Oh et al., 2003 [118], that internal defects has a negative impact on the elastic modulus of solid structure. We have observed similar behavior also for porous structure. The highest elastic gradient was observed in the group had the HIP treatment and it is 5% higher than as-built porous samples.

The HIP process is further able to eliminate the internal defect and decrease the residual stress which can improve ductility behavior [119]. Also, this effect could be observed in the porous samples within this study. The effect of HIP treatment is not due to the reduction of internal defects only but it also delivers more uniform microstructure for solid component [115].

As-built samples (SNHHTNS) have the highest compressive proof stress with 38.70 MPa respectively on the average. HIP treatment Samples (SWHET) have a slightly lower value than the as-built group (SWHET) with 0.3%. HIP process tends to have a negative effect on compressive proof stress and the similar result was found in the Hrabe et al., 2016 study [120].

First maximum stress result of porous samples follow the same trend as compressive proof stress, Figure 5.24 and Figure 5.25. The highest first maximum stress values were found in the as-built samples groups (SNHHTNS). HIP treatment lowered porous structure first maximum stress by 7%. HIP process decreases the internal defects and provide higher elongation however, it reduces first maximum and compressive proof stress due to microstructure coarsening [121].

Level of surface treatment affects mechanical performance due to the fact that strut thickness diameter is decreased by surface etching and this technique can be also used to create hybrid porous component with different relative density [131]. As-built samples with 6-minute surface treatment (SWS6T) has the lowest elastic modulus with 1.23 GPa respectively on the average. Sample with both HIP and surface treatment has still higher elastic modules than as-built samples with surface treatment, Figure 4.26. Compressive proof stress can be decreased by surface etching. 6-minute surface treatment can reduce compressive proof stress by 25%.

Sample with HIP and 6-minute etching (SHITS6T) has the lowest value 28.49 MPa respectively on the average.

Mechanical properties of porous samples with surface treatment and HIP can be a good match with bone mechanical properties. Close mechanical properties of bone and porous structure would decrease the stress shielding which can extend the lifetime of the implant [122]. Surface etching also provides the excellent clean product which is crucial for biomedical applications. Preventing the release of titanium particles from the implant is crucial for any biomedical application, Heringa et al., 2018 study shows that titanium accumulation in the human body can damage liver [111]. Woodman et al., 1984 research also shows ion release from titanium-based implants effect and damage to human vital organs, namely liver, and kidney [123]. It was suggested that separation of any un-melted powder from the porous structure would lead to critical liver failure [124] and therefore surface treatment is highly recommended for the commercial orthopedic product.

The results of the study indicate the effect of HIP and surface etching on mechanical properties of porous samples. However, there are also other factors that should be considered in a biomedical application. In this study, the investigation was carried out with static compression test in the air however, porous structure in the human body is supposed to deal with dynamic loading in blood-like material and body fluids environment. The fluids and cells penetrate the structure and it may affect the corrosions of the implant [107]. The in-vivo environment could increase the porous structure density and strength with interpenetrating phase composites effect.
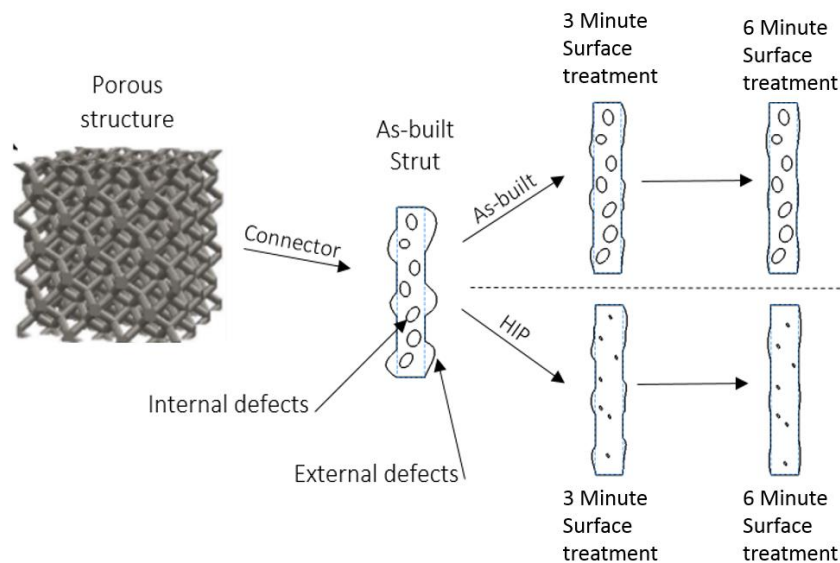
Figure 6.2 Post-treatment effect on titanium alloy porous structure

Figure 6.2 illustrates the work flow of the post-treatment, the HIP process can reduce internal defect and surface treatment can deduct external defects.

6.4 Analytic and numerical approach of porous 2D structure

Metallic open cell foam can be simplified as honeycombs for the 2D approach. Man-made honeycombs can be seen in different industries. It can be found in nature where structures have to deal with a different type of loading. Understanding the mechanical properties of cellular solids can lead to improved materials design and performance. Open cell 2D geometrical model was developed for analytic and numerical approach according to *Gibson and Ashby et. Al.*, 1997 [125] research.

In this study, unit cell mechanical analytic and numerical behavior were compared. The computational investigation was carefully carried out for complex 2D structure. Models were developed for without units for understanding to the comparison.

Elastic modulu and yield strength compared for unit cell development for both analytic and numerical approach. Finite element analysis result for elastic gradient was calculated in x- and y-direction. It was expected that Ex and Ey have to be equal. In our calculation, there was 0.4% difference occurred. This is still satisfied result to carry out 2D complex numerical calculation.

2D complex geometrical model consists of dry connectors during the numerical calculation, Figure 4.9. Honeycombs or trabecular shape do not always have regular order, in nature there plenty of example of irregular honeycombs. It is shown that Von-Mises stress concentration can be adjusted by the order of open-cell organization. It may also help to improve the fundamental idea of changing the highest stress location.

SLM laser beam follows the hatching path to melt the metal powder. It creates the component layer by layer, in some cases, laser can miss the pattern and create a missing connector. The similar scenario can be faced with software collapse. Each case, the highest stress concentration can change the location, Figure 6.3.
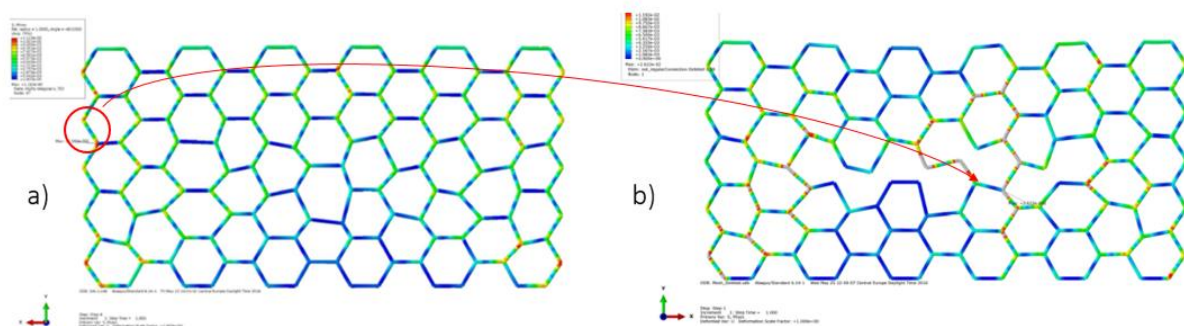
Figure 6.3 Irregular 2D honeycombs stress distribution a) irregular honeycombs and b) irregular missing strut honeycombs [62]

6.5 Analytic and numerical approach of porous 3D structure

The analytical solution for the elastic properties of a rhombic dodecahedron was calculated with unit-cell approach. We derive analytical relationships for the effective mechanical properties of an open rhombic dodecahedron unit cell and tessellated cellular structure with periodic boundary conditions using fundamental concepts of mechanics of materials (small enough deformations). We present analytical models to calculate the effective elastic-plastic properties of a rhombic dodecahedron unit cell and periodic tessellated cellular structure. The cell edge material behavior was taken as elastic and comprised the elastic modulus and yield strength [126].

Babaee et. al., 2012 [76] shows that bulk material definition was used widely for the analytic approach of struts mechanical properties. Our previous studies show that AM strut size and orientation has an influence on mechanical properties significantly.

Analytic investigation and mechanical test of elastic modulus difference is 28%. *Babaee et. al.,* 2012 used bulk material properties in his calculation. However, powder type also can change the elastic module. Another effect is that SLM machine accuracy, the analytic calculation was planned for designed diameters with smooth connectors however, in printed samples connectors slightly bigger and contains surface roughness. It may also change the cross-sectional area and load bearing diameter.

Finite element models of both unit cell and tessellated cellular structures was developed and used them to establish the validity of the analytical models. The elastic properties and yield strength of the cellular structure were calculated from the force-displacement response of the structure in each basic loading direction. The effective elastic modulus is the initial slope of the response.

Elastic modulus of analytic calculation 57% difference than numerical calculation. Elasticity and plasticity data were used from our previous study during the calculation. This difference can be caused by the mathematical model contact accuracy which can be improved. Deformation behaviour and collapse area are quite similar to mechanical testing, there is still 75% elastic modules difference remaining.

The mathematical model is developed and executed according to the same procedure of mechanical test and analytic calculation. However, material data input plays a crucial role during the calculation. Single strut mechanical properties were used for finite element approach, result present that single porous structure mechanical behaviour quite homogenous even though single struts mechanical properties are depending on building orientation and their size.

6.6 Mechanical response of titanium alloy porous structure under dynamic loading

Orthopaedic metal implant is surrounded by tissue fluid during the stay in the human body. The in-vivo system contains water, complex organic compounds, dissolved oxygen, sodium, chloride, bicarbonate, potassium, calcium, magnesium, phosphate, amino acids, proteins, plasma, lymph, saliva [127]. Although porous samples were tested in the air in the literature, commercial porous implants seldom bear with compressive load in the human body condition and it can be either dynamic or quasi-static [116][117].

Previous studies focus dynamic test on aluminum foam and its energy absorption capability since the automotive industry widely use foams for good impact force performance [130]. In this experiment high speed (2m/s) impact test was carried out for impact force and energy absorption performance of porous titanium alloy and applied post-treatment methods. The same testing method was applied in blood like material (BLM) and water as well in order to mimic human body condition. Dynamic impact force results were very similar for porous sample in air, water, and blood like material, Figure 6.5. It is shown that an experiment can be carried out in the air since impact force results in liquid environments can be tolerated. On the other hand, the dynamic test stress-strain diagram shows that stress trend of porous structure in the air very similar to test in water and blood like material, Figure 6.4. Current research shows that mechanical tests can be carried out in the air for porous structures.
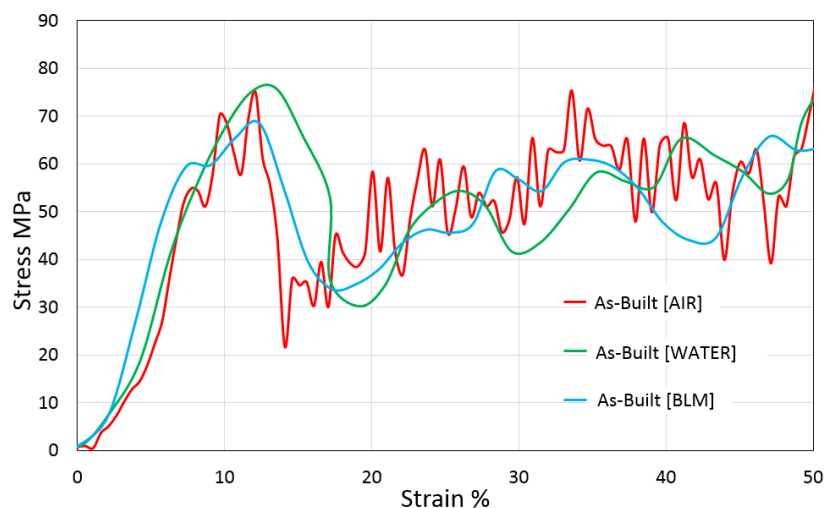
Figure 6.4 Stress-Strain diagram of dynamic compression test for as-built sample

In addition, post-treatment method also has an effect on the mechanical performance of the dynamic test. As it was mentioned in previous sections, surface etching tends to decrease strut diameter and density as a result of that load bearing area is decreased. On the other hand, behaviour of the porous structure with surface etching very similar to as-built samples. Eroding sample can increase the pore size however, it still acts as an open-cell regular structure.
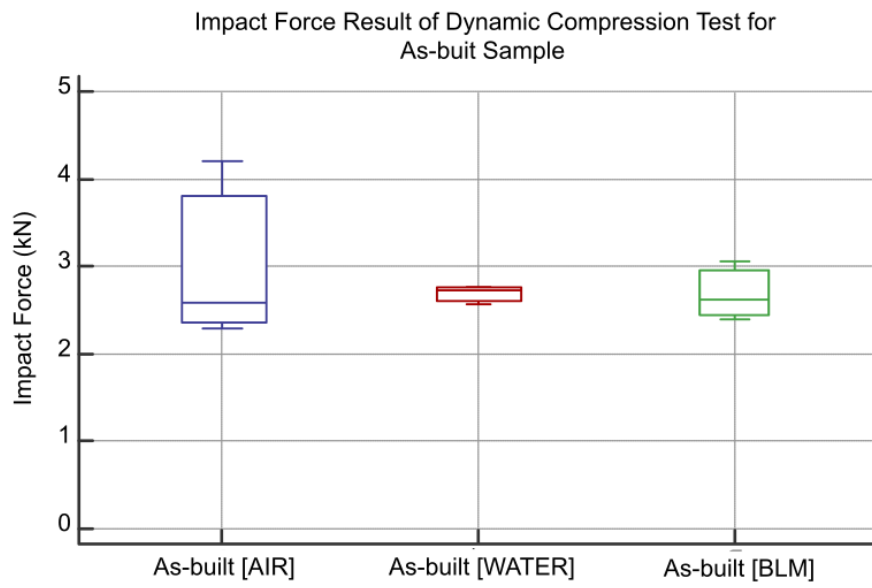
Figure 6.5 Impact force result of dynamic compression test for as-built sample

Chapter 7: Conclusion

Additive manufacturing (AM) does not only provide design freedoms or low-density components, but it also helps to develop regular porous surface. AM porous structure mechanical properties are influenced by manufacturing set-up, material, mesh architecture and post treatments. Improving mechanical properties of AM porous surface of orthopedic implant can increase bone integration and decrease implant loosening. In this study, the mechanical response of porous structure was investigated intensively with the approach of mesh architecture, post-treatment methods, and material consideration.

Connectors or struts are core elements of the open cell porous structure and they have a different orientation in the cellular architecture. It has been experimentally shown in this study, single strut properties were affected by the size and building orientation. The building orientation direction effect is much less pronounced in larger samples [84]. Single strut mechanical properties have been used for analytic and numerical calculation since previous studies were designed by using bulk material data. We can conclude that material properties definition plays a vital role in analytical and numerical calculation approach. Predicting the mechanical properties of porous structure has been challenging since strut material definition can be decisive. Quasi-static tests showed that mechanical responses of porous samples manufactured from two different suppliers had different results even though the same pure titanium powder were used.

In this research, conventional and new post-treatment methods have been used for improving porous structure functional properties for biomedical application. Surface etching decreases the strut diameter dramatically. On the other hand, it helps to prevent porous structure struts together under the compressive deformation. This feature can be enchanted with HIP treatment as well. Although compromising the strength of porous structure is inevitable but it is still suitable for orthopedic biomedical applications [66].

Porous structure dynamic test was carried out in air, water, and blood like material since titanium cellular structure frequently interacts with body fluid. We show that dynamic test result of porous structure in the air was very similar to water and blood like material environment. It shows that future mechanical test can be carried out in air conditions.

To conclude, the building orientation and geometrical accuracy of AM are one of the parameters that should be considered the design of the complex truss porous structures. The surface etching is a suitable method for post-processing of the porous structure [66]. In this study, we have also shown that HIP treatment is not significantly effective for porous structure mechanical properties.

List of Tables

List of Figures

Bibliography

[1]   WANG, Xiaojian, Shanqing XU, Shiwei ZHOU, Wei XU, Martin LEARY, Peter CHOONG, M. QIAN, Milan BRANDT a Yi Min XIE. Topological design and additive manufacturing of porous metals for bone scaffolds and orthopaedic implants: A review. *Biomaterials* [online]. 2016, **83**, 127–141. ISSN 18785905. Dostupné z: doi:10.1016/j.biomaterials.2016.01.012

[2]   HAGEDORN, Y. Laser additive manufacturing of ceramic components. In: *Laser Additive Manufacturing* [online]. B.m.: Elsevier, 2017, s. 163–180. ISBN 9780081004340. Dostupné z: doi:10.1016/B978-0-08-100433-3.00006-3

[3]   MULLEN, Lewis, Robin C. STAMP, Wesley K. BROOKS, Eric JONES a Christopher J. SUTCLIFFE. Selective laser melting: A regular unit cell approach for the manufacture of porous, titanium, bone in-growth constructs, suitable for orthopedic applications. *Journal of Biomedical Materials Research - Part B Applied Biomaterials* [online]. 2009, **89**(2), 325–334. ISSN 15524973. Dostupné z: doi:10.1002/jbm.b.31219

[4]   A.CHAMAY a P.TSCHANTZ. Mechanical influences in bone remodeling. Experimental research on Wolff's law. *Journal of Biomechanics* [online]. 1972, **5**(2), 173–180. ISSN 00219290. Dostupné z: doi:10.1016/0021-9290(72)90053-X

[5]   BIGERELLE, M. a K. ANSELME. A kinetic approach to osteoblast adhesion on biomaterial surface. *Journal of Biomedical Materials Research - Part A* [online]. 2005, **75**(3), 530–540. ISSN 15493296. Dostupné z: doi:10.1002/jbm.a.30473

[6]   HOLLISTER, S J. Porous scaffold design for tissue engineering. *Nature Materials* [online]. 2005, **4**(7), 518–524. ISSN 1476-1122. Dostupné z: doi:10.1038/nmat1421

[7]   BOMBAČ, David, Miha BROJAN, Peter FAJFAR, Franc KOSEL a Rado TURK. Review of materials in medical applications. *RMZ – Materials and Geoenvironment* [online]. 2007, **54**(54), 471–499. Dostupné z: http://www.rmz-mg.com/letniki/rmz54/RMZ54_0471-0499.pdf

[8]   ELIAS, C. N., J. H C LIMA, R. VALIEV a M. A. MEYERS. Biomedical applications of titanium and its alloys. *Jom* [online]. 2008, **60**(3), 46–49. ISSN 10474838. Dostupné

z: doi:10.1007/s11837-008-0031-1

[9]   WIEDING, Jan, Anika JONITZ a Rainer BADER. The effect of structural design on mechanical properties and cellular response of additive manufactured titanium scaffolds. *Materials* [online]. 2012, **5**(8), 1336–1347. ISSN 19961944. Dostupné z: doi:10.3390/ma5081336

[10]   DO, Dang Khoa a Peifeng LI. The effect of laser energy input on the microstructure , physical and mechanical properties of Ti-6Al-4V alloys by selective laser melting [online]. 2016, **2759**(March). Dostupné z: doi:10.1080/17452759.2016.1142215

[11]   OKAZAKI, Yoshimitsu, Yoshimasa ITO, Kenj KYO a Tetsuya TATEISHI. Corrosion resistance and corrosion fatigue strength of new titanium alloys for medical implants without V and Al. *Materials Science and Engineering A* [online]. 1996, **213**(1–2), 138–147. ISSN 09215093. Dostupné z: doi:10.1016/0921-5093(96)10247-1

[12]   VAN BAEL, S., Y. C. CHAI, S. TRUSCELLO, M. MOESEN, G. KERCKHOFS, H. VAN OOSTERWYCK, J. P. KRUTH a J. SCHROOTEN. The effect of pore geometry on the in vitro biological behavior of human periosteum-derived cells seeded on selective laser-melted Ti6Al4V bone scaffolds. *Acta Biomaterialia* [online]. 2012, **8**(7), 2824–2834. ISSN 17427061. Dostupné z: doi:10.1016/j.actbio.2012.04.001

[13]   ZADPOOR, Amir A. Bone tissue regeneration: The role of scaffold geometry. *Biomaterials Science* [online]. 2015, **3**(2), 231–245. ISSN 20474849. Dostupné z: doi:10.1039/c4bm00291a

[14]   DZUGAN, J., M. SEIFI, R. PROCHAZKA, M. RUND, P. PODANY, P. KONOPIK a J. J. LEWANDOWSKI. Effects of thickness and orientation on the small scale fracture behaviour of additively manufactured Ti-6Al-4V. *Materials Characterization* [online]. 2018, **143**(February), 94–109. ISSN 10445803. Dostupné z: doi:10.1016/j.matchar.2018.04.003

[15]   ATTAR, H, M CALIN, L C ZHANG, S SCUDINO a J ECKERT. Materials Science & Engineering A Manufacture by selective laser melting and mechanical behavior of commercially pure titanium. *Materials Science & Engineering A* [online]. 2014, **593**, 170–177. ISSN 0921-5093. Dostupné z: doi:10.1016/j.msea.2013.11.038

[16]   SERCOMBE, T B, X LI, T B SERCOMBE a X LI. Selective laser melting of aluminium and aluminium metal matrix composites : review Selective laser melting of aluminium and aluminium metal matrix composites : review [online]. 2016, **7857**(May). Dostupné z: doi:10.1179/1753555715Y.0000000078

[17]   MOMBELLI, Andrea, Dena HASHIM a Norbert CIONCA. What is the impact of titanium particles and biocorrosion on implant survival and complications ? A critical review [online]. 2018, **29**(March), 37–53. Dostupné z: doi:10.1111/clr.13305

[18]   JOSEF, Hlinka, Kvíčala MIROSLAV a Lasek STANISLAV. CORROSION PROPERTIES OF POROUS TITANIUM SINTERES WITH SODIUM CHLORIDE. In: *24th International Conference on Metallurgy and Materials 2015 Brno, Czech Republic, EU*. 2015, s. 3–8.

[19]   FRISKEN, K W, G W DANDIE, S LUGOWSKI a G JORDAN. A study of titanium release into body organs following the insertion of single threaded screw implants into the mandibles of sheep. *Australian Dental Journal*. 2002, (3), 214–217.

[20]   Ã, Lorna J Gibson. Biomechanics of cellular solids. *Journal of Biomechanics* [online]. 2005, **38**, 377–399. Dostupné z: doi:10.1016/j.jbiomech.2004.09.027

[21]   GIBSON, L.J. The mechanical behaviour of cancellous bone. *Journal of Biomechanics* [online]. 1985, **18**(5), 317–328. ISSN 00219290. Dostupné z: doi:10.1016/0021-9290(85)90287-8

[22]   GIBSON, Lorna J. *Cellular Solids : Structure , Properties and Applications*. nedatováno.

[23]   OPPENHEIMER, Scott a David C. DUNAND. Solid-state foaming of Ti-6A1-4V by creep or superplastic expansion of argon-filled pores. *Acta Materialia* [online]. 2010, **58**(13), 4387–4397. ISSN 13596454. Dostupné z: doi:10.1016/j.actamat.2010.04.034

[24]   GIBSON, L.J. a M F ASHBY. *Cellular Solids Structure and Properties*. B.m.: Cambridge University Press, 1999.

[25]   CAMPBELL, JE. *Metal and polymer foam hybrid materials: Design, fabrication and analysis*. B.m., 2009. University of Toronto.

[26]   RODR, A, A RUSINEK, R KLEPACZKO a B PE. *Materials and Design* [online]. 2009. ISBN 9780080982052. Dostupné z: doi:10.1016/j.matdes.2008.09.043

[27] IAN GIBSON, David ROSEN a BRENT STUCKER. *Additive Manufacturing Technologies* [online]. Second Edi. B.m.: ASTM International, 2013. ISBN 9781493921126. Dostupné z: doi:10.1520/F2792-12A.2

[28] SLOTWINSKI, J. A., P. E. STUTZMAN, C. F. FERRARIS, S. S. WATSON, M. A. PELTZ a E. J. GARBOCZI. Physical and chemical characterization techniques for metallic powders. *AIP Conference Proceedings* [online]. 2014, **1581 33**(January), 1178–1183. ISSN 15517616. Dostupné z: doi:10.1063/1.4864954

[29] CAFFREY, Tim, Terry WOHLERS a R.I. CAMPBELL. *Executive summary of the Wohlers Report 2016* [online]. 2016. Dostupné z: https://dspace.lboro.ac.uk/dspace-jspui/bitstream/2134/21223/1/Wohlers Report 2016 Executive Summary.pdf

[30] BADIRU, Adedeji B., Vhance V. VALENCIA a David LIU. *Additive Manufacturing Handbook: Product Development for the Defense Industry* [online]. B.m.: CRC Press, 2017. ISBN 9781351645393. Dostupné z: doi:10.1201/9781315119106

[31] BERNARD, Alain a A. FISCHER. New trends in rapid product development. *CIRP Annals - Manufacturing Technology* [online]. 2002, **51**(2), 635–652. ISSN 00078506. Dostupné z: doi:10.1016/S0007-8506(07)61704-1

[32] MURR, Lawrence E, Sara M GAYTAN, Diana A RAMIREZ, Edwin MARTINEZ, Jennifer HERNANDEZ, Krista N AMATO, Patrick W SHINDO, Francisco R MEDINA a Ryan B WICKER. • Invited Review Metal Fabrication by Additive Manufacturing Using Laser and Electron Beam Melting Technologies. *Journal of Materials Science & Technology* [online]. 2012, **28**(1), 1–14. ISSN 1005-0302. Dostupné z: doi:10.1016/S1005-0302(12)60016-4

[33] HEDIN, Oscar. *Production Technology for Additive Manufacturing The Arcam EBM ® process: A walkthrough* [online]. 2012. Dostupné z: http://www.omtecexpo.com/images/stories/Oscar_Hedin_OMTEC_Presentation.pdf

[34] ASTM INTERNATIONAL. F2792-12a - Standard Terminology for Additive Manufacturing Technologies. *Rapid Manufacturing Association* [online]. 2013, 10–12. ISSN 1882-675X. Dostupné z: doi:10.1520/F2792-12A.2

[35] SIDAMBE, Alfred T. Biocompatibility of advanced manufactured titanium implants-A review. *Materials* [online]. 2014, **7**(12), 8168–8188. ISSN 19961944. Dostupné z: doi:10.3390/ma7128168

[36] VAYRE, Benjamin, Frédéric VIGNAT a François VILLENEUVE. Metallic additive manufacturing: state-of-the-art review and prospects. *Mechanics & Industry* [online]. 2012, **13**(2), 89–96. ISSN 2257-7777. Dostupné z: doi:10.1051/meca/2012003

[37] ALIAKBARI, Mina. *Additive Manufacturing: State-of-the-Art, Capabilities, and Sample Applications with Cost Analysis*. B.m., 2012. KTH.

[38] OSAKADA, Kozo a Masanori SHIOMI. Flexible manufacturing of metallic products by selective laser melting of powder. *International Journal of Machine Tools and Manufacture* [online]. 2006, **46**(11 SPEC. ISS.), 1188–1193. ISSN 08906955. Dostupné z: doi:10.1016/j.ijmachtools.2006.01.024

[39] LEVY, a.B. Spierings; K. Wegener; G. Designing Material Properties Locally with Additive Manufacturing technology SLM. *Sff 2012* [online]. 2012, 447–455. Dostupné z: doi:https://doi.org/10.3929/ethz-a-010335595

[40] BUGEDA, Gabriel, Miguel CERVERA a Guillermo LOMBERA. Numerical prediction of temperature and density distributions in selective laser sintering processes. *Rapid Prototyping Journal Rapid Prototyping Journal* [online]. 1999, **5**(1), 21–26. ISSN 13552546 (ISSN). Dostupné z: doi:10.1108/13552549910251846

[41] RIGO, Olivier a Carsten ENGEL. *Selective Laser Melting versus Electron Beam Melting*. 2013.

[42] GIBSON, Ian, David ROSEN a Brent STUCKER. *F2792-12a - Standard Terminology for Additive Manufacturing Technologies* [online]. B.m.: ASTM International, 2013. ISBN 9781493921126. Dostupné z: doi:10.1520/F2792-12A.2

[43] STRATASYS. *Five Ways 3D Printing Is Transforming the Automotive Industry* [online]. nedatováno. Dostupné z: https://www.stratasys.com/-/media/files/white-papers-new/wp_du_fivewaysauto.pdf

[44] JARDINI, André Luiz, Maria Aparecida LAROSA, Rubens Maciel FILHO, Cecília Amélia De

Carvalho ZAVAGLIA, Luis Fernando BERNARDES, Carlos Salles LAMBERT, Davi Reis CALDERONI a Paulo KHARMANDAYAN. Cranial reconstruction: 3D biomodel and custom-built implant created using additive manufacturing. *Journal of Cranio-Maxillofacial Surgery* [online]. 2014, **42**(8), 1877–1884. ISSN 18784119. Dostupné z: doi:10.1016/j.jcms.2014.07.006

[45] HAFEZ, Mahmoud. Custom-Made Cutting Guides for Total Knee Arthroplasty. *Joint Replacement and Its Alternatives* [online]. 2012, (July), 1240–1254. Dostupné z: doi:10.1016/b978-1-4377-1503-3.00153-0

[46] BYROM, Richard. William Fairbairn, Karl Culmann and the Origin of Wolff's Law. *The International Journal for the History of Engineering & Technology* [online]. 2014, **84**(1), 52–58. ISSN 1758-1206. Dostupné z: doi:10.1179/1758120613z.00000000036

[47] MILLIS, Darryl L. *Responses of Musculoskeletal Tissues to Disuse and Remobilization* [online]. Second Edi. B.m.: Elsevier Inc., 2004. ISBN 9780721695556. Dostupné z: doi:10.1016/B978-0-7216-9555-6.50011-5

[48] PENG, Liang, Jing BAI, Xiaoli ZENG a Yongxin ZHOU. Comparison of isotropic and orthotropic material property assignments on femoral finite element models under two loading conditions. *Medical Engineering and Physics* [online]. 2006, **28**(3), 227–233. ISSN 13504533. Dostupné z: doi:10.1016/j.medengphy.2005.06.003

[49] WYCISK, Eric, Claus EMMELMANN, Shafaqat SIDDIQUE a Frank WALTHER. High Cycle Fatigue (HCF) Performance of Ti-6Al-4V Alloy Processed by Selective Laser Melting. *Advanced Materials Research* [online]. 2013, **816–817**(September), 134–139. ISSN 1662-8985. Dostupné z: doi:10.4028/www.scientific.net/AMR.816-817.134

[50] LEICHT, Alexander; a Elon Oskar WANNBERG. *Analyzing the Mechanical Behavior of Additive Manufactured Ti-6Al-4V Using Digital Image Correlation Analyzing the Mechanical Behavior of Additive Manufactured Ti-6Al-4V Using Digital Image Correlation*. B.m., 2015. CHALMERS UNIVERSITY OF TECHNOLOGY.

[51] BOBYN, J. D., G. J. STACKPOOL, S. A. HACKING, M. TANZER a J. J. KRYGIER. Characteristics of bone ingrowth and interface mechanics of a new porous tantalum biomaterial. *The Journal of Bone and Joint Surgery* [online]. 1999, **81**(5), 907–914.

ISSN 00000000. Dostupné z: doi:10.1302/0301-620X.81B5.9283

[52]   E.PEHLIVAN, M. ROUDNICKA, J.DZUGAN, V. KRÁLÍK, V.DALIBOR, M.SEIFI, J. LEWADOWSKID a M. DANIEL. Effect of build orientation and geometry on the mechanical response of tiny wire samples manufactured by selective laser melting Eren Pehlivan. *Additive Manufacturing(In-Reviewing)*. 2018, 1–21.

[53]   CONCEPT LASER. *CL 42TI Commercially Pure Titanium-Material data* [online]. nedatováno.   Dostupné   z: https://www.ge.com/additive/sites/default/files/2018-12/CLMAT_42Ti_DS_EN_US_2_v1.pdf

[54]   VRANCKEN, Bey, Lore THIJS, Jean Pierre KRUTH a Jan VAN HUMBEECK. Heat treatment of Ti6Al4V produced by Selective Laser Melting: Microstructure and mechanical properties. *Journal of Alloys and Compounds* [online]. 2012, **541**, 177–185. ISSN 09258388. Dostupné z: doi:10.1016/j.jallcom.2012.07.022

[55]   CONCEPT LASER. *M2 cusing Metal laser melting system* [online]. 2018. Dostupné z: www.ge.com/additive

[56]   TER HAAR, Gerrit M. a Thorsten H. BECKER. Selective laser melting produced Ti-6-Al-4V: Post-process heat treatments to achieve superior tensile properties. *Materials* [online]. 2018, **11**(1). ISSN 19961944. Dostupné z: doi:10.3390/ma11010146

[57]   ASTM WK49229. *Standard Guide for Orientation and Location Dependence Mechanical Properties for Metal Additive Manufacturing*. 2017

[58]   ASTM E8-Standard Test Methods for Tension Testing of Metallic Materials. *ASTM International* [online]. 2012, **946**, 133–140. ISSN 16130073. Dostupné z: doi:10.1520/E0008_E0008M-13A

[59]   *COMTES FHT Company presentation* [online]. 2012. Dostupné z: https://www.comtesfht.com/media/document/comtes-fht-presentation-en-2013-05-1.pdf

[60]   REDLUX. *Case Study : Rush University Medical Center Figuring Out Why Artificial Joints Fail* [online]. 2016. Dostupné z: https://secure.toolkitfiles.co.uk/clients/19010/sitedata/PDFs/Reference-Rush-

University-20170503.pdf

[61]   GÁLVEZ, Oscar Efraín Sotomayor a A. *Numerical Modeling of Random 2D and 3D Structural Foams Using Voronoi Diagrams : A Study of Cell Regularity and Compression Response*. B.m., 2013. Auburn Universit.

[62]   PEHLIVAN, Eren. Cellular Material Fatigue Estimation And Development. *Student's conference Czech Technical University in Prague | Faculty of Mechanical Engineering layer*. 2017, 1-6.

[63]   ZEIN, Iwan, Dietmar W HUTMACHER, Kim Cheng TAN a Swee Hin TEOH. Fused deposition modeling of novel scaffold architectures for tissue engineering applications. *Biomaterials* [online]. 2002, **23**(4), 1169–1185. ISSN 01429612. Dostupné z: doi:10.1016/S0142-9612(01)00232-0

[64]   PEHLIVAN, Eren. Porosity Structure Fatigue Estimation And Improvement. *20th Workshop Of Applied Mechanics 2016 Prague, June 10th 2016, Czech Republic*. 2016.

[65]   VAJJHALA, Surek. *Finite Element Analysis of Voronoi Cellular Solids*. B.m., 1996. Massachusetts Institute of Technology.

[66]   E.PEHLIVAN, J.DZUGAN, R.SEDLACEK, J.FOJT, J.LEWADOWSKID, M.SEIFI a M.DANIEL. AM porous structures compressive mechanical behaviour after HIP and surface treatment Eren Pehlivan. *Materials Science and Engineering: C (in-reviewing)*. 2019, 1–18.

[67]   ISO 13314 Mechanical testing of metals Ductility testing Compression test for porous and cellular metals. *International Standard ISO* [online]. 2011, **2011**. Dostupné z: http://118.144.34.51/zqyj/201311/P020131111349407278750.pdf

[68]   GONG, Haijun, Khalid RAFI, Hengfeng GU, Thomas STARR a Brent STUCKER. Analysis of defect generation in Ti-6Al-4V parts made using powder bed fusion additive manufacturing processes. *Additive Manufacturing* [online]. 2014, **1**, 87–98. ISSN 22148604. Dostupné z: doi:10.1016/j.addma.2014.08.002

[69]   DOUBENSKAIA, M., D. KOTOBAN a I. ZHIRNOV. Study of oxygen effect on the melting pool temperature during selective laser melting. *Mechanics & Industry* [online]. 2016,

17(7), 707. ISSN 2257-7777. Dostupné z: doi:10.1051/meca/2016067

[70]   LTD, OSAKA Titanium technologies Co. *OTC Titanium Powder data sheet* [online]. Dostupné z: http://www.osaka-ti.co.jp/e/e_product/development/hunmatu.html

[71]   NIINOMI, Mitsuo. Mechanical properties of biomedical titanium alloys. *Materials Science and Engineering: A* [online]. 2002, **243**(1–2), 231–236. ISSN 09215093. Dostupné z: doi:10.1016/s0921-5093(97)00806-x

[72]   ENGH, C A, J D BOBYN a A H GLASSMAN. Porous Coated Hip Replacement - Factors Governing Bone In-growth, Stress Shielding and Clinical Results. 1987, **69**(1).

[73]   NAGELS, Jochem, Mariëlle STOKDIJK a Piet M ROZING. Stress shielding and bone resorption in shoulder arthroplasty. Journal of Shoulder and Elbow Surgery [online]. 2003, **12**(1), 35–39. ISSN 10582746. Dostupné z: doi:10.1067/mse.2003.22

[74]   CONCEPTLASER. *Titanium alloy grade 23 CL 41TI ELI* [online]. nedatováno. Dostupné z: https://www.ge.com/additive/sites/default/files/2018-12/CLMAT_41TI ELI_DS_EN_US_2_v1.pdf

[75]   MEDING, John B, Scott R Small MS, Mary E JONES, Michael E BEREND a Merrill A RITTER. Acetabular Cup Design Influences Deformational Response in Total Hip Arthroplasty. *ClinicalOrthopaedics and Related Research* [online]. 2013, 403–409. Dostupné z: doi:10.1007/s11999-012-2553-7

[76]   BABAEE, Sahab, Babak Haghpanah JAHROMI, Amin AJDARI, Hamid NAYEB-HASHEMI a Ashkan VAZIRI. Mechanical properties of open-cell rhombic dodecahedron cellular structures. *Acta Materialia* [online]. 2012, **60**(6–7), 2873–2885. ISSN 13596454. Dostupné z: doi:10.1016/j.actamat.2012.01.052

[77]   HEDAYATI, R., M. SADIGHI, M. MOHAMMADI-AGHDAM a A. A. ZADPOOR. Effect of mass multiple counting on the elastic properties of open-cell regular porous biomaterials. *Materials and Design* [online]. 2016, **89**, 9–20. ISSN 18734197. Dostupné z: doi:10.1016/j.matdes.2015.09.052

[78]   AHMADI, Seyed Mohammad, Saber Amin YAVARI, Ruebn WAUTHLE, Behdad POURAN, Jan SCHROOTEN, Harrie WEINANS a Amir A. ZADPOOR. Additively manufactured open-

cell porous biomaterials made from six different space-filling unit cells: The mechanical and morphological properties. *Materials* [online]. 2015, **8**(4), 1871–1896. ISSN 19961944. Dostupné z: doi:10.3390/ma8041871

[79] ZADPOOR, Amir Abbas a Reza HEDAYATI. Analytical relationships for prediction of the mechanical properties of additively manufactured porous biomaterials. *Journal of Biomedical Materials Research - Part A* [online]. 2016, **104**(12), 3164–3174. ISSN 15524965. Dostupné z: doi:10.1002/jbm.a.35855

[80] MICHAEL SCHEFFLER, Paolo Colombo. *Cellular Ceramics Structure, Manufacturing, Properties and Applications Edited*. 2005. ISBN 9783527313204.

[81] DASSAULT SYSTEMS SIMULIA CORP. *Getting Started With Abaqus*. nedatováno.

[82] IMATEK. *Technical Specification IM10R-10 System* [online]. nedatováno. Dostupné z: http://www.reoterm.com.br/public/uploads/especificacoes/_53594e8216ac6.pdf

[83] PRESS, Pergamon a Editor D LERCHE. STUDIES OF FLUIDS SIMULATING BLOOD-LIKE RHEOLOGICAL PROPERTIES AND APPLICATIONS IN MODELS OF ARTERIAL BRANCHES. In: *SEVENTH INTERNATIONAL CONGRESS OF BIORHEOLOGY*. 1989, s. 39–52.

[84] E.PEHLIVAN, M.MATEJ a J.DZUGAN. Additively Manufactured CP-Ti (Grade 2) Single Strut Size Effect of Mechanical Response Under Building Direction. *IOP Conference Series: Materials Science and Engineering* [online]. 2018, **461**(Grade 2), 012066. ISSN 1757-899X. Dostupné z: doi:10.1088/1757-899X/461/1/012066

[85] CAO, Huiliang, Xuanyong LIU, Fanhao MENG a Paul K. CHU. Biological actions of silver nanoparticles embedded in titanium controlled by micro-galvanic effects. *Biomaterials* [online]. 2011, **32**(3), 693–705. ISSN 01429612. Dostupné z: doi:10.1016/j.biomaterials.2010.09.066

[86] SANSONE, Valerio, Davide PAGANI a Marco MELATO. The effects on bone cells of metal ions released from orthopaedic implants. A review. *Clinical Cases in Mineral and Bone Metabolism*. 2013, **10**(1), 34–40. ISSN 17248914.

[87] TAMMAS-WILLIAMS, Samuel, Philip J WITHERS, Iain TODD a Philip B PRANGNELL. Communication The Effectiveness of Hot Isostatic Pressing for Closing Porosity in

Selective Electron Beam Melting. *Metallurgical and Materials Transactions A* [online]. 2016, **47**(5), 1939–1946. ISSN 1543-1940. Dostupné z: doi:10.1007/s11661-016-3429-3

[88]   YAN, Chunze, Liang HAO, Ahmed HUSSEIN a Philippe YOUNG. Ti-6Al-4V triply periodic minimal surface structures for bone implants fabricated via selective laser melting. *Journal of the Mechanical Behavior of Biomedical Materials* [online]. 2015, **51**, 61–73. ISSN 18780180. Dostupné z: doi:10.1016/j.jmbbm.2015.06.024

[89]   WARNKE, Patrick H, Timothy DOUGLAS, Patrick WOLLNY, Eugene SHERRY, Martin STEINER, Sebastian GALONSKA, Stephan T BECKER, Ingo N SPRINGER, Jörg WILTFANG a Sureshan SIVANANTHAN. Rapid prototyping: porous titanium alloy scaffolds produced by selective laser melting for bone tissue engineering. *Tissue engineering. Part C, Methods* [online]. 2009, **15**(2), 115–24. ISSN 1937-3392. Dostupné z: doi:10.1089/ten.tec.2008.0288

[90]   OKABE, Hiroshi a Martin J. BLUNT. Prediction of permeability for porous media reconstructed using multiple-point statistics. *Physical Review E - Statistical Physics, Plasmas, Fluids, and Related Interdisciplinary Topics* [online]. 2004, **70**(6), 10. ISSN 1063651X. Dostupné z: doi:10.1103/PhysRevE.70.066135

[91]   YOO, Dong Jin. Heterogeneous porous scaffold design for tissue engineering using triply periodic minimal surfaces. In: *International Journal of Precision Engineering and Manufacturing* [online]. 2012, s. 527–537. ISSN 12298557. Dostupné z: doi:10.1007/s12541-012-0068-5

[92]   LIU, Xiangmei, Shuilin WU, Kelvin W.K. YEUNG, Y. L. CHAN, Tao HU, Zushun XU, Xuanyong LIU, Jonathan C.Y. CHUNG, Kenneth M.C. CHEUNG a Paul K. CHU. Relationship between osseointegration and superelastic biomechanics in porous NiTi scaffolds. *Biomaterials* [online]. 2011, **32**(2), 330–338. ISSN 01429612. Dostupné z: doi:10.1016/j.biomaterials.2010.08.102

[93]   MATASSI, Fabrizio, Alessandra BOTTI, Luigi SIRLEO, Christian CARULLI a Massimo INNOCENTI. Porous metal for orthopedics implants. *Clinical Cases in Mineral and Bone Metabolism* [online]. 2013, **10**(2), 111–115. ISSN 17248914. Dostupné

z: doi:10.11138/ccmbm/2013.10.2.111

[94]   RAO, Prashanth J, Matthew H PELLETIER, William R WALSH a Ralph J MOBBS. Spine
       Interbody Implants: Material Selection and Modification, Functionalization and
       Bioactivation of Surfaces to Improve Osseointegration. *Orthopaedic Surgery* [online].
       2014, **6**(2), 81–89. Dostupné z: doi:10.1111/os.12098

[95]   LI, K., X. L. GAO a G. SUBHASH. Effects of cell shape and strut cross-sectional area
       variations on the elastic properties of three-dimensional open-cell foams. *Journal of
       the Mechanics and Physics of Solids* [online]. 2006, **54**(4), 783–806. ISSN 00225096.
       Dostupné z: doi:10.1016/j.jmps.2005.10.007

[96]   JIANG, Bin, Zejun WANG a Naiqin ZHAO. Effect of pore size and relative density on the
       mechanical properties of open cell aluminum foams. *Scripta Materialia* [online]. 2007,
       56(2), 169–172. ISSN 13596462. Dostupné z: doi:10.1016/j.scriptamat.2006.08.070

[97]   BOBYN, J D, R M PILLIAR, H U CAMERON a G C WEATHERLY. The optimum pore size for
       the fixation of porous-surfaced metal implants by the ingrowth of bone. *Clinical
       orthopaedics and related research* [online]. nedatováno, (150), 263–70. ISSN 0009-
       921X. Dostupné z: http://www.ncbi.nlm.nih.gov/pubmed/7428231

[98]   PACURAR, Razvan, Nicolae BALC a Florica PREM. Research on how to improve the
       accuracy of the SLM metallic parts. *AIP Conference Proceedings* [online]. 2011,
       1353(103), 1385–1390. ISSN 0094243X. Dostupné z: doi:10.1063/1.3589710

[99]   SLOTWINSKI, John A., Edward J. GARBOCZI a Keith M. HEBENSTREIT. Porosity
       Measurements and Analysis for Metal Additive Manufacturing Process Control. *Journal
       of Research of the National Institute of Standards and Technology* [online]. 2014, **119**,
       494. ISSN 2165-7254. Dostupné z: doi:10.6028/jres.119.019

[100] YADOLLAHI, Aref, Nima SHAMSAEI, Scott M. THOMPSON, Alaa ELWANY a Linkan BIAN.
       Effects of building orientation and heat treatment on fatigue behavior of selective laser
       melted 17-4 PH stainless steel. *International Journal of Fatigue* [online]. 2017, **94**, 218–
       235. ISSN 01421123. Dostupné z: doi:10.1016/j.ijfatigue.2016.03.014

[101] WEGNER, Andreas a Gerd WITT. Correlation of Process Parameters and Part Properties
       in Laser Sintering using Response Surface Modeling. *Physics Procedia* [online]. 2012,

39, 480–490. ISSN 18753892. Dostupné z: doi:10.1016/j.phpro.2012.10.064

[102] NEGI, Sushant, Suresh DHIMAN a Rajesh Kumar SHARMA. Determining the effect of sintering conditions on mechanical properties of laser sintered glass filled polyamide parts using RSM. *Measurement: Journal of the International Measurement Confederation* [online]. 2015, **68**, 205–218. ISSN 02632241. Dostupné z: doi:10.1016/j.measurement.2015.02.057

[103] CAULFIELD, B., P. E. MCHUGH a S. LOHFELD. Dependence of mechanical properties of polyamide components on build parameters in the SLS process. *Journal of Materials Processing Technology* [online]. 2007, **182**(1–3), 477–488. ISSN 09240136. Dostupné z: doi:10.1016/j.jmatprotec.2006.09.007

[104] ZHANG, Haidong a Saniya LEBLANC. Processing Parameters for Selective Laser Sintering or Melting of Oxide Ceramics. *Additive Manufacturing of High-performance Metals and Alloys - Modeling and Optimization* [online]. 2018. Dostupné z: doi:10.5772/intechopen.75832

[105] GHOUSE, Shaaz, Sarat BABU, Richard J. VAN ARKEL, Kenneth NAI, Paul A. HOOPER a Jonathan R.T. JEFFERS. The influence of laser parameters and scanning strategies on the mechanical properties of a stochastic porous material. *Materials and Design* [online]. 2017, **131**, 498–508. ISSN 18734197. Dostupné z: doi:10.1016/j.matdes.2017.06.041

[106] CHASTAND, Victor, Astrid TEZENAS, Yannick CADORET, Philippe QUAEGEBEUR, Wilson MAIA a Eric CHARKALUK. Fatigue characterization of Titanium Ti-6Al-4V samples produced by Additive Manufacturing. *Procedia Structural Integrity* [online]. 2016, **2**, 3168–3176. ISSN 24523216. Dostupné z: doi:10.1016/j.prostr.2016.06.395

[107] SHIRAZI, Seyed Farid Seyed, Samira GHAREHKHANI, Mehdi MEHRALI, Hooman YARMAND, Hendrik Simon Cornelis METSELAAR, Nahrizul ADIB KADRI a Noor Azuan Abu OSMAN. A review on powder-based additive manufacturing for tissue engineering: Selective laser sintering and inkjet 3D printing. *Science and Technology of Advanced Materials* [online]. 2015, **16**(3). ISSN 14686996. Dostupné z: doi:10.1088/1468-6996/16/3/033502

[108] WANG, Hongtao, Z. Zak FANG a Pei SUN. A critical review of mechanical properties of powder metallurgy titanium. *International Journal of Powder Metallurgy (Princeton, New Jersey)* [online]. 2010, **46**(5), 45–57. ISSN 08887462. Dostupné z: doi:10.3390/met5041902

[109] MAZUR, Maciej, Martin LEARY, Shoujin SUN, Martin VCELKA, Darpan SHIDID a Milan BRANDT. Deformation and failure behaviour of Ti-6Al-4V lattice structures manufactured by selective laser melting (SLM). *International Journal of Advanced Manufacturing Technology* [online]. 2016, **84**(5–8), 1391–1411. ISSN 14333015. Dostupné z: doi:10.1007/s00170-015-7655-4

[110] CHENG, X. Y., S. J. LI, L. E. MURR, Z. B. ZHANG, Y. L. HAO, R. YANG, F. MEDINA a R. B. WICKER. Compression deformation behavior of Ti-6Al-4V alloy with cellular structures fabricated by electron beam melting. *Journal of the Mechanical Behavior of Biomedical Materials* [online]. 2012, **16**(1), 153–162. ISSN 18780180. Dostupné z: doi:10.1016/j.jmbbm.2012.10.005

[111] HERINGA, M B, R. J.B. PETERS, R. L.A.W. BLEYS, M. K. VAN DER LEE, P C TROMP, P. C.E. VAN KESTEREN, J. C.H. VAN EIJKEREN, A. K. UNDAS, A. G. OOMEN a H. BOUWMEESTER. Detection of titanium particles in human liver and spleen and possible health implications. *Particle and Fibre Toxicology* [online]. 2018, **15**(1), 1–9. ISSN 17438977. Dostupné z: doi:10.1186/s12989-018-0251-7

[112] WALLY, Zena, William VAN GRUNSVEN, Frederik CLAEYSSENS, Russell GOODALL a Gwendolen REILLY. Porous Titanium for Dental Implant Applications. *Metals* [online]. 2015, **5**(4), 1902–1920. Dostupné z: doi:10.3390/met5041902

[113] DUCHEYNE, P., G. WILLEMS, M. MARTENS a J. HELSEN. In vivo metal-ion release from porous titanium-fiber material. *Journal of Biomedical Materials Research* [online]. 1984, **18**(3), 293–308. ISSN 10974636. Dostupné z: doi:10.1002/jbm.820180306

[114] SHAO, Shuai, Mohammad J. MAHTABI, Nima SHAMSAEI a Scott M. THOMPSON. Solubility of argon in laser additive manufactured α-titanium under hot isostatic pressing condition. *Computational Materials Science* [online]. 2017, **131**, 209–219. ISSN 09270256. Dostupné z: doi:10.1016/j.commatsci.2017.01.040

[115] MOLAEI, Reza, Ali FATEMI a Nam PHAN. Significance of hot isostatic pressing (HIP) on multiaxial deformation and fatigue behaviors of additive manufactured Ti-6Al-4V including build orientation and surface roughness effects. *International Journal of Fatigue* [online]. 2018, **117**, 352–370. ISSN 01421123. Dostupné z: doi:10.1016/j.ijfatigue.2018.07.035

[116] AL-BERMANI, S. S., M. L. BLACKMORE, W. ZHANG a I. TODD. The origin of microstructural diversity, texture, and mechanical properties in electron beam melted Ti-6Al-4V. *Metallurgical and Materials Transactions A: Physical Metallurgy and Materials Science* [online]. 2010, **41**(13), 3422–3434. ISSN 10735623. Dostupné z: doi:10.1007/s11661-010-0397-x

[117] SONG, Y., D.S. XU, R. YANG, D. LI, W.T. WU a Z.X. GUO. Theoretical study of the effects of alloying elements on the strength and modulus of β-type bio-titanium alloys. *Materials Science and Engineering: A* [online]. 2002, **260**(1–2), 269–274. ISSN 09215093. Dostupné z: doi:10.1016/s0921-5093(98)00886-7

[118] OH, Ik Hyun, Naoyuki NOMURA, Naoya MASAHASHI a Shuji HANADA. Microstructures and Mechanical Properties of Porous Titanium Compacts Prepared By Powder Sintering. *Materials Transactions* [online]. 2003, **49**(12), 1197–1202. ISSN 13596462. Dostupné z: doi:10.1016/j.scriptamat.2003.08.018

[119] MURR, L. E., S. A. QUINONES, S. M. GAYTAN, M. I. LOPEZ, A. RODELA, E. Y. MARTINEZ, D. H. HERNANDEZ, E. MARTINEZ, F. MEDINA a R. B. WICKER. Microstructure and mechanical behavior of Ti-6Al-4V produced by rapid-layer manufacturing, for biomedical applications. *Journal of the Mechanical Behavior of Biomedical Materials* [online]. 2009, **2**(1), 20–32. ISSN 17516161. Dostupné z: doi:10.1016/j.jmbbm.2008.05.004

[120] HRABE, Nikolas, Thomas GNÄUPEL-HEROLD a Timothy QUINN. Fatigue properties of a titanium alloy (Ti–6Al–4V) fabricated via electron beam melting (EBM): Effects of internal defects and residual stress. *International Journal of Fatigue* [online]. 2017, **94**, 202–210. ISSN 01421123. Dostupné z: doi:10.1016/j.ijfatigue.2016.04.022

[121] TILEY, J., T. SEARLES, E. LEE, S. KAR, R. BANERJEE, J. C. RUSS a H. L. FRASER.

Quantification of microstructural features in α/β titanium alloys. *Materials Science and Engineering A* [online]. 2004, **372**(1–2), 191–198. ISSN 09215093. Dostupné z: doi:10.1016/j.msea.2003.12.008

[122] KRISHNA, B. Vamsi, Susmita BOSE a Amit BANDYOPADHYAY. Low stiffness porous Ti structures for load-bearing implants. *Acta Biomaterialia* [online]. 2007, **3**(6), 997–1006. ISSN 17427061. Dostupné z: doi:10.1016/j.actbio.2007.03.008

[123] WOODMAN, J L, J J JACOBS, J. O. GALANTE a R M URBAN. Metal ion release from titanium-based prosthetic segmental replacements of long bones in baboons: A long-term study. *Journal of Orthopaedic Research* [online]. 1983, **1**(4), 421–430. ISSN 1554527X. Dostupné z: doi:10.1002/jor.1100010411

[124] FRISKEN, K W, G W DANDIE, S LUGOWSKI a G JORDAN. A study of titanium release into body organs following the insertion of single threaded screw implants into the mandibles of sheep. *Australian Dental Journal* [online]. 2002, **47**(3), 214–217. ISSN 00450421. Dostupné z: doi:10.1111/j.1834-7819.2002.tb00331.x

[125] MURR, L. E. Additive manufacturing of biomedical devices: an overview. *Materials Technology* [online]. 2018, **33**(1), 57–70. ISSN 17535557. Dostupné z: doi:10.1080/10667857.2017.1389052

[126] XUE, Zhenyu a John W HUTCHINSON. Constitutive model for quasi-static deformation of metallic sandwich cores. *International Journal for Numerical Methods in Engineering* [online]. 2004, **61**(13), 2205–2238. ISSN 00295981. Dostupné z: doi:10.1002/nme.1142

[127] HANSEN DOUGLAS C. Metal Corrosion in the Human Body: The Ultimate Bio-Corrosion Scenario. *Electrochemical Society Interface* [online]. 2008, 31–34. Dostupné z: http://electrochem.org/dl/interface/sum/sum08/su08_p31-34.pdf

[128] WANG, Di, Yongqiang YANG, Ruicheng LIU, Dongming XIAO a Jianfeng SUN. Study on the designing rules and processability of porous structure based on selective laser melting (SLM). *Journal of Materials Processing Technology* [online]. 2013, **213**(10), 1734–1742. ISSN 09240136. Dostupné z: doi:10.1016/j.jmatprotec.2013.05.001

[129] LI, JIAN, DIANSHENG CHEN, HUIQIN LUAN, WEI YAN a YUBO FAN. Mechanical Performance of Porous Implant With Different Unit Cells. *Journal of Mechanics in*

Medicine and Biology [online]. 2017, **17**(06), 1750101. ISSN 0219-5194. Dostupné z: doi:10.1142/s0219519417501019

[130] DESHPANDE, V. S. a N. A. FLECK. High strain rate compressive behaviour of aluminum alloy foams. *International Journal of Impact Engineering* [online]. 2000, **24**(3), 277–298. ISSN 0734743X. Dostupné z: doi:10.1016/S0734-743X(99)00153-0

[131] ING. PEHLIVAN EREN. UŽITNÝ VZOR:Necementovaná celoporézní acetabulární komponenta. CZ 32805 U1. 2019. Czech Republic, 1-3.

List of author publications

[84] E.PEHLIVAN, M.MATEJ a J.DZUGAN. Additively Manufactured CP-Ti (Grade 2) Single Strut Size Effect of Mechanical Response Under Building Direction. IOP Conference Series: Materials Science and Engineering [online]. 2018, 461(Grade 2), 012066. ISSN 1757-899X. Dostupné z: doi:10.1088/1757-899X/461/1/012066.

[131] ING. PEHLIVAN EREN. UŽITNÝ VZOR: Necementovaná celoporézní acetabulární komponenta. CZ 32805 U1. 2019. Czech Republic, 1-3.

[62] PEHLIVAN, Eren. Cellular Material Fatigue Estimation And Development. Student's conference Czech Technical University in Prague | Faculty of Mechanical Engineering layer. 2017, 1-6.

[64] PEHLIVAN, Eren. Porosity Structure Fatigue Estimation And Improvement. 20th Workshop Of Applied Mechanics 2016 Prague, June 10th 2016, CZECH REPUBLIC. 2016.

[52] E.PEHLIVAN, M. ROUDNICKA, J.DZUGAN, V. KRÁLÍK, V.DALIBOR, M.SEIFI, J. LEWADOWSKID a M. DANIEL. Effect of build orientation and geometry on the mechanical response of tiny wire samples manufactured by selective laser melting Eren Pehlivan. Additive Manufacturing (In-Reviewing). 2018, 1–21.

[66] E.PEHLIVAN, J.DZUGAN, R.SEDLACEK, J.FOJT, M.DANIEL. AM porous structures compressive mechanical behaviour after HIP and surface treatment. PLOS ONE (in-reviewing). 2019, 1–18.